W. Pabst / E. Gregorová

Characterization of particles and particle systems

ICT Prague 2007

Tyto studijní materiály vznikly v rámci projektu FRVŠ 674 / 2007 F1 / b
Tvorba předmětu “Charakterizace částic a částicových soustav“.

CPPS–1. Introduction – Particle size + equivalent diameters

1.0 Introduction

Particle size is one of the most important parameters in materials science and technology as well as many other branches of science and technology, from medicine, pharmacology and biology to ecology, energy technology and the geosciences. In this introduction we give an overview on the content of this lecture course and define the most important measures of size (equivalent diameters).

1.1 A brief guide through the contents of this course

This course concerns the characterization of individual particles (size, shape and surface) as well as many-particle systems. The theoretical backbone is the *statistics of small particles*. Except for sieve classification (which has lost its significance for particle size analysis today, although it remains an important tool for classification) the most important particle size analysis methods are treated in some detail, in particular

- *sedimentation methods*,
- *laser diffraction*,
- *microscopic image analysis*,

as well as *other methods* (dynamic light scattering, electrozone sensing, optical particle counting, XRD line profile analysis, adsorption techniques and mercury intrusion). Concerning image analysis, the reader is referred also to our lecture course "Microstructure and properties of porous materials" at the ICT Prague, where complementary information is given, which goes beyond the scope of the present lecture.

The two final units concern timely practical applications (*aerosols and nanoparticles*, *suspension rheology and nanofluids*). Apart from specific appendices to individual course units, there are three major inter-unit appendices, which are based on the knowledge of several course units and concern in particular

- *isometric particles* (size characterization by laser diffraction and image analysis),
- *oblate particles* (size and shape characterization, sedimentation and laser diffraction),
- *prolate particles* (size and shape characterization, image analysis + laser diffraction),

as well as suspension rheology.

1.2 Equivalent diameters

Particle size, in the sense commonly used, is a linear length measure, measured in SI unit [m]. In this sense it can be uniquely defined only for spheres, where it is the diameter (or radius). For all other shapes, particle size must be clearly defined via the measuring procedure. So-called derived diameters are determined by measuring a size-dependent property of the particle and relating it to a single linear dimension. The most widely used of these are the *equivalent diameters*, in particular the equivalent spherical diameters.

Ningde Amperex Tech. Exhibit No. 2043
Zhuhai CosMX Battery Co. Ltd. v. Ningde Amperex Tech.
IPR2025-00432, U.S. Patent No. 11,575,148
Page 2 of 123

Important equivalent diameters are:

- Volume-equivalent sphere diameter D_{volume} = diameter of a sphere with the same volume as the particle $V_{particle}$, i.e.

$$D_{volume} = \left(\frac{6}{\pi} V_{particle} \right)^{1/3}$$

e.g. for a cube with edge length 1 μm (volume 1 μm^3) we have $D_{volume} = 1.24$ μm.

- Surface-equivalent sphere diameter $D_{surface}$ = diameter of a sphere with the same surface as the particle $S_{particle}$, i.e.

$$D_{surface} = \left(\frac{6}{\pi} S_{particle} \right)^{1/2}$$

e.g. for a cube with edge length 1 μm (surface 6 μm^2) we have $D_{surface} = 1.38$ μm.

- Stokes diameter D_S (= equivalent diameter corresponding to the diameter of a sphere with the same final settling velocity as the particle undergoing laminar flow in a fluid of the same density and viscosity), defined via the Stokes relation

$$D_S = \sqrt{\frac{18 \eta v}{(\rho_S - \rho_L) g}},$$

where η is the viscosity (of the pure liquid medium without particles), ρ_S the density of the solid particles, ρ_L the density of the pure liquid, g the gravitational acceleration and v the final settling velocity.

- Hydrodynamic equivalent diameter D_H (= diameter of a sphere with the same translational diffusion coefficient $D_{translation}$ as the particle in the same fluid under the same conditions), defined via the Stokes-Einstein relation

$$D_H = \frac{kT}{3\pi \, \eta \, D_{translation}},$$

where k is the Boltzmann constant, T the absolute temperature and η the viscosity of the liquid medium (the diffusion coefficient must be extrapolated to zero concentration).

- Sieve diameter D_{sieve} (= equivalent diameter corresponding to the diameter of a sphere passing through a sieve of defined mesh size with square or circular apertures).

Ningde Amperex Tech. Exhibit No. 2043
Zhuhai CosMX Battery Co. Ltd. v. Ningde Amperex Tech.
IPR2025-00432, U.S. Patent No. 11,575,148
Page 3 of 123

- Laser diffraction equivalent diameter D_L (= diameter of a sphere yielding on the same detector geometry the same electronic response from the optical signal, i.e. the diffraction pattern, as the particle); when the Fraunhofer approximation is valid, D_L should correspond to the projected area diameter of the particle in random orientation.

- Projected area diameter D_P (= equivalent diameter corresponding to the diameter of a sphere or circle with the same projected area as the particle); in general, D_P, is orientation-dependent, particularly for anisometric particles; the equivalent area diameter measured via microscopic image analysis, D_M, usually refers to preferential (non-random) "stable" orientation and thus is not the same as D_P for random orientation; another equivalent area diameter, conceptually analogous to the projected area diameter, is the random section area diameter, which can be measured from random cuts (planar sections, polished sections) via image analysis → see CPPS-10.

- Volume-surface diameter D_{SV} (Sauter diameter) = ratio of the cube of the volume-equivalent diameter to the square of the surface-equivalent diameter, i.e.

$$D_{SV} = \frac{D_V^3}{D_S^2}.$$

This diameter is inversely proportional to the surface density (surface area per unit volume) S_V, or the specific surface area (surface area per unit mass), i.e. $S_M = S_V / \rho$, where ρ is the density. The relation between D_{SV} and S_V is (with values for k_{SV} given in Table 1.1)

$$S_V = \frac{k_{SV}}{D_{SV}}.$$

Table 1.1. *Shape factors k_{SV} for spheres and the Platonic solids (regular polyhedra).*

Shape	k_{SV}
Sphere	6
Tetrahedron	8.94
Octahedron	8.06
Cube	7.44
Dodecahedron (pentagonal faces)	6.59
Icosahedron (triangular faces)	6.39

Other equivalent diameters are thinkable, but less frequently used, e.g. the perimeter-equivalent diameter of a particle outline etc. Apart form the equivalent diameters there are other size measures which can be used to quantify particle size, mainly in microscopic image analysis of 2D particle outlines, among them the chord or intercept lengths (including the Martin diameter, i.e. the length of the chord dividing the projected particle area into two equal halves) and the caliper or Feret diameters (including the maximum and minimum Feret diameter) → see CPPS-9.

Ningde Amperex Tech. Exhibit No. 2043
Zhuhai CosMX Battery Co. Ltd. v. Ningde Amperex Tech.
IPR2025-00432, U.S. Patent No. 11,575,148
Page 4 of 123

CPPS–2. Particle shape and surface

2.0 Introduction

Particle shape is a complex geometric characteristic. It involves the form and habit of the particle as well as features like convexity and surface roughness. The literature on shape characterization is enormous and so is the number of possible definitions of shape factors. Here we give only the minimum set of definitions which are absolutely necessary for understanding (the literature on) particle shape characterization. Since the distinction of shape and surface topology is more or less a question of scale, we introduce fractal concepts as well.

2.1 Shape characterization and measures of shape

Particle shape has at least two different meanings:

- Shape (form) in the sense of deviations from spherical shape (e.g. regular polyhedra),
- Shape (habit) in the sense of deviations from isometric shape (e.g. spheroids).

Apart from these two meanings shape can denote the deviation from roundness (rounded versus angular) and deviations from convexity (convex versus concave shape). We define an isometric shape as a shape of an object (particle) for which, roughly speaking, the extension (particle size) is approximately the same in any direction. More precisely, for a particle to be isometric, the ratio of the maximum and minimum length of chords intersecting the center of gravity of the convex hull of the particle should not exceed the ratio of the least isometric regular polyhedron, i.e. the tetrahedron (simplex in 3D). For many practical purposes, isometric particles can approximately be considered (modeled) as spherical particles. A size measure (e.g. an equivalent diameter) is often sufficient for a description of isometric particles. Note that the term ”(an-) isometric” refers to external shape of objects (particles), while the term “(an-) isotropic” refers to the internal structure of media (materials).

Anisometric particles have significantly different extensions in different directions. When the particles (or their convex hulls) are centrally symmetric (at least approximately or in a statistical sense), i.e. possess a center of symmetry, they can be modeled as ellipsoids or rectangular parallelepipeds. In the general (triaxial) case at least three numbers are needed to satisfactorily describe the size and shape of such particles (e.g. hydroxyapatite platelets in bones). However, in practice many anisometric particles may be considered as rotationally symmetric, i.e. possessing an axis of rotational symmetry (e.g. disks / platelets and rods / fibers). In this case, only two numbers suffice for a description of size and shape, e.g. the extension in the direction of the rotational axis (maximum Feret diameter) and the maximum extension in the direction perpendicular to it (minimum Feret diameter), or an equivalent diameter and an aspect ratio. Although prismatic shapes frequently occur in practice, the simplest and therefore most popular model shapes for rotationally symmetric particles are

- Cylinders (with height H and diameter D) and
- Spheroids, i.e. rotary ellipsoids (with extension H in the direction of the rotational axis and maximum extension D in the direction perpendicular to the rotational axis); they can be oblate (flattened, e.g. disks / platelets) or prolate (elongated, e.g. rods / fibers).

Ningde Amperex Tech. Exhibit No. 2043
Zhuhai CosMX Battery Co. Ltd. v. Ningde Amperex Tech.
IPR2025-00432, U.S. Patent No. 11,575,148
Page 5 of 123

In both cases an aspect ratio can be defined as

$$R = \frac{H}{D}$$

or vice versa. All other possible shape measures for these model shapes can be reduced to the aspect ratio. In contrast to cylinders, spheroids contain spheres as a special case ($R = 1$).

In principle, for arbitrary particle shapes in 2D (particle outlines) the chord lengths intersecting the center of gravity can be determined in various directions; thus for each particle a plot of chord length (in m) versus orientation angle (in radians) can be obtained, which may be evaluated via Fourier analysis: using polar coordinates, the shape of the particle outline can be considered to be a wave form having a value of radius r, for values of θ lying between 0 and 2π. This wave form can be expressed as a harmonic (Fourier) series, i.e.

$$r(\theta) = a_0 + \sum_{n=1}^{\infty} \left(a_n \cos n\theta + b_n \sin n\theta \right).$$

→ Fourier coefficients a_n and b_0 describing particle shape. In principle, complete shape information is contained in the coefficients. A major practical difficulty, however, is to know the point at which the series can be stopped (higher order terms are needed for more angular and irregular particles). Moreover, the values of the coefficients depend on the choice of the origin. Obviously, for many-particle systems this procedure is usually not economical.

2.2 Fractal geometry and surface roughness

The total length T of a line consisting of n identical units, each with length a, is $T = na^1$. Similarly, the total area T of a square of n units with area a^2, is $T = na^2$, and the total volume T of a cube of n units with volume a^3, is $T = na^3$. Thus, in general,

$$T = na^{\delta},$$

where δ is an integer. In all the above cases the shape (hypervolume) can be considered to be completely filled. Partial filling can be represented by noninteger values of δ, with the degree of filling increasing as the value of δ becomes greater. Thus an irregular particle can be described by an exponent δ (non-Euclidean or fractal dimension), which contains information about the degree of volume filling, surface roughness or ruggedness of the perimeter of the 2D particle outline (projection or section). Irregular particles with a rough surface or agglomerates can have fractal dimensions between 2 and 3. The fractal dimension of the perimeter of a 2D outline of an irregular particle with a rough surface is between 1 and 2. That means, if the perimeter (surface) is measured (tiled) with smaller and smaller probes, then their total length (area) increases → the surface area of a particle (and similarly, the perimeter of a 2D particle outline) is not a uniquely defined value, but dependent on the size of the probe used. The fractal dimension δ is obtained from the slope of the straight line fit in log-log-plots (n versus a). The straight line fit in the log-log-plot (or, equivalently, the power law fit in the lin-lin-plot) implies geometrical similarity on different length scales, i.e. different degrees of magnification (scale-invariance, self-similarity), at least in a limited range. For details on measuring techniques see CPPS-12.3.

Ningde Amperex Tech. Exhibit No. 2043
Zhuhai CosMX Battery Co. Ltd. v. Ningde Amperex Tech.
IPR2025-00432, U.S. Patent No. 11,575,148
Page 6 of 123

CPPS–3. Particle packing, coordination numbers and fractals

3.0 Introduction

The packing of particles is of utmost practical importance in materials science and technology as well as other branches of science where e.g. packed beds are used (chemical engineering, reactor technology), the products consist of particular materials (pharmacology) or the systems involved are intrinsically granular and porous (geosciences, petroleum engineering). In particular, when classical power processing techniques are used for the production of ceramic or metal bodies a knowledge of particle packing is essential to control the subsequent high-temperature and / or high-pressure processing steps. The basic quantification of particle packing involves the relative packing density (packing fraction) and the coordination number. A more detailed characterization of particle systems, in particular those exhibiting geometric self-similarity in a certain range of length scales, is possible via concepts of fractal geometry.

3.1 Packing fraction and coordination numbers

For monosized spherical particles the densest packing is that with a packing fraction (relative packing density = solids volume fractions) of $\pi/18 \approx 0.74$ (Kepler's conjecture 1611, proved by Hales 1998; this apparently obvious result gains its importance from the fact that in 3D space one can create suboptimal global packings with finite-sized clusters of spheres, e.g. tetrahedral or icosahedral clusters, with local densities higher than the global maximum – at the expense of having large voids elsewhere, i.e. these high-density clusters cannot be space-filling; e.g. identical non-overlapping regular tetrahedra cannot tile 3D space and the system is geometrically "frustrated", meaning that local optimal packing rules are inconsistent with global packing constraints). This maximum packing fraction of 0.74 for monosized spheres corresponds to hexagonal closest packing (hcp) or face-centered cubic (fcc) and its stacking variants, all with a coordination number of 12 (i.e. a chosen particles has 12 nearest neighbors in direct point contact). Simple cubic packing, on the other hand, has a packing fraction of 0.52 and a coordination number of 6. It is not known whether stable packings of monosized spheres with lower packing fraction and coordination number exist in 3D space (diamond packing with a packing fraction of 0.34 and a coordination number of 4 is unstable). Table 3.1 lists other ordered packings of monosized spheres.

Table 3.2. *Packing fraction and coordination number of ordered packings of monosized spheres in 3D space.*

Packing type	Packing fraction	Coordination number
Closest packing (fcc / hcp)	0.7405	12
Tetragonal-sphenoidal	0.708	10
Body-centered cubic	0.680	8
Orthorhombic	0.605	8
Simple cubic	0.524	6
Diamond	0.340	4

Ningde Amperex Tech. Exhibit No. 2043
Zhuhai CosMX Battery Co. Ltd. v. Ningde Amperex Tech.
IPR2025-00432, U.S. Patent No. 11,575,148
Page 7 of 123

Inspite of the fact that there are two recognized packings with a coordination number of eight, there have been attempts to approximately correlate the packing fraction ϕ_S and the coordination number N_C, e.g. by the relations

$$N_C = \frac{\pi}{1-\phi_S},$$

$$N_C = 14 - 10.4\left(1-\phi_S\right)^{0.38}.$$

The latter relation predicts that the coordination number for densely arranged particles approaches 14 when the packing fraction approaches 1, i.e. 100 %. Therefore, the Kelvin tetra-kai-decahedron (truncated octahedron with 14 faces, i.e. 6 squares and 8 hexagons) has become the preferred basic model shape for sintered microstructures → see the course "Technology of Ceramics" at the ICT Prague.

When the packing is random (i.e. not ordered), the packing fraction for monosized spheres is approx. 0.64, and the average coordination number is 7. Traditionally, this packing type has been called random-close packing (rcp structure). Although Torquato (2000, 2002) has shown that the rcp structure is ill defined and has replaced it by the concept of the "maximally random jammed" state (mrj structure), the best estimate for the mrj packing fraction is still 0.64 in the case of monosized spheres.

Higher packing fractions can be achieved by polydisperse particle systems and non-spherical (e.g. polyhedral or anisometric) particles, but reliable theoretical predictions are difficult in these cases. In practice, empirical rules and experience with real systems are invoked → see the course "Technology of Ceramics" at the ICT Prague.

3.2 Mass and surface fractals

When particles aggregate, e.g. from a particulate sol or a macromolecular solution with polyfunctional monomers, they commonly form fractal structures. A mass fractal (object) is distinguished from a conventional Euclidean object by the fact that its mass M increases with its size (equivalent radius) according to the relation

$$M \propto r^{d_m},$$

where d_m is the mass fractal dimension ($0 \le d_m \le 3$). For a Euclidean object $M \propto r^3$, but for a fractal $d_m < 3$, that means the density of the object ($\rho \propto M/r^3$) decreases as it gets bigger; a tree-like structure is an example of a mass fractal. A surface fractal (object) has a surface area S increasing more steeply than proportional to r^2, i.e.

$$S \propto r^{d_s},$$

where d_s is the surface fractal dimension ($2 \le d_s \le 3$); a crumpled piece of paper is an example of a surface fractal (it is not a mass fractal, however, since its mass increases as $M \propto r^3$).

Ningde Amperex Tech. Exhibit No. 2043
Zhuhai CosMX Battery Co. Ltd. v. Ningde Amperex Tech.
IPR2025-00432, U.S. Patent No. 11,575,148
Page 8 of 123

For Euclidean objects (nonfractal with a smooth surface) $d_m = 3$ and $d_s = 2$, for mass fractal objects $d_m = d_s$, for surface fractal objects the mass fractal dimension equals the Euclidean dimension, i.e. $d_m = 3$, and $2 < d_s < 3$. The three most popular techniques to determine fractal dimensions are:

- Adsorption of gas or solute molecules (specific surface measurements) – Pfeifer-Avnir approach:

$$a \propto \sigma^{-d_m/2} D^{d_m - 3},$$

  where a is the amount of adsorbate adsorbed on the adsorbent (e.g. number of adsorbate molecules per unit volume of adsorbent or moles of adsorbate per unit mass of adsorbent), σ is the equivalent area or cross-section of the adsorbate molecule (when a linear size measure, e.g. an equivalent diameter, is used the exponent is $-d_m$ instead of $-d_m/2$) and D is a linear measure of particle size (e.g. an independently measured mean equivalent diameter); theoretically, either σ or D can be varied (in practice usually σ). Alternative variants of the adsorption technique use a modified Frenkel-Halsey Hill equation or the Kiselev equation (Neimark-Kiselev approach) → see CPPS-12.3.

- Mercury intrusion (volume-weighted pore-size distribution measurements):

$$\frac{dV(r)}{dr} \propto r^{2-d_s},$$

  → further details see CPPS-12.3.

- Small-angle scattering (Porod region): Small-angle scattering can use neutrons (SANS), X-rays (SAXS), or visible light (static light scattering or dynamic / quasi-elastic light scattering – QELS) → length scales from 0.1 nm to 1 μm. The scattering curve, i.e. the log-log plot of scattered intensity as a function of the inverse length measure

$$k = \frac{4\pi}{\lambda} \sin\frac{\theta}{2},$$

  where λ is the wavelength and θ the scattering angle, can be divided into three regions:

  - Bragg region at large scattering angles ($k\beta \approx 1$, where β is the bond length), from which information concerning interatomic spacings is obtained via Bragg's law (in amorphous systems diffuse peaks → radial distribution curves).

  - Guinier region at very small scattering angles ($k\gamma \approx 1$), for which the scattered intensity is exponentially related to the radius of gyration γ, i.e.

Ningde Amperex Tech. Exhibit No. 2043
Zhuhai CosMX Battery Co. Ltd. v. Ningde Amperex Tech.
IPR2025-00432, U.S. Patent No. 11,575,148
Page 9 of 123

$$I(k) \propto \exp\left(-k^2\gamma^2/3\right)$$

→ information on the mass or radius of macromolecules.

- Porod region at intermediate scattering angles ($\gamma >> k^{-1} >> \beta$), for which the scattered intensity decays acccording to a power law, i.e. as

$$I(k) \propto k^P,$$

where P is the Porod slope, which can be interpreted in terms of fractal dimensions as

$$P = d_s - 2d_m.$$

Since for mass fractal objects $d_m = d_s \rightarrow P = -d_m$, i.e. the mass fractal dimension is obtained directly from the slope. For surface fractal objects $d_m = 3 \rightarrow P = d_s - 6$. However, polydispersivity of pore sizes (interstitial voids in an aggregate / agglomerate of particles) with a number-weighted pore size distribution corresponding to a power law also yields a power-law decay for the scattered intensity. That means, physically meaningful fractal dimensions can be derived from the Porod plot only when the type and degree of polydispersivity is known. Table 3.2 gives examples of Porod slopes for various structures of particles aggreagates / agglomerates.

Table 3.2. *Porod slopes for various structures of particles aggreagates / agglomerates.*

Structure	Porod slope	Type of fractal
Linear polymer (random walk)	– 2	Mass
Linear polymer – swollen (self-avoiding walk)	– 5/3 ≈ 1.67	Mass
Branched polymer	– 16/7 ≈ 2.29	Mass
Branched polymer – swollen	– 2	Mass
Diffusion-limited aggregate	– 2.5	Mass
Multiparticle diffusion-limited aggregate	– 1.8	Mass
Percolation cluster	– 2.5 to – 2.6	Mass
Fractally rough surface	– 3 to – 4	Surface
Agglomerate of particles or porous medium with smooth surfaces	– 4	Non-fractal

Ningde Amperex Tech. Exhibit No. 2043
Zhuhai CosMX Battery Co. Ltd. v. Ningde Amperex Tech.
IPR2025-00432, U.S. Patent No. 11,575,148
Page 10 of 123

CPPS–4. Small particle statistics

4.0 Introduction

Small particle statistics is treated in detail in Herdan's book (1960). In the pre-computer era, analytical functions (and the corresponding special graphical papers) were used whenever possible to represent measured particle size distributions. These functions have the advantage that they can be characterized by a few fit parameters, from which all statistical values can be determined. Real particle size distributions, however, do usually not fit any analytical function exactly, and therefore today a numerical (tabular or graphical) representation is preferred. In order to reduce the information contained in a complete distribution, statistics can be applied.

4.1 Graphical representation of size distributions

Particle size distributions can be represented as histograms (discrete distributions) or as continuous curves, when the size classes are sufficiently close (usually the bin width of a size class is chosen by dividing the overall width of the distribution by the square root of the number of measured particles). The size measure (usually an equivalent diameter x_i, corresponding to the average in a size class i) is given on the abscissa (x-axis), while the ordinate (y-axis) shows the statistical weight of each size class. This statistical weight can be

- the number of particles in a size class → *number-weighted* distribution (with index 0),
- the total length of all particles (= sum of all equivalent diameters) in the selected size class → *length-weighted* distribution (with index 1),
- the total surface of all particles (= sum of the surface areas of equivalent spheres, as calculated from the equivalent diameters) in the selected size class → *surface-weighted* distribution (with index 2),
- the total volume of all particles (= sum of the volumes of equivalent spheres, as calculated from the equivalent diameters) in the selected size class → *volume-weighted* distribution (with index 3),
- the total mass of all particles in the selected size class → *mass-weighted* distribution (which is identical to the volume-weighted distribution when all particles in a sample have the same density).

Particle size distributions can be represented either in differential form as frequency curves / histograms or, more precisely, probability density distributions (denoted q_r),

$$q_r(x_i) = \frac{n_i\, x_i^r}{\sum n_i\, x_i^r},$$

where n_i is the number of particles in the i-th size class with average size (equivalent diameter) x_i, or in integral form as cumulative curves / histograms (denoted Q_r), which can be undersize,

Ningde Amperex Tech. Exhibit No. 2043
Zhuhai CosMX Battery Co. Ltd. v. Ningde Amperex Tech.
IPR2025-00432, U.S. Patent No. 11,575,148
Page 11 of 123

$$Q_r(x_i) = \sum_{n=1}^{i} q_r(x_n)\,\Delta x_n = \int_{x_{\min}}^{x_i} q_r(x)\,dx$$

or oversize,

$$Q_r^{oversize}(x_i) = 1 - Q_r(x_i)$$

(in this course we always refer to the undersize distribution, if not explicitly stated otherwise).

Number-weighted particle size distributions (q_0, Q_0) are the primary results of counting methods such as microscopic image analysis, while volume-weighted distributions (q_3, Q_3) are the primary results of ensemble methods such as laser diffraction. (The mass-weighted distributions obtained using sedimentation methods are identical to the volume-weighted distributions if the density of all particles is the same.) Length- and surface-weighted distributions are rather uncommon in practice. Note that number-weighted and volume-weighted distributions cannot be directly compared. They can be compared only after one of them has been transformed into the other (which requires either the assumption that the shape is size-invariant or an independent measurement of the shape-size dependence). Although comparable after applying this kind of transformation, (q_0, Q_0) $\rightarrow$ (q_3, Q_3) or (q_3, Q_3) $\rightarrow$ (q_0, Q_0), the results cannot be expected to coincide in general, because different methods measure different equivalent diameters. Only for spherical particles (or approximately for isometric particles) coincidence may be expected in principle ($\rightarrow$ standard reference materials for calibration purposes). In practice, the degree of coincidence can be limited by the different measuring ranges and other method-specific errors.

4.2 Statistical mean values

In general, the mean values for the different types of distributions are:

$$\bar{x}_k = \left(\frac{\sum x_i^k x_i^r n_i}{\sum x_i^r n_i} \right)^{1/k} = \left(\frac{\sum x_i^{k+r} n_i}{\sum x_i^r n_i} \right)^{1/k},$$

where r denotes the type of distribution (r = 0, 1, 2, 3 for number-weighted, length-weighted, surface-weighted and volume-weighted, respectively) and k denotes the type of average (e.g. harmonic mean $k = -1$, geometric mean $k = 0$, arithmetic mean $k = 1$, quadratic mean $k = 2$ etc.). For these averages Cauchy's majority relation holds:

$$\ldots\ \bar{x}_H \le \bar{x}_G \le \bar{x}_A \le \bar{x}_Q\ \ldots$$

The geometric mean is calculated via the relation

$$\log \bar{x}_G = \frac{\sum x_i^r n_i \log x_i}{\sum x_i^r n_i} = \frac{\sum q_r(x_i) \log x_i}{\sum q_r(x_i)}.$$

Ningde Amperex Tech. Exhibit No. 2043
Zhuhai CosMX Battery Co. Ltd. v. Ningde Amperex Tech.
IPR2025-00432, U.S. Patent No. 11,575,148
Page 12 of 123

It can be shown that the harmonic mean of the volume-weighted distribution equals the arithmetic mean of the surface-weighted distribution (Herdan's theorem). Therefore the specific surface (surface density) is inversely proportional to the harmonic mean of the volume-weighted distribution, also called "natural" mean or Sauter mean (mean volume-to-surface particle size). Its reciprocal, i.e. the ratio between the second and third moment (se below) is proportional to the specific surface of the powder, the proportionality factor being 6 for spheres and greater than 6 for other particle shapes.

4.3 Other basic parameters characterizing size distributions

Other parameters, which are not statistical mean values (averages), can be used to characterize particle size distributions. The most important of them are:

- *Quantiles*: particle sizes corresponding to a selected cumulative weight; the most important quantiles are the lower decile (x_{10}), the median value (x_{50}), and the upper decile (x_{90}) $\rightarrow$ their physical meaning is evident from the cumulative (undersize) curve (histogram): 10 % (with respect to number in Q_0, with respect to volume in Q_3 etc.) are smaller than x_{10} etc.

- *Median*: the special quantile x_{50}, which divides the particle population into two equal parts (with respect to number in Q_0, with respect to volume in Q_3 etc.)

- *Span*: a measure of the width (breadth) of a distribution, defined as

$$Span = \frac{x_{90} - x_{10}}{x_{50}}.$$

- *Mode*: the most frequent value (with respect to number in Q_0, with respect to volume in Q_3 etc.) in a distribution, corresponding to the maximum in the frequency curve (or more precisely, probability density distribution); distributions and particle systems with one mode are called monomodal, with two bi- and with three tri-modal (in general multimodal); particle systems with one very narrow mode are called monodisperse, with two bidisperse etc. (in contrast to polydisperse systems, which exhibit a broad distribution); in the extreme case of strictly monodisperse spheres, the frequency curve would be a Dirac delta distribution and the corresponding cumulative curve a Heaviside step function.

- *Variance* (σ^2): a measure of the width (breadth) of a distribution, defined as

$$\sigma^2 = \frac{\sum q_r(x_i)(x_i - \bar{x}_A)^2}{N-1},$$

where $N = \sum n_i$ for number-weighted distributions and $N = \sum x_i^r n_i$ in general. The *standard deviation* is the square root of the variance (σ) and the *coefficient of variation* is the standard deviation divided by the arithmetic mean ($\sigma/\bar{x}_A$).

Ningde Amperex Tech. Exhibit No. 2043
Zhuhai CosMX Battery Co. Ltd. v. Ningde Amperex Tech.
IPR2025-00432, U.S. Patent No. 11,575,148
Page 13 of 123

- *Skewness:* a measure of the distortion from a symmetrical distribution, defined as

$$S = \frac{N}{(N-1)(N-2)} \frac{\sum q_r(x_i)(x_i - \bar{x}_A)^3}{\sigma^3} \approx \frac{\sum q_r(x_i)(x_i - \bar{x}_A)^3}{N\,\sigma^3}.$$

  A symmetric distribution is defined as having zero skewness. S is positive if the distribution is right-skewed (steep rise on the left, long tail on the right side, i.e. more material in the coarse size range) and negative if left-skewed.

- Kurtosis: a measure of the peakedness (shape) of the distribution, defined as

$$K = \frac{N(N-1)}{(N-1)(N-2)(N-3)} \frac{\sum q_r(x_i)(x_i - \bar{x}_A)^4}{\sigma^4} - \frac{3(N-1)^2}{(N-2)(N-3)} \approx \frac{\sum q_r(x_i)(x_i - \bar{x}_A)^4}{N\,\sigma^4} - 3$$

  A normal distribution (Gauss distribution) is defined as having zero kurtosis (being mesokurtic). K is positive if the distribution is leptokurtic (sharper or narrower than the normal distribution) and negative of platykurtic (flattened maximum).

Of course, all these parameters are different for each type of distribution (of the same sample), i.e. number-weighted, length-weighted, surface-weighted and volume-weighted.

4.4 The moment notation

In the *moment notation*, mean values are defined through the moments of different types of distributions. When the differential area $q_r(x)dx$ below the frequency curve (probability density distribution) $q_r(x)$ (with $r = 0, 1, 2, 3$ denoting a number-weighted, length-weighted, surface-weighted and volume-weighted distribution, respectively) is multiplied by the "lever" x^k ($k = \ldots$-3, -2, -1, 0, 1, 2, 3 …), the so-called *moments* result.

Complete general moment (of k-th order) of the $q_r(x)$ distribution:

$$M_{k,r} = \int_{x_{\min}}^{x_{\max}} x^k q_r(x)dx = \frac{1}{k+1} \sum_{i=1}^{N} q_{r,i} \left(x_i^{k+1} - x_{i-1}^{k+1}\right).$$

This general moment is called complete, because the integration extends over all particle sizes. The corresponding incomplete general moment would be defined by the integral between two selected values $x_1 \geq x_{\min}$ and $x_2 \leq x_{\max}$. Note that $M_{0,0} = 1$.

Complete central moment (of k-th order) of the $q_r(x)$ distribution:

$$m_{k,r} = \int_{x_{\min}}^{x_{\max}} \left(x - \bar{x}_{1,r}\right)^k q_r(x)dx,$$

Ningde Amperex Tech. Exhibit No. 2043
Zhuhai CosMX Battery Co. Ltd. v. Ningde Amperex Tech.
IPR2025-00432, U.S. Patent No. 11,575,148
Page 14 of 123

where $\bar{x}_{1,r}$ is the average size (arithmetic mean diameter) defined as

$$\bar{x}_{1,r} = M_{1,r} = \frac{M_{1+r,0}}{M_{r,0}}$$

(arithmetic mean, i.e. the abscissa value of the center of gravity of the $q_r(x)$ curve), which is a special case (for $k = 1$) of the general mean

$$\bar{x}_{k,r} = \sqrt[k]{M_{k,r}} = \sqrt[k]{\frac{M_{k+r,0}}{M_{r,0}}} = \sqrt[k]{\frac{M_{k+r-e,e}}{M_{r-e,e}}} .$$

Note that the normalization condition for general moments is

$$M_{0,r} = \int_{x_{\min}}^{x_{\max}} q_r(x)dx = 1 .$$

Important is the expectation value (k-th general moment of the number-weighted distribution)

$$E(x^k) = M_{k,0} = \int_{x_{\min}}^{x_{\max}} x^k q_0(x)dx$$

and the variance (second central moment of the number-weighted distribution)

$$s^2 = m_{2,0} = \int_{x_{\min}}^{x_{\max}} (x - \bar{x}_{1,0})^2 q_0(x)dx .$$

The k-th moment of a $q_r(x)$ distribution can be determined from a given $q_0(x)$ distribution via the equation

$$M_{k,r} = \frac{M_{k+r,0}}{M_{r,0}} .$$

This equation also allows a physical interpretation of the moments, e.g. $M_{-1,3} = M_{2,0}/M_{3,0}$ corresponds to a surface-volume ratio and $M_{-3,3} = M_{0,0}/M_{3,0} = 1/M_{3,0}$ to a reciprocal volume. More generally, the k-th moment of a $q_r(x)$ distribution can be determined from a given $q_e(x)$ distribution via the equation

$$M_{k,r} = \frac{M_{k+r-e,e}}{M_{r-e,e}} .$$

Using two different moments, any mean value of the distribution can be calculated.

Ningde Amperex Tech. Exhibit No. 2043
Zhuhai CosMX Battery Co. Ltd. v. Ningde Amperex Tech.
IPR2025-00432, U.S. Patent No. 11,575,148
Page 15 of 123

4.5 The moment-ratio notation

In the *moment-ratio notation*, mean values are expressed as the ratio between two moments of the number-weighted distribution of the size measure x (usually an equivalent diameter). The quantity $\overline{D}_{p,q}$ is the mean size obtained from summing discrete individual x values to the power of p (relationship between the signal and x) and normalizing by a sum of x values to the power of q (relationship between the statistical weight of each particle to its x value), i.e.

$$\overline{D}_{p,q} = \left(\frac{\sum x_i^p}{\sum x_i^q} \right)^{\frac{1}{p-q}} \qquad \text{for} \qquad p \neq q$$

$$\overline{D}_{p,q} = \exp\left(\frac{\sum x_i^p \ln x_i}{\sum x_i^p} \right) \qquad \text{for} \qquad p = q$$

In other words, $\overline{D}_{p,q}$ (after extraction of a proper root) is the arithmetic mean of the distribution obtained by plotting x^q against x^{p-q}. When a certain required mean value cannot be measured directly, but two other mean size values are known, then the required mean size can be calculated using the relation

$$\overline{D}_{p,q} = \frac{\left(\overline{D}_{p,c}\right)^{\frac{p-c}{p-q}}}{\left(\overline{D}_{q,c}\right)^{\frac{q-c}{p-q}}} \qquad \text{for} \qquad p \neq q\,.$$

For example, a graticule (grid) can be used to measure the total intercept length from random sections (cuts) of all particles by optical or electron microscopy; divided by the number of particles this yields the mean intercept length $\overline{D}_{1,0}$ (arithmetic mean of the number-weighted distribution). If digital image analysis is used to measure the projected areas of all particles and the total projected area is divided by the number of particles this yields $\overline{D}_{2,0}$. Similarly, the Coulter principle measures $\overline{D}_{3,0}$ and laser diffraction, sedimentation and sieving $\overline{D}_{4,3}$.

In dynamic light scattering (DLS), also called photon correlation spectroscopy (PCS), the scattering intensity is proportional to the volume squared or the sixth power of the particle dimension, when the particles are smaller than the wavelength of light (Rayleigh-Debye-Gans theory, first-order approximation). Thus, the mean size obtained from DLS (PCS) is

$$\left(\overline{D^{-1}}\right)^{-1} = \overline{D}_{6,5} = \frac{\sum I_i}{\sum\left(\frac{I_i}{D_i}\right)} = \frac{\sum D_i^6}{\sum D_i^5}\,.$$

This mean size value ($\overline{D}_{6,5}$) is always smaller than the weight average $\overline{D}_{4,.3}$. For larger particles, the DLS (PCS) mean size $\left(\overline{D^{-1}}\right)^{-1}$ is smaller than $\overline{D}_{6,5}$.

Ningde Amperex Tech. Exhibit No. 2043
Zhuhai CosMX Battery Co. Ltd. v. Ningde Amperex Tech.
IPR2025-00432, U.S. Patent No. 11,575,148
Page 16 of 123

CPPS–5. Sedimentation methods

5.0 Introduction

Apart from sieve classification, which has lost its former significance for particle sizing, sedimentation methods are the most prominent traditional methods used for particle size analysis. Advantages are their conceptual clarity and practical simplicity, without the need of sophisticated equipment. Disadvantages are that sedimentation methods are relatively time-consuming, the measuring range is relatively narrow and the results are very sensitive to sample preparation. In particular it is essential to achieve optimal deagglomeration. Too large particles develop turbulent motion, too small particles agglomerate and are subject to Brownian motion → range 1–100 μm (centrifugal sedimentation down to 0.1 μm).

5.1 Measuring principle, equipment and procedure

Principle of sedimentation methods: from a polydisperse particle system suspended in a liquid medium large particles exhibit faster settling under the influence of gravitation (and possibly centrifugal forces) than small particles.

Common traditional equipment is the Andreasen pipette → after preparing the suspension according to a standardized recipe (deagglomeration by deflocculants, stirring, agitating, ultrasonication, possibly boiling etc.) the suspension is allowed to settle. At predetermined time intervals small volume (10 ml) samples are taken by the pipette from a fixed position in the sedimentation column (600 ml, more than 20 cm high) to determine the concentration of solids which are still in suspension (after the larger size fractions have already settled out). For efficient measurements sampling time intervals should grow in a geometric series, so that a complete measurement can last several days when submicron particles are present.

Other common equipment for particle sizing via sedimentation methods are sedimentation balances, in which the mass increment of the sediment is continuously recorded, or photo- and X-ray sedimentographs, in which the cuvette (sedimentation column) is scanned in order to determine the particle concentration via attenuation of light or X-rays. With the latter, the measurement times can be reduced to a few minutes.

Necessary conditions for reliable results are the absence of particle-particle interactions (→ dilute suspensions) and laminar flow (→ Reynolds numbers below approx. 1; therefore large particles have to be eliminated before measurement, usually by using 63 μm sieves; the sieve fraction > 63 μm can be included in the final result).

5.2 Standard data evaluation

The standard evaluation of sedimentation measurements is performed by the classical Stokes formula for settling spheres → Stokes diameter D_S (equivalent sphere diameter):

$$D_S = \sqrt{\frac{18\eta h}{(\rho_S - \rho_L)\, g\, t}},$$

Ningde Amperex Tech. Exhibit No. 2043
Zhuhai CosMX Battery Co. Ltd. v. Ningde Amperex Tech.
IPR2025-00432, U.S. Patent No. 11,575,148
Page 17 of 123

where η is the viscosity (of the pure liquid medium without particles), ρ_S the density of the solid particles, ρ_L the density of the (pure) liquid, g the gravitational acceleration, h the sedimentation path (height of the column above the sampling point) and t the sedimentation time (sampling time). Note that the velocity is $v = h/t$ only under steady-state conditions, i.e. when the acceleration stage has been exceeded and the final settling velocity has been reached. This is usually the case after a few seconds. The Stokes equation can be derived from the force equilibrium

$$F_B - F_G + F_R = 0 ,$$

where F_B is the lift force (buoyancy force) acting on the particle in the (specifically lighter) liquid medium

$$F_B = \frac{4}{3}\pi R^3 \rho_L \, g ,$$

F_G the gravitational force acting on the particle

$$F_G = \frac{4}{3}\pi R^3 \rho_S \, g ,$$

and F_R the resistance force (friction force) exerted by the viscous liquid medium on the particle

$$F_R = 6\pi \eta R v ,$$

with v being the (final) velocity of the particle relative to the liquid medium and $R = D_S / 2$ the "particle" radius (equivalent sphere radius). Apart from several assumptions of physical character (laminarity of flow, steady flow with final velocity), the validity of the Stokes equation is essentially based on the geometrical assumption that the particles are spherical. Since this is usually not the case for real systems, the Stokes diameters D_S correspond to equivalent diameters of hypothetical spheres with the same settling behavior as the irregular, anisometric particles in question.

The results of sedimentation methods are mass-weighted size distributions. When all particles have the same density, these results can be considered as identical to volume-weighted size distributions, i.e. Q_3 curves.

5.3 Nonstandard data evaluation and shape determination of oblate particles

The Stokes equation can be modified and adapted to flat cylinders and oblate spheroids. This modified Stokes equation can be used to reinterpret the results in the case of oblate particles. Based on this reinterpretation, particle shape can be quantified when the sedimentation results are known and the size distribuition has been independently measured by image analysis or laser diffraction → see CPPS-Appendix-oblate.

Ningde Amperex Tech. Exhibit No. 2043
Zhuhai CosMX Battery Co. Ltd. v. Ningde Amperex Tech.
IPR2025-00432, U.S. Patent No. 11,575,148
Page 18 of 123

CPPS–6. Laser diffraction I – Theory

6.0 Introduction

The theory of laser diffraction is a special branch of electromagnetic scattering theory. In its classical (i.e. non-quantum-mechanical) form it is based on the Maxwell equations and its solutions. Mie theory is the exact classical theory of light scattering with small particles. It is elaborated for spheres and numerical solutions are available today, which can be implemented in computer algorithms. Alternatively, approximate analytical solutions are available for particles much smaller or larger than the wavelength of light (Rayleigh / Rayleigh-Debye-Gans scattering and Fraunhofer diffraction, respectively). The Fraunhofer approximation, which is closer to geometrical optics than the other approximations, is commonly used in laser diffraction instruments for particle sizing.

6.1 Interaction between light and matter

Light is electromagnetic radiation in the frequency range (ν) from approx. 10^{13} Hz (IR) to 10^{17} Hz (UV), corresponding to the wavelength range (λ) from 3 nm to 30 µm. The conversion between frequency and wavelength is via the speed of light $c = \lambda\nu$ (in vacuum 300 000 km/s). Visible light (i.e. the part of the electromagnetic spectrum to which the human eye is sensitive) ranges from approx. 400 nm (violet) to 750 nm (red).

The optical properties of matter (particles) are described by the complex refractive index,

$$N = n + i\kappa,$$

where the real part accounts for refraction according to Snell's law and the imaginary part is related to the absorption coefficient a via the relation

$$a = \frac{4\pi\,\kappa}{\lambda}.$$

This absorption coefficient occurs in the Lambert-Beer law describing the exponential attenuation of light intensity (irradiance) I as the light wave traverses a medium of thickness z, i.e.

$$I = I_0 \exp(-a\,z),$$

where I_0 is the intensity of the incident light (magnitude of the Poynting vector). Generally, extinction of light in a medium occurs by the combination of absorption and scattering. The absorbed radiation energy can be transformed into heat or re-radiated as fluorescence or phosphorescence. Scattering generally occurs in all directions and includes refraction and reflection as special cases. Light is characterized by the wave vector $\mathbf{k}$ (directing into the direction of propagation of the transverse light wave), whose magnitude is the wave number $k = 2\pi/\lambda$. A relative refractive index between two media can be defined as $m = N_1/N_2$.

Ningde Amperex Tech. Exhibit No. 2043
Zhuhai CosMX Battery Co. Ltd. v. Ningde Amperex Tech.
IPR2025-00432, U.S. Patent No. 11,575,148
Page 19 of 123

6.2 Rayleigh scattering, Rayleigh-Debye-Gans approximation, and Mie theory

When the particle is much smaller than the wavelength of light ($D << \lambda$ and $D \cdot |m| << \lambda$), then each part of the particle experiences the same homogeneous electric and magnetic field of incident light and the particle behaves like a dipole radiating in all directions, irrespective of its shape → Rayleigh scattering (with scattering angle θ):

$$I \propto I_0 \frac{D^6}{\lambda^4} \left| \frac{m^2 - 1}{m^2 + 2} \right|^2 \left(1 + \cos^2 \theta\right).$$

Thus, if the quantity $\left|\left(m^2 - 1\right)/\left(m^2 + 2\right)\right|^2$ is independent of the wavelength (this is not always true, because the complex refractive index generally depends on frequency, mainly for metallic particles), the scattered intensity is inversely proportional to λ^4, as long as extinction is dominated by scattering. When extinction is dominated by absorption, the intensity is inversely proportional to λ. In either case shorter wavelengths are extinguished more than longer ones → reddening of the spectrum of light upon transmission through hetergeneous media (aerosols, particle suspensions, fluids with density fluctuations) → blue sky during daytime, red sky at sunrise / sunset, use of red traffic lights in dust, fog / mist and haze.

When the particles are too large to be treated as single dipoles but still small enough to be treated as independent Rayleigh scatterers, they can be treated in the Rayleigh-Debye-Gans approximation if their refractive index is close to that of the medium (i.e. $|m - 1| << 1$) and the condition $D \cdot |m - 1| << \lambda$ is fulfilled (in practice up to a few 100 nm). When the shape of the particles is known (which implies knowledge of the shape-dependent scattering factor), size information can be extracted by measuring the angular scattering intensity (without knowledge of the refractive index of the particle).

For particles of arbitrary size, Mie theory can be applied to evaluate scattering data (numerical solution). In order to apply Mie theory, the complex refractive index of the particle (and the medium) must be known (for the light wavelength used). With increasing particle size the scattered intensity becomes preferentially directed to the forward direction. Note that Mie theory has been derived for optically isotropic particles of spherical shape.

6.3 Fraunhofer approximation

When the particle size is much larger than the wavelength of light $D >> \lambda$, the particle removes an amount of light energy corresponding to twice its cross-section area (extinction paradox). One areal cross-section is removed by reflection, refraction and absorption, and one via diffraction. Diffraction by particles is an edge effect (comparable to diffraction by an aperture), and for large particles, interference arises mainly from the particle outline, i.e. only the projected area perpendicular to the light propagation direction matters, not the volume and the internal structure (optical properties) of the particles → Fraunhofer approximation. More precisely, the Fraunhofer diffraction pattern is the Fourier transform of the particle projection. Analytical solutions are known for a variety of shapes. For spheres, which scatter as if they were opaque disks, the Fraunhofer diffraction equation is

Ningde Amperex Tech. Exhibit No. 2043
Zhuhai CosMX Battery Co. Ltd. v. Ningde Amperex Tech.
IPR2025-00432, U.S. Patent No. 11,575,148
Page 20 of 123

$$I \propto I_0 \left(\frac{J_1(\alpha \sin\theta)}{\alpha \sin\theta} \right)^2 ,$$

where $\alpha = \pi D/\lambda$ is a dimensionless size parameter and $J_1(...)$ the spherical Bessel function of first kind. In practice the Fraunhofer approximation applies to particles larger than a few µm, or highly absorptive particles (with absorption coefficients higher than 0.5), or particles with significant different refractive index contrast relative to the medium (m > 1.2). Because for large particles the scattering intensity is concentrated in the forward direction, typically at angles smaller than 10 °, Fraunhofer diffraction is also known as forward scattering or low-angle laser light scattering (LALLS). In Fraunhofer diffraction by a sphere, the angle of the first minimum of scattering intensity is simply related to the particle size via the relation

$$\sin\theta\,(\textit{first minimum}) = \frac{1.22\,\lambda}{D},$$

and most of the scattering intensity is concentrated close to the center of the interference pattern, see Table 6.1.

Table 6.1. *Intensity distribution of Fraunhofer diffraction from a sphere.*

Intensity ring	Radial position	Relative intensity I/I_0	Integral intensity in the whole ring [%]
Central max.	0	1	83.8
First min.	$\arcsin(1.22\,\lambda/D)$	0	0
Second max.	$\arcsin(1.64\,\lambda/D)$	0.0175	7.2
Second min.	$\arcsin(2.23\,\lambda/D)$	0	0
Third max.	$\arcsin(2.68\,\lambda/D)$	0.0042	2.8
Third min.	$\arcsin(3.24\,\lambda/D)$	0	0
Fourth max.	$\arcsin(3.70\,\lambda/D)$	0.0016	1.5
Fourth min.	$\arcsin(4.24\,\lambda/D)$	0	0

Table 6.2. *Common laser light sources.*

Laser type	Power [mW]	Wavelength [nm]	Remark
He-Ne gas laser	1 – 50	543.5, 594.1, 612.0, 632.8	
Ar ion laser	30 – 2000	488, 514.5	Water-cooling needed
Diode laser	0.1 - 200	405, 450, 635, 650, 670, 685, 750, 780	Low cost

Ningde Amperex Tech. Exhibit No. 2043
Zhuhai CosMX Battery Co. Ltd. v. Ningde Amperex Tech.
IPR2025-00432, U.S. Patent No. 11,575,148
Page 21 of 123

CPPS–7. Laser diffraction II – Practice

7.0 Introduction

Laser diffraction is the most widely used method for particle size analysis today. Although the underlying physical principles of scattering and diffraction were known for more than 100 years (Mie theory, 1908), particle sizers based on the diffraction principle could be developed only after the invention of the laser (around 1960), and the routine use of these instruments in practice required powerful computers (since the 1970es and 1980es). Commercial instruments today are fast, flexible (from laboratory batch measurements to in-line production control, from suspensions to dry powders, from nanometers to millimeters) and yield highly reproducible results. Therefore they are gradually replacing other particle sizing methods, in particular sedimentation methods, in most branches of industry.

7.1 Typical equipment and sample treatment

A typical laser diffraction instrument (particle sizer) consists of a light source (the laser), a sample chamber in the form of a flow-through cell (e.g. a glass cuvette connected to a liquid reservoir, approx. 500 ml) and a photodetector (e.g. a half-circle, quarter-circle or wedge-shaped segmented detector or a CCD-type detector), which transforms the optical signal (interference pattern, i.e. the light intensity in dependence of the scattering angle) into an electric signal (from the individual photodetector segments), which is then transferred to the computer and used for data generation. The geometry of the photodetector may become important when size measurement is to be coupled with shape measurement (based the deviation of the interference pattern from circular symmetry) or orientation measurement of anisometric particles (fibers) → current research. The distance between laser, sample chamber and photodetector as well as the position and spatial resolution of the photodetector (distance of detector segments) determine the measuring range which can be achieved. Typically it is from 0.1 μm to more than 1 mm, but new instruments principally enable measurements in the nanosize range as well. Fourier optics (with a Fourier lens between the sample chamber and the detector) or reverse Fourier optics (using a convergent laser beam with a Fourier lens between laser and sample chamber) is used to ensure that light scattered at a specific angle will fall onto a particular detector element, regardless of the particle's position in the beam.

The liquid reservoir (which can be an external beaker) contains the suspension (usually a powder sample dispersed in water) and is mechanically agitated by ultrasonics and possibly a stirrer. One of the advantages of laser diffraction, in contrast to other sizing methods, is the fact that ultrasonication can be used even during measurement (and not only as an auxiliary technique for sample preparation before measurement). During measurement the suspension is steadily pumped with a chosen flow velocity (adjustable according to the density of the particles to avoid settling in the system) through the flow-through cell. Alternatively, a dry-dispersion unit can be used in some instruments, from which the sample is conveyed through the glass cuvette by a air stream as a dry powder. Sample preparation has to be adapted to the character of the particles (type of material as well as particle size), but is usually less demanding than for sedimentation and other sizing methods. Of course, submicron and especially nanosized particles tend to exhibit strong agglomeration effects, and powerful deflocculants or other tricks may have to be used to achieve deagglomeration.

Ningde Amperex Tech. Exhibit No. 2043
Zhuhai CosMX Battery Co. Ltd. v. Ningde Amperex Tech.
IPR2025-00432, U.S. Patent No. 11,575,148
Page 22 of 123

7.2 Measuring principle and data evaluation

Laser diffraction is an ensemble method, i.e. a large number of particles is illuminated simultaneously and the diffraction pattern recorded by the photodetector is assumed to be the superposition of the interference patterns of the individual particles. In order to ensure that the latter is really the case, the concentration of the particle system (usually a suspension) has to be sufficiently low so that particle overlap and multiple scattering is avoided. On the other hand, the concentration must be high enough to achieve a reasoanble signal-to-noise ratio.

The standard method for data evaluation in laser diffraction is based on the Fraunhofer approximation. For a polydisperse powder sample the usual evaluation procedure consists in a deconvolution of the diffraction pattern according to the integral equation

$$I \propto I_0 \int_0^\infty \left(\frac{J_1(\alpha \sin\theta)}{\alpha \sin\theta} \right)^2 f(D)\, dD \ ,$$

where the function $f(D)$ is the desired particle size distribution (probability density). This is a so-called inverse problem (in mathematical terms ill-posed and ill-conditioned), for which questions of existence and uniqueness of the solutions generally arise. In commercial equipment the solution is usually based on proprietary algorithms. When the particles are not large enough to justify the application of the Fraunhofer approximation (valid for $D >> \lambda$), the exact Mie theory should be used for data evaluation (highly recommended for particles smaller than 1 µm), i.e. the complex refractive index of the materials should be known.

7.3 Data interpretation

The primary results of laser diffraction measurements are volume-weighted size distribution curves or histograms. These can be transformed into surface-, length- or number-weighted curves (histograms), each with its own statistical values → see Appendix-CPPS-7-A.

Exercise problem

Given the numerical values in Appendix-CPPS-7-A (alumina powder) tabulate the cumulative percentage values of the Q_3 distribution in steps of 0.2 µm, i.e. 0.2, 0.4, 0.6 etc. from 0.2 µm to 6 µm. Based on these values calculate (assuming of sphercial shape wherever necessary)

1. the probability density distribution (frequency histogram) q_3,
2. the surface-, length- and number-weighted distributions (q_2, q_1, q_0 and Q_2, Q_1, Q_0)
3. the harmonic, geometric, arithmetic, and quadratic mean for each distribution,
4. the mode, median and span of each distribution,
5. the variances, standard deviations, coefficients of variation, skewnesses and kurtoses,
6. the general moments $M_{-3,0}$, $M_{-2,0}$, $M_{-1,0}$, $M_{0,0}$, $M_{1,0}$, $M_{1,1}$, $M_{1,2}$, $M_{1,3}$, $M_{2,0}$, $M_{3,0}$, $M_{4,0}$, as well as the central moment $m_{2,0}$,
7. the moment ratios from $D_{0,0}$ to $D_{6,6}$ (i.e. those with index pairs 00, 10, 11, 20, 21, 22, 30, 31, 32, 33, 40, 41, 42, 43, 44, 50, 51, 52, 53, 54, 55, 60, 61, 62, 63, 64, 65, 66),

and compare the results with the computer printouts given in Appendix-CPPS-7-A.

Ningde Amperex Tech. Exhibit No. 2043
Zhuhai CosMX Battery Co. Ltd. v. Ningde Amperex Tech.
IPR2025-00432, U.S. Patent No. 11,575,148
Page 23 of 123

CPPS–8. Other methods – Dynamic light scattering, electrozone sensing, optical particle counting

8.0 Introduction

Particle sizing methods can be divided into ensemble techniques and counting techniques. Ensemble techniques have typically low resolution and low sensitivity, but a broad dynamic size range and high statistical accuracy. Examples are sieving, sedimentation, laser diffraction and dynamic light scattering (see below). On the other hand, counting techniques are typically high-resolution, high-sensitivity techniques with narrow dynamic size range and low statistical accuracy. Examples are microscopic image analysis, electrozone sensing and optical particle counting (see below). Counting techniques are better suited to detect a few small or large particles lying beyond selected size limits.

8.1 Dynamic light scattering (photon correlation spectroscopy)

Dynamic light scattering (DLS, also called photon correlation spectroscopy – PCS, a special case of quasi-elastic light scattering - QELS) is the method of choice for sizing submicron particles (< 1 μm).

Measuring principle: Fluctuations of the scattered light intensity (i.e. temporal variation in the μs to ms time scale) are recorded (at a given scattering angle) and analyzed → decay constant of the autocorrelation function (ACF) → diffusion coefficient → size information. Lower size limit (a few nm, depending on the relative refractive index) determined by experimental noise, upper size limit (a few μm, depending on particle density and fluid viscosity) by sedimentation (particles to be analyzed must be stably suspended). No optical properties of the particle and no calibration needed.

Instrumental equipment and sample concentration: Light source (e.g. He-Ne, Ar ion or diode laser) for coherent and possibly lineraly polarized light (note that coherence describes light waves that are in phase both in time and space – temporal and spatial coherence → coherence length = coherence time · speed of light), delivering and collecting optics (e.g. fiber optics), sample module (e.g. glass cuvette), photodetector system (photodiode or photomultiplier tubes), electronic system (amplifier and pulse discriminator) and correlator (hardware or software to measure the ACF). The scattering angle (range) is chosen in order maximize information and to increase the signal-to-noise ratio. The masureing time should be long enough to produce a smooth ACF. The particle concentration should be low enough to avoid multiple scattering and particle-particle interactions (→ mean distance between particles should be at least 20 times their diameter), but high enough to achieve a good signal-to-noise ratio (→ difficult to achieve for particles larger than 1 μm).

Data evaluation and interpretation: The ACF decays with time, e.g. for monodisperse particles according to

$$C(t') = A \cdot \exp\left(-\frac{t'}{\tau}\right) + B,$$

where $A = \langle I_S^2(t)\rangle - \langle I_S(t)\rangle^2$ and $B = \langle I_S^2(t)\rangle^2$ and the characteristic decay time τ (for polydisperse systems a spectrum of decay times, which has to be deconvoluted) is related to

Ningde Amperex Tech. Exhibit No. 2043
Zhuhai CosMX Battery Co. Ltd. v. Ningde Amperex Tech.
IPR2025-00432, U.S. Patent No. 11,575,148
Page 24 of 123

the diffusion coefficient D_T (for spherical particles only translational diffusion due to Brownian motion; for anisometric particles rotational diffusion can also be measured) via the relation

$$D_T = \frac{1}{K^2 \tau},$$

where K is the magnitude of the scattered wave vector

$$K = \left(\frac{4\pi\, n}{\lambda}\right) \sin\frac{\theta}{2},$$

which is a constant, not containing information on the particle's optical properties (n is the refractive index of the liquid medium). On the other hand, the hydrodynamic equivalent radius R_H is related to the diffusion coefficient via the Stokes-Einstein relation, e.g. for spherical particles

$$D_T = \frac{kT}{6\pi\, \eta\, R_H},$$

where k is the Boltzmann constant, T the absolute temperature and η the viscosity of the liquid medium (the diffusion coefficient must be extrapolated to zero concentration). Similar relations are available for non-spherical particles.

The primarily intensity-weighted distribution can be transformed into a volume-weighted ot number-weighted distribution via appropriate weighting factors (for Rayleigh scattering, Rayleigh-Debye-Gans scattering or Mie theory, depending on particle size). Additionally, in macromolecular solutions DLS can be used to determine the volume- or number-averaged molecular weight.

8.2 Electrozone sensing (Coulter counter technique)

The electrical sensing zone method (Coulter counter) was invented in the early 1950es and since then it has become one of the most widely used particle sizing techniques in medicine and pharmaceutical technology. The instrumental equipment is based on a tube with an orifice (aperture, "sensing zone") placed in an electrolyte solution containing a low concentration of particles. The device has two electrodes, one inside and one outside the orifice and a current flows between them through the electrolyte solution. When particles pass through the orifice or sensing zone (via liquid flow driven by suction in the inner container), a volume of electrolyte equivalent to the immersed volume of the particle is displaced, causing a short-term change in the conductivity across the orifice (i.e. the current between the two electrodes decreases when the particles are electrically insulating). This resistance change can be measured either as a voltage pulse or a current pulse. By measuring the number of pulses and their amplitudes, one can obtain information about the number of particles and the volume of each individual particle (independent of particle shape). → number of pulses – number of particles, pulse amplitude – proportional to the particle volume:

Ningde Amperex Tech. Exhibit No. 2043
Zhuhai CosMX Battery Co. Ltd. v. Ningde Amperex Tech.
IPR2025-00432, U.S. Patent No. 11,575,148
Page 25 of 123

$$U \propto \frac{V\sigma I}{R^4},$$

(U is the amplitude of the voltage pulse, V the particle volume, σ the electrolyte resistivity, I the aperture current, R the aperture radius). The electrical response is independent of particle shape. The lower size limit (0.4 μm) is determined by the signal-to-noise ratio, the upper size limit (several hundred μm) by the ability to suspend particles uniformly in the beaker (sedimentation). For measurements in a wide range, two or more apertures have to be used and the results overlapped to provide a complete size distribution.

The particle size can be channelized using a pulse height analyzer and a number-weighted particle size distribution is obtained (q_0, Q_0). The advantage of this counting method are that it measures a particle volume (→ equivalent volume diameter D_V), unbiased by particle shape. It counts and sizes with high resolution, sensitivity and reproducibility. The limitations (drawbacks) are that electrically conducting particles (metals) cannot be measured, that an electrolyte solution must be used (i.e. pure organic solvents, e.g. ethanol, cannot be used). Orifice blocking by large particles may lead to information loss concerning small particles. Errors are to be expected when the particles are porous, since open pores may or may not be filled with electrolyte solution, so that the effectively displaced volume can be considerably smaller than the convex hull of the particle. Although standard measurements can be in a few minutes, reasonable statistics may require long runs (more than 30 min). Stray signals (electronic noise, e.g. from an electron microscope in the same room) can cause high background counts.

8.3 Optical particle counting (single-particle optical sensing)

Optical particle counting (OPC, also called single particle optical sensing - SPOS) is one of the main technologies for environmental monitoring (atmospheric aerosol monitoring, clean room monitoring, clean water control) and industrial quality control (of liquid- or gas-borne particle systems), due to its ability to make in-situ measurements (especially when simple monitors are used). Similar to electrozone sensing and image analysis it is a counting method (in contrast to sedimentation, laser diffraction and DLS, which are ensemble methods), yielding a number-weighted size distribution. Compared to ensemble methods which have relatively low resolution, but a broad dynamical range and high statistical accuracy, OPC is a high-resolution technique, but with relatively narrow dynamical range and low statistical accuracy. It is ideally suited to detect unwanted single particles with a size lying outside specified limits, but the shape of the size distribution is not very reliable.

Measuring principle: Light scattering technique (for small particles down to approx. 50 nm, mainly air-borne powders and aerosols) or light extinction technique (for large particle from approx. 0.5 μm to more than 1 mm, mainly liquid-borne particles); the scattered intensity is dependent on the sixth power of size for small particles (Rayleigh regime) and on the second power of size for large or highly absorptive particles (Fraunhofer regime); in the Fraunhofer regime (typically > 1-10 μm, depending on absorption) light extinction OPC (light blockage OPC) measures the projected area diameter. Each time the particle traverses the beam, some part of the beam is blocked (via scattering or absorption by the particle), the light flux detected by the photodetector is reduced and a negative signal pulse is produced (pulse amplitude → particle size).

Instrumental equipment and sample concentration: Light source (e.g. gas or diode laser), sensing zone (e.g. a glass cuvette), collecting optics and photodetector (usually in

Ningde Amperex Tech. Exhibit No. 2043
Zhuhai CosMX Battery Co. Ltd. v. Ningde Amperex Tech.
IPR2025-00432, U.S. Patent No. 11,575,148
Page 26 of 123

forward direction; for scattering OPC sometimes at 90 °); volumetric designs illuminate the whole cross-section (→ absolute frequencies), in-situ designs only a part ("spectrometer design" for the size distribution, "monitor design" only to detect contamination single particles). In OPC often the absolute concentration (counts per unit volume) is of interest → volumetric metering and flow control. The electronic system converts light intensity pulses to electronic pulses, counts the individual pulses and sorts them according to their amplitude into predefined channels (pulse-height analyzer, multichannel analyzer - MCA and / or charge-coupled device - CCD). For OPC measurements the particle concentration must be very low; extremely clean vehicle fluids must be used to prepare the highly dilute suspensions.

Data evaluation and interpretation: Data evaluation is based on matrix inversion schemes (e.g. Phillips-Twomey regularization), but do not require complicated mathematical models like laser diffraction. OPC intruments need calibration with particles of the same optical properties (otherwise the results are only "optically equivalent diameters", which are not comparable even for spherical particles); if propertly calibrated, good correlation of OPC and EZS results can be expected. For non-spherical particles the size measured closely approaches the volume-equivalent diameter when the particle size is smaller than the light wavelength and the projected area diameter in the Fraunhofer regime. In general, the results depend on particle size, shape and orientation, as well as light wavelength, flow rate and relative refractive index.

Ningde Amperex Tech. Exhibit No. 2043
Zhuhai CosMX Battery Co. Ltd. v. Ningde Amperex Tech.
IPR2025-00432, U.S. Patent No. 11,575,148
Page 27 of 123

CPPS–9. Image analysis I – Free particles, quantitative size and shape determination

9.0 Introduction

The aim of image analysis is the reduction of the complex visual information contained in images to easily interpretable quantitative information in the form of simple graphs (e.g. size distributions) or even a few numbers (e.g. average or mean values). Thus, inevitably, some information is lost, and the user must ensure that the essential information is extracted.

Projection is the basic technique to obtain size and shape information for particles and particle systems via microscopic image analysis. Thus, in the case of anisometric particles (disks / platelets or needles / fibers) it has to be taken into account that the orientation during measurement is usually not random, unless special methods of sample preparation are used. Therefore, for example, the thickness (height) of platelets is usually not accessible via image analysis. Apart from this, sample preparation has to ensure that agglomeration of particles is avoided as far as possible (difficult mainly for fibers and nanoparticles).

Since the resolution limit of optical microscopy (light microscopy) is of order 1 μm, particles of such a size and smaller should be characterized by SEM (down to approx. 10 nm), TEM (down to approx. 1 nm) or scanning probe microscopes (scanning tunneling microscope – STM, atomic force microscope – AFM). Due to diffraction fringes occurring for small particles, only dimensions larger than a few μm can be reliably measured by optical microscopy.

Image analysis is traditionally performed with static micrographs, although dynamic real-time or even in-line measurement systems are available today. Image analysis can be done manually (by selecting and marking each object "by hand", i.e. via the user interface, e.g. the computer) or automatically. Automatic image analysis generally requires much higher image quality (e.g. contrast) and usually also image processing (i.e. digital image modification to obtain a binary image according to the operator's specifications) prior to image analysis proper. Automatic image analysis (and the image processing steps required) is useful for routine measurements (mainly in industry), but is beyond the scope of this course.

9.1 Basic size and shape measures

- Caliper diameter (Feret diameter): Normal distance between two parallel tangent planes touching the particle surface (in 3D) or two parallel tangents touching the particle outline (in 2D); these values are dependent on particle orientation, therefore a single measurement has little significance → either measurements in all directions (for one single particle) or measurement of a sufficient number of particles in random orientation (if all particles are of the same size and shape) or measurement of two mutually perpendicular normal values for each particle such that the area of the rectangle enclosing the particle outline becomes a minimum (determined by the "minimum Feret diameter" $D_F^{\min}$ and the dimension perpendicular to it, the so-called "maximum Feret diameter" $D_F^{\max}$) → aspect ratio R for each particle (or aspect ratio distribution for an ensemble of particles),

Ningde Amperex Tech. Exhibit No. 2043
Zhuhai CosMX Battery Co. Ltd. v. Ningde Amperex Tech.
IPR2025-00432, U.S. Patent No. 11,575,148
Page 28 of 123

$$R = \frac{D_F^{\max}}{D_F^{\min}} .$$

(Sometimes the inverse definition is used, and many other shape factors have been defined in the literature – generally the definition has to be given in each context.)

For a completely convex particle outline in 2D the average Feret diameter $\langle D_F \rangle$ (averaged over all directions) is related to the particle perimeter P via the relation

$$\langle D_F \rangle = \frac{P}{\pi} .$$

The caliper or Feret diameters can be considered as 1D projections of 2D particle outlines onto a line, i.e. the average Feret diameter corresponds to an "average projection" (ensemble average for a system of randomly oriented particles). Note, however, that the errors in determining perimeters from digitalized pixel images are usually large and therefore D_F thus calculated is usually not very reliable, especially for small particles (for alternative methods to measure the perimeter by image analysis → see our course "Microstructure and properties of porous materials" (ICT Prague).

- Chord length (intercept length): Secant length inside the particle (dependent on direction and position); the mean chord length (in 2D or 3D) of a single particle (or identical particles in random orientation and position) is principally defined as the average of "all" (in practice, many) parallel chord lengths in a single direction, averaged over "all" (in practice, a few) directions. It is related in 2D to the area-to-perimeter ratio via the relation

$$\langle D_C \rangle = \pi \frac{A}{P}$$

and in 3D to the volume-to-surface ratio via the relation

$$\langle D_C \rangle = 4 \frac{V}{S} .$$

These relations are valid for each single particle as well as for systems of particles (interpreted as ensemble averages).

- Projected area diameter: Equivalent diameter D_P of a circle with the same area as the 2D projection of the particle (projected area A_P):

$$D_P = \sqrt{\frac{4\, A_P}{\pi}} .$$

The projected area can be considered as a 2D projection of a 3D particle and in the case of completely convex particles its average value is related to the particle surface S via the Cauchy relation (Cauchy's stereological theorem, 1840):

Ningde Amperex Tech. Exhibit No. 2043
Zhuhai CosMX Battery Co. Ltd. v. Ningde Amperex Tech.
IPR2025-00432, U.S. Patent No. 11,575,148
Page 29 of 123

$$\langle A_P \rangle = \frac{S}{4}$$

(ensemble average for a system of randomly oriented particles). In contrast to perimeters the measurement of areas from digitalized pixel images gives quite reliable results.

Three types of shape factors are commonly used:

- Aspect ratio (axial ratio, Heywood's elongation ratio, 1946): Ratio of maximum to minimum Feret diameter or vice versa, i.e.

$$Aspect\ ratio = \frac{maximum\ Feret\ diameter}{minimum\ Feret\ diameter}$$

(values from 1 to ∞ or from 0 to 1, depending on the definition variant); a measure of elongation or flattening (anisometry) of the convex hull of particles; note, however, that only for prolate spheroids (rods) the aspect ratio determined via image analysis in 2D is (close to) the true 3D aspect ratio.

- Circularity (roundness): Ratio of the perimeter squared to the projected area times 4π, i.e.

$$Circularity = \frac{P^2}{4\pi A_P}$$

(values $\geq$ 1, i.e. = 1 for circles and > 1 for non-circles); a combined measure of irregularity (anisometry and non-smoothness) for convex and non-convex particles; an analogous shape factor in 3D in Waddell's sphericity factor (Waddell 1932), defined as

$$Sphericity = \frac{surface\ area\ of\ \ sphere\ of\ \ same\ volume}{surface\ area\ of\ \ particle},$$

which is simply the squared ratio of the volume-equivalent and surface-equivalent diameter, i.e. $(D_V / D_S)^2$.

- Concavity (non-convexity): Ratio of the diameter of the smallest circumscribed circle (sphere) to the diameter of the largest inscribed circle (sphere) centered in the center-of-mass of the particle, i.e.

$$Concavity = \frac{diameter\ of\ \ circumscribed\ circle\ (sphere)}{diameter\ of\ \ inscribed\ circle\ (sphere)}$$

(values from ∞ for star-like objects to 1 for circles); only useful for isometric particles.

Ningde Amperex Tech. Exhibit No. 2043
Zhuhai CosMX Battery Co. Ltd. v. Ningde Amperex Tech.
IPR2025-00432, U.S. Patent No. 11,575,148
Page 30 of 123

CPPS–10. Image analysis II – Grains in polycrystalline materials, stereology

10.0 Introduction

Sectioning is the basic technique to obtain 2D images from which information on 3D microstructures can be extracted. Planar sections (polished sections) are the simplest and most typical type of probe available to investigate the microstructure of polycrystalline materials. Other probes, which are beyond the scope of this course, are thin sections and so-called disector probes and finally tomographic sectioning techniques. These are treated in our course "Microstructure and properties of porous materials" at the ICT Prague. Stereology can be considered as a subdiscipline of stochastic geometry and aims at obtaining information on the 3D microstructure from 2D cuts (planar sections). Classical stereology is based on the assumption that there exist mean values characterizing the microstructure of the material, which are invariant under affine transformations (i.e. non-distorting translations and rotations). Therefore, unless stated otherwise, we assume that the microstructure of the material under investigation is isotropic, uniform and random (IUR assumption). More general cases are treated in our course "Microstructure and properties of porous materials".

10.1 Stereological terminology and the Delesse-Rosiwal law

The basic symbols used in stereology and their corresponding physical dimensions (units) are

- P = number of points (e.g. pixels or intersection points in a measuring grid)
- N = number of objects (e.g. grains or pores)
- L = line or curve length (of a probe or a feature !) [m]
- A = area of microstructural features in a planar section (always plane) [m^2]
- S = surface or interface area of features in 3D space (generally curved) [m^2]
- V = volume of microstructural features in 3D space [m^3]
- M = curvature (integral mean curvature) [m].

Note that N makes sense only when individual objects can be distinguished. This is not the case for a bicontinuous microstructure, for example. All other quantities are applicable to arbitrary microstructures, if the microstructural features of interest are clearly distinguishable (phases or grains). It is common practice in stereology to write ratios as indexed quantities instead of fractions. Hence, we have the following shorthand notation for stereological ratios:

- P_P = point fraction = number of points hitting the feature (phase or grain) of interest divided by the total number of points placed on the image,
- L_L = line fraction = cumulative length of lines hitting the feature (phase or grain) of interest divided by the total length of lines placed on the image,
- A_A = area fraction = cumulative area of a feature (phase or grain) divided by the total area of the measured image,
- V_V = volume fraction of a microstructural feature in 3D space (when the feature of interest are pores, i.e. the void phase, $V_V = \phi$ is the porosity).

Ningde Amperex Tech. Exhibit No. 2043
Zhuhai CosMX Battery Co. Ltd. v. Ningde Amperex Tech.
IPR2025-00432, U.S. Patent No. 11,575,148
Page 31 of 123

In general, microstructures can be anisotropic (e.g. transversally isotropic composites) and non-uniform (e.g. gradient materials). In order to obtain a reliable and correct quantitative description of arbitrary microstructures in 3D, the sampling procedure must ensure that the probes intersect the microstructure isotropically, uniformly and randomly (IUR requirement on the probes). That means, probing should take all orientations and positions into equal account and sampling should not be influenced by microstructural systematicity (e.g. periodicity). On the other hand, if the microstructure itself is isotropic, uniform and random (IUR microstructures), then any probe is as good as any other. Of course, in both cases statistical accuracy requires additionally a sufficient number of measurements (and measured "events"). The most fundamental stereological relationship is the Delesse-Rosiwal law,

$$V_V = A_A = L_L = P_P .$$

That means, the volume fraction of a phase can be determined by measuring the area fraction of that phase on a planar section or, equivalently, by using a superimposed line grid or point grid to measure the cumulative line length or the number of points hitting the phase, respectively. As mentioned before, in the case of arbitrary microstructures, probing (sampling) must satisfy the IUR requirement, while for IUR microstructures, one planar section is in principle sufficient if only the number of measured "events" (hits) is large enough to make the ratio accurate from the viewpoint of statistics. Note that, for reasons of simplicity, we omit angular brackets with stereological quantities, but with the implicit understanding that stereological theorems have to be interpreted as "expected value theorems" and the corresponding microstructural quantities as "estimators" → more details see our course "Microstructure and properties of porous materials".

Other fundamental ratios used in stereology are

- P_L = number of intersection points with feature lines or curves (e.g. grain section perimeters) per unit length of a probe line (e.g. a line in a superimposed grid) [m^{-1}],
- N_L = number of objects per unit length of a probe line [m^{-1}],
- N_A = number of objects per unit area of a planar section [m^{-2}],
- N_V = number of objects per unit volume in 3D space [m^{-3}],
- L_A = cumulative length of feature lines or curves (e.g. grain section perimeters) per unit area in a planar section [m^{-1}],
- L_V = cumulative length of feature lines or curves per unit volume in 3D space [m^{-2}], sometimes misleadingly called "specific line length" (should be: "line length density" or shortly "line density"),
- S_V = cumulative surface or interface area of features per unit volume in 3D space [m^{-1}], sometimes misleadingly called "specific surface area" (should be: "surface area density" or shortly "surface density")
- M_V = curvature density (intergral mean curvature per unit volume) [m^{-2}].

Note that the topological characteristics N_V (number density) and C_V (connectivity density, not treated here), provide basic information on arbitrary 3D microstructures, irrespective of the objects being convex or even well-defined inclusions or not → Euler characteristic, measures of curvature (see our course "Microstructure and Properties of Porous Materials")

Ningde Amperex Tech. Exhibit No. 2043
Zhuhai CosMX Battery Co. Ltd. v. Ningde Amperex Tech.
IPR2025-00432, U.S. Patent No. 11,575,148
Page 32 of 123

10.2 Basic stereological relations

Usually the quantities "per unit volume" (i.e. N_V, L_V, S_V, M_V) cannot be directly measured directly (except for N_V, when the disector probe is used → see our course "Microstructure and properties of porous materials") and it is one of the main tasks of stereology to determine them indirectly via the other, directly measureable, quantities (P_L, N_A, L_A).

This is done using the following stereological relations:

- Surface area density (from line intercept count or length per area): $S_V = 2P_L = \frac{4}{\pi} L_A$,
- Line length density (from the area object or point count): $L_V = 2N_A = 2P_A$,
- Curvature density (from the area tangent count): $M_V = \pi T_A$.

The following averages can be defined for all microstructural features:

- Mean intercept length in 3D [m]: $\langle D_C \rangle = \frac{4V_V}{S_V}$ (in 2D: $\frac{\pi \cdot mean\ projected\ area}{mean\ perimeter}$)
- Mean cross section [m^2]: $\langle A \rangle = \frac{A_A}{N_A} = \frac{2\pi V_V}{M_V}$
- Mean surface curvature (average curvature of the whole surface) [m^{-1}]: $\langle H \rangle = \frac{M_V}{S_V}$.

If the microstructural features are individual objects (i.e. the microstructure is an ensemble of objects), the following averages can be defined additionally:

- Mean volume [m^3]: $\langle V \rangle = V_V / N_V$
- Mean surface [m^2]: $\langle S \rangle = S_V / N_V$
- Mean caliper diameter ("mean height", defined only for convex bodies but of otherwise arbitrary shape) [m]: $\langle D \rangle = \frac{N_A}{N_V} = \frac{M_V}{2\pi N_V}$
- Mean chord length [m]: $\langle Y \rangle = L_L / N_L$

The number of objects per unit volume can be either measured directly from transparent slices (via the so-called disector count, which is a 3D equivalent of the 2D area tangent count used to determine the curvature density) or determined from the mean diameter (if known)

$$N_V = \frac{N_A}{\langle D \rangle} = \frac{2\pi M_V}{\langle D \rangle}.$$

In most cases, however, the size distribution (and thus the mean diameter) is not known a priori, and the inverse problem must be solved (so-called "unfolding" of size distributions).

Ningde Amperex Tech. Exhibit No. 2043
Zhuhai CosMX Battery Co. Ltd. v. Ningde Amperex Tech.
IPR2025-00432, U.S. Patent No. 11,575,148
Page 33 of 123

10.3 Unfolding size distributions

Without shape assumptions it is not possible to infer the true 3D size (distribution) of (convex) objects (inclusions, e.g. grains or pores, in a matrix) from measurements on 2D plane sections. From the mathematical viewpoint the problem is ill-posed and ill-conditioned, i.e. small statistical variations in the 2D measurements lead to large errors in the 3D results. Even if it is assumed that the shape is the same for all objects (inclusions) and size-invariant, the solution is not trivial.

When the objects (inclusions) are spheres, one could in principle apply a simple graphical unfolding procedure (Lord-Willis procedure, unfolding of linear intercepts), which is based on the fact that the frequency distribution of linear intercepts in a single sphere is a triangular distribution (→ see our course "Microstructure and properties of porous materials"), but the large errors introduced in the small-size fraction devaluates the method in practice.

An alternative method is based on the simultaneous solution of a system of equations (Saltykov method). In practice the largest diameter observed in the planar section is assumed to be the true maximum sphere diameter and based on this value, the whole size range is subdivided into n size classes (usually up to 10 – 15 classes of bin width δ). Then the n-dimensional vector N_{Ai} (i.e. the N_A values for each size class, corresponding to the measured circle diameters) is transformed into another n-dimensional vector N_{Vj} (i.e. the required N_V values for each size class, corresponding to the desired true sphere diameters) via a quadratic matrix (Saltykov-matrix, see below). Using the Einstein summation convention, this Saltykov-transformation can be written briefly as

$$N_{Vj} = \left(\frac{1}{\delta}\right) \alpha_{ij} \cdot N_{Ai} .$$

Similar transformation matrices are available for other isometric shapes as well (e.g. polyhedra and cylinders), but it has to be emphasized that the results are only reasonable when the assumption of a unique, size-invariant shape is at least approximately fulfilled. In the case of rotational ellipsoids (spheroids), which can be useful model shapes for all kinds of anisometric inclusions a generalized version of the Saltykov transformation is available (DeHoff-transformation),

$$N_{Vj} = \left(\frac{K(R)}{\delta}\right) \alpha_{ij} \cdot N_{Ai} ,$$

where K is a function of the aspect ratio (axial ratio) R (here defined to be always < 1; the values of $K(R)$ are > 1 for prolate and < 1 for oblate spheroids). In order to decide from a 2D planar section whether the shape is prolate or oblate, one considers the most isometric (equiaxed) sections. If their diameter corresponds to the length of the anisometric sections, the inclusions (e.g. grains or pores) are oblate, otherwise prolate. It is in principle thinkable to extend this matrix unfolding approach to convex features that do not all have the same shape (using a fourth-order transformation matrix). Statistical errors, however, devaluate this idea in practice.

Ningde Amperex Tech. Exhibit No. 2043
Zhuhai CosMX Battery Co. Ltd. v. Ningde Amperex Tech.
IPR2025-00432, U.S. Patent No. 11,575,148
Page 34 of 123

	$N_A(1)$	$N_A(2)$	$N_A(3)$	$N_A(4)$	$N_A(5)$	$N_A(6)$	$N_A(7)$	$N_A(8)$	$N_A(9)$	$N_A(10)$	$N_A(11)$	$N_A(12)$	$N_A(13)$	$N_A(14)$	$N_A(15)$
$N_A(1)$	0.1857	−0.0750	−0.0261	−0.0132	−0.0080	−0.0054	−0.0039	−0.0028	−0.0022	−0.0016	−0.0013	−0.0009	−0.0007	−0.0004	−0.0001
$N_A(2)$		0.1925	−0.0776	−0.0270	−0.0136	−0.0083	−0.0055	−0.0039	−0.0029	−0.0022	−0.0016	−0.0012	−0.0007	−0.0006	−0.0002
$N_A(3)$			0.2000	−0.0804	−0.0280	−0.0140	−0.0085	−0.0056	−0.0040	−0.0028	−0.0021	−0.0016	−0.0010	−0.0006	−0.0003
$N_A(4)$				0.2085	−0.0836	−0.0290	−0.0146	−0.0088	−0.0057	−0.0041	−0.0028	−0.002	−0.0013	−0.0009	−0.0004
$N_A(5)$					0.2182	−0.0872	−0.0301	−0.0151	−0.0090	−0.0058	−0.0040	−0.0027	−0.0018	−0.0010	−0.0005
$N_A(6)$						0.2294	−0.0913	−0.0319	−0.0155	−0.0091	−0.0059	−0.0038	−0.0026	−0.0015	−0.0006
$N_A(7)$							0.2425	−0.0961	−0.0329	−0.0163	−0.0094	−0.0058	−0.0037	−0.0021	−0.0009
$N_A(8)$								0.2582	−0.1016	−0.0346	−0.0168	−0.0095	−0.0057	−0.0031	−0.0013
$N_A(9)$									0.2773	−0.1081	−0.0366	−0.0174	−0.0093	−0.0051	−0.0020
$N_A10)$										0.3015	−0.1161	−0.0386	−0.0178	−0.0087	−0.0033
$N_A(11)$											0.3333	−0.1260	−0.0408	−0.0171	−0.0061
$N_A(12)$												0.3779	−0.1382	−0.0420	−0.0130
$N_A(13)$													0.4472	−0.1529	−0.0360
$N_A(14)$														0.5774	−0.1547
$N_A(15)$															1.0000

Figure 10.1. *Saltykov matrix.*

Ningde Amperex Tech. Exhibit No. 2043
Zhuhai CosMX Battery Co. Ltd. v. Ningde Amperex Tech.
IPR2025-00432, U.S. Patent No. 11,575,148
Page 35 of 123

CPPS–11. Crystallite size from XRD line profile analysis

11.0 Introduction

The shape and broadening (breadth) of XRD line profiles provides microstructural information, including the average size, size distribution and shape of crystallites in the range 5 – 100 nm (i.e. crystalline nanoparticles and nanocrystalline materials), lattice faulting / twinning and density and spatial arrangement of dislocations. This microstructural information is generally convoluted together and can be grouped into size-broadening and strain- / distortion-broadening contributions. Line profile analysis attempts to extract microstructural information from the observed (recorded) line profiles. This commonly involves the solution of an inverse problem (integral equation), for which questions of existence and uniqueness may arise. Therefore, currently, line profile analysis still is a field of intense research activities. Concomitantly with the progress in nanotechnology and the need for a straightforward routine size and shape analysis in the nanosize range, there are many attempts to develop and select suitable standard materials, and to compare the size distributions and shape information obtained by XRD methods with the results of image analysis using SEM, TEM and possibly, scanning probe microscopes such as the scanning tunneling microscope (STM) and the atomic force microscope (AFM). XRD line profile analysis seems to be a promising tool to be applied in fast and convenient routine measurements (as soon as reliable evaluation procedures are established and the physical interpretation of the results is clarified).

11.1 Scherrer formula and Williamson-Hall plot

When the crystallite size is smaller than approx. 100 nm XRD line profile broadening becomes a measurable effect. The classic relation used for the calculation of crystallite size is the Scherrer formula:

$$D_{Scherrer} = \frac{K\,\lambda}{\beta_{size}\cos\theta},$$

where $D_{Scherrer}$ is the volume-weighted apparent crystallite size, β_{size} the integral breadth of the line profile (XRD peak) caused by small crystallite size, 2θ the diffraction angle, λ the X-ray wavelength (e.g. 0.154 nm for $CuK_{\alpha 1}$ radiation) and K the (shape-dependent) Scherrer constant (e.g. 0.94 for cubic crystallites).

However, apart from generic instrumental broadening, another important cause for broad XRD peaks is strain broadening (distortion broadening caused by dislocations, stacking faults and twins). This broadening is related to the microstrain $\varepsilon = \Delta d/d$ (with d being the interplanar distance between *(hkl)* planes) via the relation

$$\beta_{\varepsilon} = 4\varepsilon\tan\theta\,.$$

Due to the different angular dependence of the two broadening effects, they can in principle be distinguished. Traditionally this is done using the Williamson-Hall plot, based on the relation

Ningde Amperex Tech. Exhibit No. 2043
Zhuhai CosMX Battery Co. Ltd. v. Ningde Amperex Tech.
IPR2025-00432, U.S. Patent No. 11,575,148
Page 36 of 123

$$\beta^* = \frac{\beta \cos\theta}{\lambda} = \frac{K}{D} + \frac{4\varepsilon}{\lambda}\sin\theta ,$$

where β is the observed integral breadth. When β^* values are plotted against $\sin\theta$ and fitted by linear regression, a line is obtained with a slope proportional to microdeformations and an intercept (extrapolated to θ = 0°) inversely proportional to the crystallite size $D_{Scherrer}$.

11.2 Theory of nanocrystallite size broadening of X-ray line profiles

Constructive (i.e. non-destructive) interference of the scattered (diffracted) X-ray beam in a crystal occurs only when the Bragg condition is met:

$$\vec{s}_f - \vec{s}_i = \vec{g} ,$$

where the wave vectors $\vec{s}_f$ and $\vec{s}_i$ refer to the diffracted and incident wave, respectively (with $|\vec{s}_f| = |\vec{s}_i| = 1/\lambda$, where λ is the X-ray wavelength), and $\vec{g}$ is the diffraction vector with $|\vec{g}| = 1/d$ and d being the interplanar spacing (interatomic spacing for a set of (hkl) planes). Taking into account the angle between $\vec{s}_f$ and $\vec{s}_i$ the Bragg condition can be written as

$$2d \sin\theta_0 = \lambda$$

where $2\theta_0$ is the Bragg angle. The resulting diffraction spot (in reciprocal space) is and intensity distribution (in 3D) which is infinitesimally narrow and of infinite intensity. Diffraction of monochromatic X-rays from an ideal crystal of infinite size ($D \to \infty$):

$$I(s) = A\delta(s),$$

where $\delta(...)$ denotes the Dirac delta distribution; this relation follows from

$$I(s) \approx A\left(\frac{\sin(2\pi Ds)}{2\pi ds}\right)^2 ,$$

where the reciprocal space unit is defined as:

$$s = \frac{2}{\lambda}(\sin\theta - \sin\theta_0).$$

For spherical crystallites with finite size (diameter D < 100 nm) the size-broadened line profile (Fourier transformation of the crystallite) is

$$I(s,D) = \int_{-\tau}^{+\tau} V(t,D)\cos 2\pi st \, dt ,$$

Ningde Amperex Tech. Exhibit No. 2043
Zhuhai CosMX Battery Co. Ltd. v. Ningde Amperex Tech.
IPR2025-00432, U.S. Patent No. 11,575,148
Page 37 of 123

where t defines the displacement of a crystallite shifted parallel to the diffraction vector, $V(t,D)$ is the so-called common-volume or "ghost" function of the crystallite and the dimension τ defines the maximum thickness of the crystallite parallel to the diffraction vector $\vec{g}$ (for anisometric crystallites a function of the crystallite size D in the respective direction; thus, principally, shape information can be extracted from considering the line profile differences at different angles). The diffraction spots and line profiles are Fourier transforms of the crystallites (as a direct consequence of the far-field approximation). Therefore small crystallites correspond to broad diffraction spots (line profiles). The Fourier coefficients $A(t)$ are

$$A(t) = \frac{V(t,0)}{V(0)},$$

where $V(0)$ is the volume of the crystallite. Based on these Fourier coefficients, an area-weighted average crystallite size can be defined as

$$\langle t_A \rangle^{-1} = \left. \frac{d\,A(t)}{d\,t} \right|_{t=0}.$$

Alternatively, the integral breadth β (a direct consequence of the additivity of I) can be defined in reciprocal space units as

$$\beta = \frac{1}{I_{mex}} \int_{-\infty}^{+\infty} I(s,D)\,ds = \left[2\int_0^{\tau} A(t)\,dt \right]^{-1},$$

and, based on this integral breadth, another size measure, the volume-weighted average size can be defined as

$$\langle t_V \rangle = \beta^{-1}.$$

Both $\langle t_A \rangle$ (column length) and $\langle t_V \rangle$ (domain size) correspond to the apparent size (thickness) of the crystallite in the direction of the diffraction vector $\vec{g}$. A shape assumption is required to interpret them in terms of physical crystallite dimensions. This generally requires determining the Scherrer constant in order to relate them to the actual thickness τ of the crystallite, parallel to $\vec{g}$. Given a diffraction pattern consisting only of size-broadened line profiles, each *(hkl)* defines the thickness of the crystallite in a particular direction. Using this information, an average crystallite shape can be obtained.

In a nanocrystalline material with crystallites of the same shape, but with a distribution of sizes $P(D)$, the size broadening, $f(s)$, consists of a superposition of line profiles, $I(s,D)$, weighted by $P(D)$, i.e.

$$f(s) = \int_0^{\infty} I(s,D)\,P(D)\,dD.$$

Ningde Amperex Tech. Exhibit No. 2043
Zhuhai CosMX Battery Co. Ltd. v. Ningde Amperex Tech.
IPR2025-00432, U.S. Patent No. 11,575,148
Page 38 of 123

The modified common-volume function now involves the contribution of crystallites in the size range between D and $D + dD$, i.e.

$$\widetilde{V}(t) = \int_t^\infty V(t, D)\, P(D)\, dD,$$

and the Fourier coefficients are given as

$$A(t) = \frac{\widetilde{V}(t)}{\widetilde{V}(0)}.$$

The difficulty in determining $P(D)$ from the observed line profile, $g(s)$, is that there are other contribution to line broadening which must be removed (instrumental broadening, background and noise).

The area- and volume-weighted average sizes (apparent theicknesses) can be related to a spherical nanocrystallite model → area- and volume-weighted average diameters:

$$D_A = \frac{3}{2}\langle t_A \rangle,$$

$$D_V = \frac{4}{3}\langle t_V \rangle.$$

The ratio of the two average sizes also gives a qualitative indication as to the presence of a crystallite diameter distribution: if $\langle t_A \rangle / \langle t_V \rangle = D_A / D_V = 8/9 \approx 0.89$ for spherical crystallites, then the size distribution is a Dirac delta-distribution about D_0, i.e. all crystallites gave the same size. Other values of this ratio are indicative of a size distribution with finite breadth. When a log-normal size distribution is assumed for spherical crystallites, i.e.

$$P(D) = \frac{1}{\sqrt{2\pi\, D^2 \ln^2 \sigma_0}} \exp\left[-\frac{1}{2}\left(\frac{\ln(D/D_0)}{\ln \sigma_0} \right)^2 \right],$$

D_A and D_V can be related to the median diameter D_0 and the log-normal variance σ_0^2 [Krill & Birringer 1998]. D_V corresponds to the crystallite size determined by the Scherrer formula.

A new method of crystallite size determination, proposed by [Kužel et al. 2004] and usable for thin films (foils), is based on the measurement of the small-angle diffuse scattering of the transmitted wave.

Standard reference materials for XRD line profile analysis:

- NIST SRM 660 a LaB_6 powder for correction of instrumental broadening
- NIST SRM CeO_2 powder (cubic, isometric-spherical) in the size range 10-20 nm with average crystallite diameter 17 nm (in preparation)
- NIST SRM ZnO powder (hexagonal, prismatic-cylindrical) in the size range 40-60 nm (in preparation).

Ningde Amperex Tech. Exhibit No. 2043
Zhuhai CosMX Battery Co. Ltd. v. Ningde Amperex Tech.
IPR2025-00432, U.S. Patent No. 11,575,148
Page 39 of 123

Line-broadening analysis (LBA) is the method to extract crystallite size and inhomogeneous strain (associated with local lattice deformations due to defects) from diffraction data → two main phenomenological approaches related to two different crystallite-size dimensions:

- One based on the integral breadth of the diffraction lines → volume-averaged apparent dimension in the direction normal to the reflecting planes (domain size) D_V [Klug & Alexander 1974],
- One based on the Fourier analysis of the line profile → area-averaged apparent dimension in the direction normal to the reflecting planes (column length) D_A [Bertaut 1949].

The second derivative of the Fourier coefficient is related to the column-length distribution function, while determination of the real crystallite size distribution includes the third Fourier coefficients → large errors and unreliable because of the approximations inherent in size-strain separation approaches. An unbiased determination of crystallite size and strain can be undertaken only if the diffraction lines do not overlap. Otherwise, pattern fitting and decomposition must be made before LBA. In the simplest case line profiles can be considered as a convolution of two types of analytical functions:

- Gauss functions, loosely associated with strain broadening,
- Lorentz functions (Cauchy functions), loosely associated with size broadening.

It is widely accepted that the best analytical fucntion for profile fitting is a convolution of the two, i.e. a Voigt function. Pearson VII and pseudo-Voigt functions were then introduced as satisfactory approximations to the Voigt function, but faster to evaluate → advantage in Rietveld refinement. One of the most frequently used functions for profile fitting is the Thompson-Cox-Hastings pseudo-Voigt function, where the full widths at half maximum (FWHM) of the Gauss and Lorentz components are constrained to be the same and equal to the width of the pseudo-Voigt function itself. Note, however, there is no a priori reason to believe that a simple Voigt function can sucessfully describe all size- and strain-broadening effects. For example, "super-Lorentzian" line profiles (with tails falling off more slowly than the Lorentzian function) can be more adequately modeled by a priori assuming a size distribution, e.g. multimodal or broad log-normal.

The log-normal size distribution for spherical crystallites is characterized by two parameters, the average radius R and the dispersion σ_R^2 or, alternatively, the dimensionless ratio $c = \sigma_R^2 / R^2$:

$$f(r) = \frac{1}{r\sqrt{2\pi \ln(1+c)}} \exp\left[-\frac{\ln^2\left(rR^{-1}\sqrt{1+c}\right)}{2\ln(1+c)}\right].$$

Volume-averaged and area-averaged diameters:

$$D_V = \frac{3R(1+c)^3}{2}$$

$$D_A = \frac{4R(1+c)^2}{3}$$

Ningde Amperex Tech. Exhibit No. 2043
Zhuhai CosMX Battery Co. Ltd. v. Ningde Amperex Tech.
IPR2025-00432, U.S. Patent No. 11,575,148
Page 40 of 123

In principle, the values D_V and D_A can be used to calculate the distribution parameters R and c for the log-normal distribution. However, except for materials with highest symmetry the line profiles commonly overlap and have to be reconstructed (by fitting with simple analytical functions such as the Voigt function or its approximations or by "whole-pattern fitting"), before Fourier analysis of the line profiles can be performed. When a Voigt function is used the following inequality holds between D_V and D_A:

$$\sqrt{2\pi e}\ \mathrm{erfc}\left(\frac{1}{\sqrt{2}}\right) \approx 1.31 \leq \frac{D_V}{D_A} < 2\,.$$

The lower limit of this ratio (which ensures that the column-length distribution function is always positive) constraints the dispersion parameter $c \geq 0.164$, i.e. the Voigt function is not appropriate for very narrow distributions (this lower limit is not necessary for the pseudo-Voigt function, which ensures positivity of D_A automatically). Both the Voigt and the pseudo-Voigt function are inadequate for very broad distributions ($c > 0.4$). Assuming a priori a log-normal size distribution leads to reasonable line profile fits.

Exercise problems

1. For a given XRD pattern determine the crystallite size and microstrain using the Williamson-Hall plot (neglecting instrumental broadening).
2. Calculate the average crystallite radius R and the dispersion parameter c for cubic ceria (CeO_2) when the domain size D_V is 22.2 nm and the column length D_A is 16.8 nm and a log-normal size distribution is assumed (solution: 9.0 nm and 0.181).
3. Calculate the domain size D_V and the column length D_A for cubic ceria (CeO_2) when the crystallite size distribution is log-normal with and average crystallite radius R of 16.8 nm and a dispersion parameter c of 2.82 (solution: 140.8 nm and 32.8 nm).

Ningde Amperex Tech. Exhibit No. 2043
Zhuhai CosMX Battery Co. Ltd. v. Ningde Amperex Tech.
IPR2025-00432, U.S. Patent No. 11,575,148
Page 41 of 123

CPPS–12. Adsorption methods and mercury intrusion

12.0 Introduction

The adsorption of gas molecules in a gaseous medium (or solute molecules in a liquid medium, the solvent) can be used to characterize the surface of porous and / or particulate materials. Also mercury intrusion, which is commonly used to determine porosity and pore-size distributions, can under certain circumstances be used to characterize particle size. Specific surface area measurement by adsorption methods is most frequently based on the BET model (1938), while particle sizing by mercury intrusion is usually based on the so-called Mayer-Stowe theory (1965).

12.1 Principles of adsorption, classification of isotherms, BET method

The specific surface area [m^2/g] of a powder or a porous material can be transformed into surface density [m^2/cm^3] when the helium-pycnometric density [g/cm^3] is known. Since the helium-pycnometric density differs from the true density (e.g. the theoretical X-ray density of crystalline substances) when closed (isolated) pores are present, all these characteristics usually refer only to the open void space accessible from outside.

When a solid surface is exposed to a gaseous atmosphere, gas molecules impinge on the surface and a certain percentage (depending on the partial pressure of the gas) of them sticks to the surface, i.e. is adsorbed. The equilibrium amount a of adsorbed gas in [moles/g], i.e. in moles of adsorbate on 1 g of adsorbent, or in [cm^3 at STP/g], i.e. in volume of adsorbate at standard temperature (0 °C = 273 K) and pressure (1 atm = 101.3 kPa) on 1 g of adsorbent, as a function of relative pressure $x = p/p_0$ (where p_0 is the saturation vapor pressure, e.g. 101.3 kPa for nitrogen at 77 K) at a certain constant temperature, is called an adsorption isotherm. Thus, the adsorption isotherm represents a dynamical equilibrium situation between condensation on and evaporation from the solid surface.

According to the IUPAC classification, pore sizes can be divided into micropores (< 2 nm), mesopores (2-50 nm) and macropores (> 50 nm). In micro- and mesoporous materials the adsorbed gas can attain a liquid-like state (capillary condensation) and thus the amount of gas molecules apparently adsorbed greatly exceeds that needed for monolayer (or even multilayer) adsorption → unrealistically high surface area values.

Six types of adsorption isotherms are commonly distinguished, the most important of which are:

- Type I (Langmuir): for microporous materials; monolayer adsorption, with a nearly horizontal part, from which the amount of absorbate in the monolayer (monolayer capacity) a_m can be read off and the specific micropore volume [cm^3/g] can be estimated as

  $$V_{micro} = a_m \cdot v,$$

  where v is the molar volume of the liquid adsorbate (e.g. 34.6 cm^3/mole for liquid nitrogen at 77 K).

Ningde Amperex Tech. Exhibit No. 2043
Zhuhai CosMX Battery Co. Ltd. v. Ningde Amperex Tech.
IPR2025-00432, U.S. Patent No. 11,575,148
Page 42 of 123

- Type II (Brunauer-Emmett-Teller, BET): for nonporous or macroporous materials; multilayer adsorption, which can be described in the relative pressure range $0.05 < x < 0.3$ via the equation

$$\frac{a}{a_m} = \frac{Cx}{(1-x)(1-x+Cx)},$$

where C is a constant related to the difference between heat of adsorption and heat of condensation. This BET equation can be rewritten in the alternative form

$$\frac{x}{a(1-x)} = \frac{1}{a_m C} + \frac{C-1}{a_m C} \cdot x .$$

When the l.h.s. of this equation is plotted against x and fitted by linear regression, the values of the monolayer capacity a_m and the BET constant C can be determined from the slope s and the intercept i ($a_m = 1/(s+i)$ and $C = 1 + s/i$). As soon as a_m is known, the specific BET surface can be calculated as

$$S_{BET} = a_m \cdot N_A \cdot \sigma ,$$

where N_A is Avogadro's number ($6.023 \cdot 10^{23}$ molecules per mole) and σ the average cross-sectional area of the adsorbate gas molecule (e.g. for nitrogen 0.162 nm^2 per molecule). Note that the S_{BET} value calculated from type II (and IV) isotherms corresponds to a realistic specific surface value only when micropores are absent. High values of the BET constant C (i.e. sharp knees in the isotherm) usually indicate the presence of micropores and devaluate the results. On the other hand, values $C < 2$ result, then the isotherms are of type III or V (i.e. there is no knee in the isotherm) and indicate that the interaction between adsorbate and adsorbent is weak. Also in this case the results have to be discarded.

Specific surface determinations via so-called single-point methods (e.g. using the chromatographic Nelssen-Eggertsen technique, which does not require vacuum equipment) are based on the simplifying assumption that $C \approx \infty$. In other words, the intercept in the BET graph is neglected and a straight line is drawn from the point in question to the origin; the monolayer capacity is then calculated form the slope of this line as $a_m = 1/(s+i) \approx 1/s$. The principle of this technique is that from a gas mixture containing nitrogen and hydrogen or helium, nitrogen is preferentially adsorbed when the dry sample is cooled down by inserting the sample flask into liquid nitrogen. A thermal conductivity detector is used to determine the concentration change (partial pressure change) in the gas mixture and thus the partial pressure of the adsorbate. In practice this technique is used mostly as a comparative technique, i.e. using a reference standard of known specific surface S_{ref}. The sample specific surface S is then calculated from the peak areas (signal responses) of the reference A_{ref} and sample A (with weights W_{ref} and W, respectively) as

$$\frac{S}{S_{ref}} = \frac{(A/W)}{(A_{ref}/W_{ref})} .$$

Ningde Amperex Tech. Exhibit No. 2043
Zhuhai CosMX Battery Co. Ltd. v. Ningde Amperex Tech.
IPR2025-00432, U.S. Patent No. 11,575,148
Page 43 of 123

- Type IV isotherms exhibiting hysteresis are characteristic of mesoporous materials exhibiting capillary condensation at sufficiently high relative pressures (> 0.42) and allow the determination of the specific surface S_{BET} as well as the pore size distribution (of mesopores; note that mercury porosimetry yields the size distribution of macropores). The basic equation for pore size determination is the modified Kelvin equation

$$r = \tau(x) - \frac{2\gamma\, v \cos\theta}{RT \ln x},$$

where r is the (equivalent) pore radius, γ and v the surface tension and the molar volume of the liquid adsorbate (for liquid nitrogen $\gamma = 8.88 \cdot 10^{-3}$ N/m at 77 K) and $\tau(x)$ the equilibrium thickness of the adsorbed film (before capillary condensation or during or after evaporation), for which empirical approximations are available, e.g. when $x > 0.65$ for nitrogen (with τ in nm) the Halsey relation,

$$\tau(x) = 0.354 \cdot \left(\frac{-5}{\ln x}\right)^{\frac{1}{3}},$$

or similar relations. Since during nitrogen adsorption at 77 K nitrogen is perfectly wetting, $\theta = 0°$ and thus $\cos\theta = 1$. By calculating the r values for different relative pressures (usually from the desorption isotherm) yields a pore size distribution. Note that, similar to mercury porosimetry, this pore size determination is based on the idealized model of straight, non-intersecting, cylindrical pores (capillaries) with circular cross-section. That means, for a real system (porous material) the results have to be interpreted in terms of equivalent diameters. Note that the Kelvin equation is valid only as long as the continuum approach is justified, i.e. at best down to radii of approx. 1 nm (i.e. not for micropores).

- Isotherms of type III (for nonporous materials) and type V (for mesoporous materials) may occur when the interaction between adsorbate and adsorbent is weak. They are less common in practice (similar to the stepped type VI isotherm) and no standard evaluation procedures are available to extract microstructural information from them.

12.2 Principles of mercury intrusion and Mayer-Stowe theory

Mercury intrusion porosimetry is based on the Washburn equation,

$$r = \frac{-2\gamma \cos\theta}{p},$$

where γ is the surface tension of mercury (usually conventionally taken as 0.480 N/m, although modern research favors 0.485 N/m as the best values for highly pure mercury at room temperature in vacuum), θ the mercury contact angle at the material surface (usually

Ningde Amperex Tech. Exhibit No. 2043
Zhuhai CosMX Battery Co. Ltd. v. Ningde Amperex Tech.
IPR2025-00432, U.S. Patent No. 11,575,148
Page 44 of 123

taken as 140 °, although it is strongly dependent on the substrate and temperature and varies at least between 120 and 160°) and p the hydrostatic pressure. This equation is derived from the force balance $\pi r^2 \cdot p = 2\pi r \cdot \gamma \cos\theta$ (in words, area times pressure equals perimeter times effective surface tension) and can for practical purposes be written as $r = 735/p$, with r in nm and p in MPa. Since mercury is a non-wetting liquid, high pressures are needed to fill small pores (the higher the pressure the smaller are the pores intruded by mercury). Note that at 0.1 MPa (i.e. approximately atmospheric pressure, since 1 atm = 101.325 kPa) pores larger than 7 μm are already filled, while pressures higher than 100 MPa (approx. 1000 atm) are needed to fill pores (or better pore throats, due to the idealized model of "equivalent" cylindrical pore channels) smaller than 7 nm. For pores (pore throats) larger than 7 μm a low-pressure unit with vacuum has to be used. The volume of mercury pressed into the sample is recorded electrically with a capillary dilatometer and the resulting intrusion curve can be directly converted into a cumulative pore size distribution, from which a frequency distribution can be obtained by derivation.

When powder beds are analyzed by mercury intrusion, the peak at low pressures corresponds to the size (usually in the micrometer range) of the interstitial voids between powder particles and has nothing to do with the internal porosity of the particles itself. According to a simple theory by Mayer and Stowe (1965) the breakthrough pressure p (usually determined from a re-intrusion curve, after the agglomerates have been destroyed by the first intrusion) required to force mercury into the void spaces between regularly or non-regularly packed spheres of diameter D is given by the relation

$$p = \kappa \cdot \frac{\gamma}{D},$$

where γ is the surface tension of mercury (here assumed to be 0.485 N/m) and the (dimensionless) Mayer-Stowe constant κ depends on the mercury contact angle at the particle surface and on the interstitial void space (interparticle porosity). Mayer and Stowe considered regular packings from simple cubic (void fraction 0.48) to close packed (fcc or hcp, void fraction 0.26), for which κ varies in the wide range from approx. 5 to 17 (assuming a contact angle of 130°). For random packing (void fraction approx. 0.36) the κ value is approx. 10. Experimental measurements by Pospěch & Schneider (1989) have indeed confirmed this value as a reasonable estimate e.g. for comparison with "mean particle sizes" ("integral mean size" and mode) determined from image analysis. For comparison with sedimentation data the same authors recommend a κ value lower by approx. 40 % (i.e around 7). However, experimental scatter is generally high (corresponding to κ values of 8-13 for comparison with image analysis and 6-10 for comparison with sedimentation), and thus the average particle size calculated via Mayer-Stowe theory should be considered only as a rough estimate.

12.2 Determination of fractal dimensions

Concepts of fractal geometry, elaborated by Mandelbrot from the late 1960es onwards, have been successfully applied in the study of solid surfaces. Fractal objects are self-similar, i.e. they look similar at all levels of magnification (at least in a certain range of length scales). The degree of roughness (topography) of irregular surfaces can be characterized by the fractal dimension D, which may differ from the Euclidean dimension of the surface $d = 2$. The fractal dimension of an irregularly shaped solid can vary between 2 and 3, depending on

Ningde Amperex Tech. Exhibit No. 2043
Zhuhai CosMX Battery Co. Ltd. v. Ningde Amperex Tech.
IPR2025-00432, U.S. Patent No. 11,575,148
Page 45 of 123

surface roughness and / or porosity, i.e. the surface of such solids can in some sense be "almost volume-filling". By analogy, a fractal curve has $1 < D < 2$, i.e. can almost fill an area. There exist several experimental methods to determine the fractal dimension, e.g. small-angle X-ray scattering (SAXS), small-angle neutron scattering (SANS), adsorption techniques and mercury porosimetry.

Real solids have surface areas which are proportional to r^D, where D is the fractal dimension ranging from 2 (for perfectly flat surfaces) to 3 (for extremely rough surfaces). Well-defined mathematical examples of fractal objects are the 1D Koch curve (with $D = \log 4/\log 3 = 1.26...$), the Koch surface (translated Koch curve) in 2D (with $D = 1 + \log 4/\log 3 = 2.26...$), the 3D Menger sponge (with $D = \log 20/\log 3 = 2.72...$) and the 2D Menger sieve (with $D = \log 8/\log 3 = 1.89...$). Note that the translated Menger sieve in 3D has a fractal dimension of $D = 1 + \log 8/\log 3 = 2.89...$, which is higher than that of the 3D Menger sponge, corresponding to the fact that its solid volume is larger. The Koch surface is an example of a low-*D* surface (very rough, but not volume filling), the Menger sponge of a high-*D* surface (almost volume-filling).

Curves, surfaces and volumes can be measured by isometric, regular 1D, 2D or 3D "yardsticks" (usually hypercubes or hyperspheres) characterized by a linear size r. The "size" of the object $N(r)$ is then characterized by the scaling law of the type

$$N(r) = C\, r^{-D},$$

(power law), letting $r \to 0$, where D is the fractal dimension and C is a constant, which equals $\frac{1}{2}L$, $\frac{1}{\pi}A$ and $\frac{3\pi}{4}V$ in 1D, 2D and 3D, respectively. This relation can be rewritten to define the fractal dimension as

$$D = -\lim_{r \to 0} \frac{\log N(r)}{\log r}.$$

In practice, (specific) surface areas (or surface area densities) are usually measured via the monolayer capacity n, i.e. the number of moles n of adsorbate corresponding to the formation of a monolayer on the adsorbent. Therefore the fractal dimension can in principle be determined by using different (spherical) molecules, according to the relation

$$n \propto r^{-D}.$$

When the adsorbate molecules of a series are not spherical (but geometrically similar), it is more useful to use the effective cross-section σ, i.e.

$$n \propto \sigma^{-D/2}.$$

Fractality of the surface implies a straight line of the $\log n$ - $\log r$ - (or $\log n$ - $\log \sigma$ -) plot in the scale range of self-similarity. In this range the fractal dimension can easily be determined from the slope of the line $\log n = (-D/2)\log \sigma + const$, which relates the number of adsorbate molecules n (in moles) in the adsorbed monolayer to the effective adsorbate cross-section σ (which has to be appropriately estimated).

Ningde Amperex Tech. Exhibit No. 2043
Zhuhai CosMX Battery Co. Ltd. v. Ningde Amperex Tech.
IPR2025-00432, U.S. Patent No. 11,575,148
Page 46 of 123

The aforementioned method uses yardsticks of different size. For powders and powder compacts consisting of differently sized particles, a complementary approach can be chosen: the surface area of systems with differently sized particles (each characterized by the mean diameter d) is measured with the same yardstick (adsorbate molecule). In this case the monolayer capacity (and thus the measured surface area) has the dependence

$$n \propto S \propto d^{D-3},$$

and the fractal dimension can be determined from $\log S = (D-3)\log d + const$, when d has been independently measured, e.g. by electron microscopy. Methods based on the aforementioned relations are called molecular tiling (Pfeifer-Avnir approach). To apply this methods in practice, the monolayer capacity has to be determined, usually via the BET approach. Other methods are based on a "fractal" Frenkel-Halsey-Hill equation (FHH approach)

$$N \propto -\left[\ln\left(\frac{p}{p_0}\right)\right]^{D-3}$$

or on the Kiselev equation for the adsorbate–vapor interfacial area S_{LV} in the region of capillary condensation (thermodynamic or Neimark-Kiselev approach),

$$S_{LV} = -\frac{RT}{\gamma}\int_{N}^{N_{\max}} \ln\left(\frac{p}{p_0}\right) dN .$$

Based on this equation the surface area of the adsorbed film can be interpreted as that of the adsorbent that would be measured by spheres with radius r_m, i.e. for a fractal surface we have

$$S_{LV} \propto r_m^{\,2-D},$$

and the fractal dimension can be obtained from a plot of $\ln S_{LV}$ versus $\ln r_m$. In principle a similar method can be applied to the intrusion (and extrusion) of non-wetting fluids. The pore size distribution measured by mercury porosimetry can be written as

$$-\frac{dV(r)}{dr} = \frac{p}{r}\left(\frac{dV(p)}{dp}\right) \propto r^{2-D},$$

or equivalently, using the inverse proportionality $r \propto -1/p$ (Washburn equation),

$$-\frac{dV(p)}{dp} \propto p^{D-4} .$$

Hence, the fractal dimension D can be determined directly from the slope of $\log(dV/dp)$ versus $\log p$.

Ningde Amperex Tech. Exhibit No. 2043
Zhuhai CosMX Battery Co. Ltd. v. Ningde Amperex Tech.
IPR2025-00432, U.S. Patent No. 11,575,148
Page 47 of 123

CPPS–13. Aerosols and nanoparticles

13.0 Introduction

Aerosols, i.e. dispersions of tiny particles (solid particles, liquid drops, or composite particles with a solid core covered by liquid shell) in gaseous media, e.g. ambient air, are of importance in environmental and health science and technology as well as many other fields such as meteoreology, energy technology, powder technology, and materials technology. They include dust, fumes, smoke, fog / mist / clouds, haze and smog. In materials technology aerosols play a major today in connection with gas-phase synthesis and related synthesis routes (e.g. chemical vapor synthesis) of nanopowders. Ubiquitous phenomena connected with aerosols (and with many suspensions) are coagulation, i.e. the formation of larger secondary particles ("soft" or "hard" agglomerates, the latter sometimes called aggregates) from small primary particles, as well as coalescence and sintering. Similar to other colloidal systems, aerosols exhibit interesting and unique optical properties. Nanoparticles have been used in various products for several decades, but the expected increase of production and use of newly developed materials makes the question of their safety to life and the environment increasingly important. However, fundamental knowledge concerning the toxicity of these materials is still missing or controversial.

13.1 Aerosols – Classification

Aerosol – a dispersion of solid particle, liquid drops, or composite particles (solid core with liquid shell) in a gas, usually air → traditional classification of aerosols:

- Dust: Solid particles formed by disintegration processes (e.g. crushing, grinding, drilling), can be classified by screening (sieving),
- Fumes: Solid particles produced by physicochemical reactions (e.g. combustion, sublimation) from metals, typically smaller than 1 μm (too small to be screened),
- Smoke: Solid particles produced by burning (oxidation) of organic matter (e.g. coal, wood, oil), typically smaller than 1 μm, cannot be sized on screens,
- Mist, fog, clouds: Aerosols produced by the disintegration of liquid or the condensation of vapor → spherical liquid droplets, small enough to float in moderate air currents (when > 100 μm → drizzle or rain drops),
- Haze: Solid particles in the atmosphere (in the pre-condensation state of air) with radii < 0.1 μm (Aitken cores / nuclei) grown in the presence of atmospheric moisture; foggy haze = equilibrium state achieved by condensation of moisture on large (0.1 μm < R < 1 μm) and giant (> 1 μm) particles (condensation nuclei) of soluble salts,
- Smog: Combination of smoke and fog, resulting from impurities in the atmosphere (products from photochemical reactions or volcanic activity, smoke from wood fires etc.) and their combination with water vapor, typically smaller than 1 μm.

In atmospheric physics and meteorology the term "atmospheric aerosol" is frequently used synonymously with "atmospheric haze" → subdivided into continental aerosols ("haze M", consisting of insoluble soil components such as quartz or clay minerals or hygroscopic sulfates), sea aerosols ("haze L", consisting of soluble sea salt condensation cores) and high-altitude stratospheric aerosols, including submicron particles in dust layers ("haze H").

Ningde Amperex Tech. Exhibit No. 2043
Zhuhai CosMX Battery Co. Ltd. v. Ningde Amperex Tech.
IPR2025-00432, U.S. Patent No. 11,575,148
Page 48 of 123

13.2 Condensation and evaporation phenomena in aerosols

Early investigations: Coulier 1875, Aitken 1880, Wilson 1897.

Types of nucleation: homogeneous (condensation of vapor on clusters of similar vapor molecules, supercooling is common, for water e.g. down to – 40 °C) – heterogeneous (condensation on nuclei of dissimilar material, e.g. ions or ionic clusters or small solid particles acting as condensation cores / nuclei).

Homogeneous nucleation is a three-step process:

- Vapor must become sufficiently supersaturated
- Small clusters of molecules (embryos) must form
- Vapor must condense on these embryos → nucleus → droplet

In heterogeneous nucleation the second step is omitted (nuclei can be soluble or insoluble).

The theory developed for condensation and evaporation of liquid aerosols can also be applied to the formation of solid aerosols (nanoparticles) by gas-phase reactions.

13.3 Optical properties of aerosols

Extinction: Combination of scattering and absorption. Under the assumptions of quasi-elastic independent, single scattering the extinction of light is given by Bouguer's law (1760), also called Lambert-Beer's law:

$$I = I_0 \exp(-a\,z)\,,$$

where I is the light intensity (or irradiance or luminous flux), z the path from source to receptor and a the extinction coefficient (also called attenuation coefficient or turbidity), which is inversely proportional to the particle size as long as the particle size is large enough for the extinction efficiency factor Q_{ext} to be constant (asymptotically approaching 2 with increasing particle size d). Therefore e.g. small particles produce more haze in the atmosphere than large particles. For visible light, aerosols are most optically active in the 0.1 – 1 µm diameter range where the extinction efficiency is highest. The extinction efficiency factor is defined as the ratio of energy flux extinguished by a single particle to that incident on this particle. For very small particles with even a little bit of absorption $Q_{ext} \approx Q_{abs}$, while for pure scatterers $Q_{ext} = Q_{scat}$ is given by

$$Q_{ext} = Q_{scat} = \frac{8}{3}\alpha^4 \left(\frac{N^2 - 1}{N^2 + 2} \right)^2 ,$$

where

Ningde Amperex Tech. Exhibit No. 2043
Zhuhai CosMX Battery Co. Ltd. v. Ningde Amperex Tech.
IPR2025-00432, U.S. Patent No. 11,575,148
Page 49 of 123

$$\alpha = \frac{\pi D}{\lambda},$$

with D being the particle diameter. For $\alpha << 1$ this special case of light scattering is called Rayleigh scattering (scattering of light by molecules making up the atmosphere; blue light is scattered about 9 times as efficiently as red light $\rightarrow$ blue sky at daytime, red sky during sunrise and sunset). For larger particles the relationship of Q_{ext} on D is more complex, first rising from zero according to the fourth-power relation, then oscillating (mainly for pure scatterers; absorbing particles exhibit essentially no oscillations, only a slight overshoot to values above 2) and finally attaining the asymptotic value of 2. The asymptotic value of 2 implies that a particle can remove light from an area equal to twice its cross-section ("extinction paradox"). In the case of a polydisperse aerosol we have for the extinction coefficient

$$a = \int \frac{\pi}{4} D^2 f(D) Q_{ext} dD$$

and for the particle mass concentration (mass per unit volume)

$$C = \frac{\pi}{6} \rho \int D^3 f(D) dD,$$

where ρ is the particle density (typically 2.4 – 2.7 g/cm^3) and $f(D)dD$ the number of particles per unit volume having diameters between D and $D + dD$, i.e. a probability density function with the normalization condition (total number of particles per unit volume)

$$f = \int f(D) dD.$$

Therefore, in the case of large particles ($Q_{ext} = 2$) the particle mass concentration and the extinction coefficient are related via the surface mean diameter (Sauter mean diameter)

$$C = \frac{\rho}{3} \frac{\int D^3 f(D) dD}{\int D^2 f(D) dD} \gamma = \frac{\rho}{3} D_{Sauter} a.$$

If the polydisperse aerosol can be described by a lognormal size distribution with geometric mean diameter D_G and geometric standard deviation σ_G, then

$$C = \frac{\rho}{3} a \, D_G \exp\left(2.5 \ln^2 \sigma_G\right).$$

Note, however, that the average size of atmospheric aerosol particles can vary markedly, depending on the humidity of air (and thus the moisture content of the particles). For soluble nuclei this can be even more complicated due to the hysteresis effect, which leads to different diameters for rising and falling humidity, especially when the air is moving. Therefore, mass concentration measurements derived from extinction measurement should be considered reliable only for cases where the relative humidity is less than 40 %.

Ningde Amperex Tech. Exhibit No. 2043
Zhuhai CosMX Battery Co. Ltd. v. Ningde Amperex Tech.
IPR2025-00432, U.S. Patent No. 11,575,148
Page 50 of 123

The fundamental optical parameter for aerosols is the refractive index, defined as the ratio of the speed of light in vacuum to the speed of light in the material. When there is appreciable absorption of radiation in the aerosol particle in addition to scattering it is necessary to consider the complex refractive index:

$$N = n' - in'' = n - i\kappa ,$$

where in the case of visible light the real part n is for airborne particles mostly between 1.3 and 1.7 (1.0 for vacuum and air, 1.33 for water, 1.3 for ice, 1.7 for alumina, 2.4 for diamond) and the imaginary part between 0 and 1 (typically of order 0.1). Carbon particles have a complex refractive index of approx. $N(carbon) = 2 - i$.

Note that classical Mie theory (1908) considers ccattering by homogeneous spherical particles [Kerker 1969], but aerosol particles are inhomogeneous, consisting of at least two layers (core + shell) [Babenko et al 2003]. The real and imaginary parts of the complex refractive index of the composite aerosol particles (core particles covered by with water films) can be calculated as follows:

$$\bar{n} = n_w + (n_0 - n_w)(1-\gamma)^{-1} ,$$

$$\bar{\kappa} = \kappa_w + (\kappa_0 - \kappa_w)(1-\gamma)^{-1} ,$$

where

$$\gamma = \frac{\rho_0 m_w}{\rho_w m_0} = \frac{\rho_0}{\rho_w}\bar{\mu}(\varphi)\frac{\varphi}{1-\varphi} ,$$

with φ the relative humidity and $\bar{\mu}(\varphi)$ the coefficient of mass increase due to the water film, which is given in Table 1 [Hanel 1976, Babenko et al. 2003].

φ	$\bar{\mu}(\varphi)$
0.1	0.050
0.2	0.065
0.3	0.080
0.4	0.095
0.5	0.110
0.6	0.127
0.7	0.140
0.8	0.146
0.9	0.150
0.95	0.156
0.975	0.160

Alternative expressions use the knowledge of the size change of aerosol particles in comparison to their dry cores (with D_0 being the dry particle diameter and $D(\varphi)$ the aerosol particle diameter at relative humidity φ, which can be described e.g. via a relation of the type

Ningde Amperex Tech. Exhibit No. 2043
Zhuhai CosMX Battery Co. Ltd. v. Ningde Amperex Tech.
IPR2025-00432, U.S. Patent No. 11,575,148
Page 51 of 123

$$\frac{D(\varphi)}{D_0} = (1-\varphi)^{-\varepsilon},$$

where ε is approx. 0.25 ± 0.08 (0.17 for continental aerosols, 0.33 for sea aerosols) [Kasten 1969, Babenko et al. 2003]. Then we have for the composite density [Hanel 1976]

$$\overline{\rho} = \overline{\rho}(\varphi) = \rho_w + (\rho_0 - \rho_w)(D(\varphi)/D_0)^{-3},$$

and for the real and imaginary part of the complex refractory index, respectively:

$$\overline{n} = \overline{n}(\varphi) = n_w + (n_0 - n_w)(D(\varphi)/D_0)^{-3},$$

$$\overline{\kappa} = \overline{\kappa}(\varphi) = \kappa_w + (\kappa_0 - \kappa_w)(D(\varphi)/D_0)^{-3}.$$

Popular size distribution models for aerosols are the (Junge-type) power distribution,

$$f(R) = a\, R^{-b},$$

the generalized (modified) four-parametric gamma distribution,

$$f(R) = a\, R^{\alpha} \exp(-b\, R^{\beta}),$$

and the lognormal distribution,

$$f(R) = \frac{c}{\sqrt{2\pi} R \ln\sigma} \exp\left[-\frac{1}{2}\left(\frac{\ln(R/R_0)}{\ln\sigma}\right)^2\right],$$

where *a, b, c,* α, β are fit parameters, R_0 is the median radius and $\ln\sigma$ the standard deviation.

13.4 Coagulation phenomena in aerosols and nanoparticle systems

Due to their small size and large specific surface area the short-range surface forces such as electrostatic (Coulombic) or van der Waals forces can overcompensate long-range volume forces such as gravitation and thus aerosol particles in the atmosphere (and similarly suspensions of nanoparticles dispersed in liquids) exhibit a general tendency to intreract with each other and to coagulate.

When the relative motion among particles is caused by Brownian motion (Brownian diffusion), the process is called Brownian coagulation. It is always present, but usually predominates (over other causes of coagulation) only when the particle size is very small (< 10 nm). When the relative motion arises from external forces such as gravity, electrical forces, aerodynamic forces and ultrasound the process is called kinematic coagulation (gravitational, electrostatic, turbulent and sonic coagulation or agglomeration, respectively).

The ultimate goal of coagulation theory is to describe how particle (number) concentrations, particle size (distributions) and coagulation rates change with time. The simplest theory, going back to Smoluchowski [Smoluchowski 1911, 1917], who derived it

Ningde Amperex Tech. Exhibit No. 2043
Zhuhai CosMX Battery Co. Ltd. v. Ningde Amperex Tech.
IPR2025-00432, U.S. Patent No. 11,575,148
Page 52 of 123

originally for coagulation in dilute electrolytes, concerns the Brownian coagulation of a monodisperse aerosol of spherical particles [Whytlaw-Gray & Patterson 1932]. The usual form of the coagulation equation is

$$\frac{dN}{dt} = -2K_B N^2 ,$$

where dN/dt is the change in particle number concentration (N) with time and K_B is the Brownian coagulation coefficient (in the continuum regime),

$$K_B = 2\pi d_P D_B = \frac{2kT}{3\mu} ,$$

(with particle diameter d_P and gas viscosity μ), which is related to the Brownian diffusion coefficient D_B via the Stokes-Einstein relation,

$$D_B = \frac{kT}{3\pi\mu d_P} .$$

Invoking the initial condition that $N = N_0$ at $t = 0$, the solution of the coagulation equation is

$$\frac{N}{N_0} = \frac{1}{1 + 2K_B N_0 t} .$$

Several simplifying assumptions are implict in the Smoluchowski model (particles adhere at every collision, so that only the diffusional flux toward a single central particle acting as a sink has to be considered, and only the first few particle collisions are considered, so that particle size changes so slowly that it can be neglected), but experimental data from both monodisperse and polydisperse aerosols follow this general form of the equation often surprising well. However, the coagulation constant may be appreciably larger due to other than Brownian forces (see below) and due to polydispersivity. Redefining $K = 4\,K_B$ the Smoluchowksi coagulation equation reads

$$\frac{dN}{dt} = -\frac{1}{2} K N^2 .$$

For the coagulation kinetics of polydisperse aerosols no explicit solution exists. However, for an aerosol with discrete size classes a system of differential equations can be set up, taking into account the increase in particles due to combination from smaller particles and the corresponding loss of particles in the smaller size class, i.e.

$$\frac{dN_k}{dt} = \frac{1}{2}\sum_{j=1}^{k-1} K_{j(k=j)} N_j N_{k=j} - \sum_{all\ j} K_{kj} N_k N_j .$$

The total number of particles of all sizes (per unit volume) is equal to the sum of the numbers of particles in the individual size classes (per unit volume) and can be written as

Ningde Amperex Tech. Exhibit No. 2043
Zhuhai CosMX Battery Co. Ltd. v. Ningde Amperex Tech.
IPR2025-00432, U.S. Patent No. 11,575,148
Page 53 of 123

$$N = \sum_{all\ k} N_k \ .$$

Therefore the total change in particle number concentration is

$$\frac{dN}{dt} = -\frac{1}{2} \sum_{all\ k} \sum_{all\ j} K_{kj} N_k N_j \ .$$

Note that no sources or sinks have been assumed for the coagulating particles.

For an aerosol with a continuous size distribution the corresponding population balance is given by the following nonlinear integro-differential equation (thus circumventing the problem of many equations),

$$\frac{dN(v,t)}{dt} = \frac{1}{2} \int_0^v K(\varphi, v-\varphi)\, N(\varphi,t)\, N(v-\varphi,t)\, d\varphi - \int_0^\infty K(\varphi,v)\, N(\varphi,t)\, N(v,t)\, d\varphi ,$$

where v and the integration variable φ denote particle volumes (used rather than diameters, because volumes are additive), $N(v,t)$ is the particle size distribution function at time t and $K(\varphi,v)$ is the so-called collision kernel for two particles of volume φ and v. The collision kernel is dependent on the coagulation mechanism. To determine the total number of particles per unit volume it is necessary to integrate over all particle volumes, i.e.

$$N = N(t) = \int_0^\infty N(v,t)\, dv .$$

Then the change in the total number concentration with time becomes

$$\frac{dN(t)}{dt} = -\frac{1}{2} \int_0^\infty \int_0^\infty K(\varphi,v)\, N(\varphi,t)\, N(v,t)\, dv\, d\varphi .$$

As mentioned above, the collision kernel depends ion the coagulation mechanism. For Brownian coagulation the collision kernel can be derived either by the kinetic theory of gases or by continuum diffusion theory, dependeing on particle size. Particles much smaller than the mean free path λ of the surrounding gas molecules behave like molecules, and the kinetic theory of gases must be used to derive the collision kernel, whereas for particles much larger, the continuum diffusion theory should be used. Generally the Knudsen number

$$\mathrm{Kn} = \frac{\lambda}{r}$$

is used to define the particle size regime: in the free molecule regime (fm) Kn > 50, in the continuum regime (co) Kn < 1. The corresponding collision kernels are

Ningde Amperex Tech. Exhibit No. 2043
Zhuhai CosMX Battery Co. Ltd. v. Ningde Amperex Tech.
IPR2025-00432, U.S. Patent No. 11,575,148
Page 54 of 123

$$K_{fm}(v,\varphi) = K_B^{fm}\left(v^{1/3} + \varphi^{1/3}\right)^2 \cdot \left(\frac{1}{v} + \frac{1}{\varphi}\right)^{1/2},$$

$$K_{co}(v,\varphi) = K_B\left(v^{1/3} + \varphi^{1/3}\right) \cdot \left(\frac{C(v)}{v^{1/3}} + \frac{C(\varphi)}{\varphi^{1/3}}\right),$$

where $K_B^{fm} = (3/4\pi)^{1/6}(6kT/\rho)^{1/2}$ is the Brownian coagulation coefficient form the free molecule regime (with ρ being the particle density) and $C(...) = 1 + \mathrm{Kn}[1.142 + 0.558\exp(-0.999/\mathrm{Kn})]$ is the gas slip correction factor. A correction function $f(\mathrm{Kn}_D)$ for the transition regime (1 < Kn < 50) has been given e.g. by Dahneke [Dahneke 1983]:

$$f(\mathrm{Kn}_D) = \frac{1 + \mathrm{Kn}_D}{1 + 2\,\mathrm{Kn}_D + 2\,\mathrm{Kn}_D^2},$$

where Kn_D is given by the ratio $\mathrm{Kn}_D = K_{co}(v,\varphi)/(2K_{fm}(v,\varphi))$. The corresponding general collision kernel, vaild also in the transition regime is then

$$K_B^{general}(v,\varphi) = K_B\left(v^{1/3} + \varphi^{1/3}\right) \cdot \left(\frac{C(v)}{v^{1/3}} + \frac{C(\varphi)}{\varphi^{1/3}}\right) \cdot f(\mathrm{Kn}_D).$$

The collision kernels of kinematic coagulation mechanisms (gravitational, electrostatic, turbulent and sonic) are more complicated. Depending on the conditions, gravitational coagulation (caused by the fact that the relative motion during gravitational settling caused by differing particle size leads to additional collisions) and electrostatic coagulation (caused by the surface charge of particles, leading to attraction or repulsion) may enhance or decrease the coagulation rate, while turbulences always lead to additional collisions and thus turbulent coagulation (related to the inertia of aerosol particles) can be treated in a manner similar to Brownian coagulation except that the diffusion coefficients are much larger (so-called turbulent or eddy diffusion coefficient). For particles smaller than 10 nm Brownian diffusion usually dominates. Sonic coagulation is not well understood but it is an empirically known fact that under certain circumstances the action of ultrasound can lead to agglomeration.

One of the insteresting features of coagulation is that after sufficiently long time all coagulating aerosols are predicted to attain the same (quasi-) steady-state size distribution, regardless of the aerosol's initial size distribution [Friedlander 1965, Friedlander & Wang 1966, Wand & Friedlander 1967]. When this so-called self-preserving size distribution is reached, gains by coagulation in the number of particles of a certain size class are compensated by losses from that size either by coagulation or by sedimentation (note that the self-preserving particle size distribution is only quasi-steady-state, because without a particle source the system would eventually run out of particles and exhibit a null size distribution function).

Ningde Amperex Tech. Exhibit No. 2043
Zhuhai CosMX Battery Co. Ltd. v. Ningde Amperex Tech.
IPR2025-00432, U.S. Patent No. 11,575,148
Page 55 of 123

13.5 Nanoparticles and their safety aspects

Nanoparticles are in many aspects different from their larger-sized counterparts and the corresponding bulk materials. They are on the same size scale as most elements of living cells, including proteins, nucleic acids, lipids and cell organelles. Thus, nanoparticles (and nanomaterials) can interact with biological systems in an unforseen way. On the one hand, nanosystems may be specifically engineered to interact with biological systems (e.g. for particular medical applications such as drug delivery systems). On the other hand, the production of nanoparticles or their occurrence as a by-product of combustion processes may adversely affect a wide range of organisms throughout the environment. Moreover, as a results of their increased reactivity (due to the large specific surface) aerosols with nanoparticles can be highly explosive, although their larger-size counterparts are not.

The increasing production, mainly of metal oxide nanoparticles (of commerical interest are e.g. SiO_2, TiO_2, Al_2O_3, ZrO_2, ZnO and iron oxides) and new carbon materials such as nanotubes (single-walled – SWNT - and multi-walled - MWNT) and fullerenes (e.g. C_{60}), will enhance the possible exposure at work places. Similarly, the nanoparticles unintentionally produced by combustion processes (e.g. in diesel engines or oil burners), are released into the environment and affect the whole population. Ambient aerosols may typically contain organic and elemental carbon, metals and their oxides as well as chlorides, nitrates and sulfates.

Although man-made nanoparticles have been occurring in the environment at least since the industrial revolution and have been used in various products for several decades, the expected increase of production and use of newly developed materials makes the question of their safety to life and the environment increasingly important. However, although adverse health effects based essentially on the size and shape of particles have been known for a long time from experience with workers in the silicate industry (e.g. silicose from fine quartz dust and clay minerals) as well as in the inorganic fiber industry (e.g. lung cancer from asbestos fibers), fundamental knowledge concerning the toxicity of nanoparticles and nanomaterials is still missing or controversial. Without detailed knowledge of possible adverse effects, nanoparticle exposure should be avoided at work places as well as in the population and the environment. Multiple studies (in vitro and in vivo) are necessary to clarify the biological effects of nanoparticles.

Ningde Amperex Tech. Exhibit No. 2043
Zhuhai CosMX Battery Co. Ltd. v. Ningde Amperex Tech.
IPR2025-00432, U.S. Patent No. 11,575,148
Page 56 of 123

CPPS–14. Suspensions and nanofluids

14.0 Introduction

Suspensions, i.e. dispersions of solid particles in liquid media, are ubiquitous in materials technology and many other technological and non-technological fields, including geosciences, medicine and ecology. In materials technology casting or injection molding of suspensions are popular shaping techniques, e.g. to fabricate ceramics or particulate-, fiber- or platelet-reinforced plastic parts. Suspensions used in materials technology contain particles with a size ranging from submicron (i.e. hundreds of nm) to tens of micrometers, but in principle the particles can be much larger (e.g. in mud streams occuring in geosciences). Nanofluids, on the other hand, are suspensions with nanoparticles, i.e. particles which are smaller than 100 nm in at least one dimension. Due to their small particle size (colloidal range), nanofluids are usually more stable against settling. Their preparation, however, is more involved and agglomeration can be a major problem. The main field of potential application of nanofluids is as heat transfer media. Therefore, apart from rheology, the effective thermal conductivity of nanofluids is of particular interest.

14.1 Suspension rheology

For an introduction to suspension rheology → see Appendix-CPPS-14-A. The key point of suspension rheology is the prediction of the effective viscosity of a suspension based on the knowledge of the volume fraction of particles and, possibly, particle shape. The basic equation of suspension rheology is the Einstein equation for dilute suspensions of rigid spherical particles:

$$\eta_r = 1 + 2.5\,\phi\,,$$

where ϕ is the solids volume fraction and η_r the relative suspension viscosity, defined as

$$\eta_r = \frac{\eta}{\eta_0} = \frac{viscosity\ of\ \ suspension}{viscosity\ of\ \ pure\ liquid}\,.$$

Popular extensions of the Einstein relation to non-dilute systems are:

- Eilers relation: $\eta_r = \left(1 + 1.25\,\phi \cdot \frac{1}{1-\phi_r}\right)^2$
  (contains the Einstein relation in the dilute limit),
- Mooney relation: $\eta_r = \exp\left(C\phi \cdot \frac{1}{1-\phi_r}\right)$
  (reduces to the Einstein relation if C is chosen to be 2.5),

Ningde Amperex Tech. Exhibit No. 2043
Zhuhai CosMX Battery Co. Ltd. v. Ningde Amperex Tech.
IPR2025-00432, U.S. Patent No. 11,575,148
Page 57 of 123

- Krieger relation: $\eta_r = \left(\frac{1}{1-\phi_r} \right)^N$

(reduces to the Einstein relation if N is chosen to be $2.5\,\phi_{\max}$),

where ϕ_r is the reduced volume fraction, defined as

$$\phi_r = \frac{\phi}{\phi_{\max}} = \frac{volume\ \ fraction}{maximum\ volume\ \ fraction}.$$

For anisometric particles the Einstein relation can be generalized to the Jeffery relation,

$$\eta_r = 1 + [\eta]\phi,$$

where the so-called intrinsic viscosity $[\eta]$ is a function of particle shape. This complicated problem has been solved for dilute systems of rotational ellipsoids (i.e. spheroids, prolate and oblate) with Brownian motion by Jeffery (1922) and for non-dilute systems of prolate particles (fibers) with or without Brownian motion by Brenner (1974) → see Appendix-CPPS-14-B. Today, fiber suspension are much better investigated than platelet suspensions. Nevertheless, even for fibers a prediction of suspension viscosity for non-dilute systems is usually extremely difficult, and in practice the Krieger relation is mostly used with $N = 2$ and the maximum volume fraction being linearly dependent on the aspect ratio R, i.e.

$$\phi_{\max} = a - b \cdot R.$$

14.2 Rheology and thermal conductivity of nanofluids

Predictive relations for the effective viscosity of nanofluids are in principle analogous to those for ordinary suspensions → see Appendix-CPPS-14-C. The fact (empirical finding) that the Einstein relation always underestimates the actual viscosity increase with solid volume fraction, can be accounted for either by using a nonlinear relation or, sometimes, by reinterpreting the volume fraction in terms of an "effective", "equivalent", or "apparent" volume fraction. In nanofluids, and to a certain extent in ordinary suspensions as well, the physical interpretation of this apparently enhanced volume fraction may be agglomeration. For nanofluids, additionally, the fluid surface layer on the dispersed nanoparticles, which is known to exhibit structure and properties different from the bulk fluid, may be volumetrically significant. One the most interesting models for practical use is the Chen model [Chen et al. 2007] → see Appendix-CPPS-14-C.

Nanofluids usually exhibit enhanced thermal conductivity in comparison to the base fluid and it is commonly agreed that there is measurable enhancement of thermal conductivity even for very low volume fractions of solids (< 1 %). Principally this enhancement is simply a plausible consequence of the fact that most solids have higher – sometimes considerably higher – thermal conductivity than the base fluid, cf. Table 14-C-1. Popular models for the effective thermal cobnductivity of nanofluids are the Maxwell-Eucken model, the Bruggeman-Landauer model and the Hamilton-Crosser model → see Appendix-CPPS-14-C.

Ningde Amperex Tech. Exhibit No. 2043
Zhuhai CosMX Battery Co. Ltd. v. Ningde Amperex Tech.
IPR2025-00432, U.S. Patent No. 11,575,148
Page 58 of 123

Appendix-CPPS-4

CPPS-4-A. Analytical distribution functions

In unit CPPS-4 we have focused on those parts of statistics which are specific to systems of small particles and therefore usually not included in standard textbooks of general statistics. Therefore we do not give a complete account of analytical functions that can be used to approximate size distributions and to perform statistical data analysis → see standard textbooks of mathematics and statistics. A few popular analytical distribution functions are:

1. Normal distribution (Gauss-Laplace) for $-\infty < x < \infty$

$$f(x) = \frac{1}{\sigma\sqrt{2\pi}} \exp\left[-\frac{1}{2}\left(\frac{x-\bar{x}_A}{\sigma}\right)^2\right]$$

$$F(x) = \frac{1}{\sigma\sqrt{2\pi}} \int_{-\infty}^{x} \exp\left[-\frac{1}{2}\left(\frac{t-\bar{x}_A}{\sigma}\right)^2\right] dt$$

$\bar{x}_A$ = arithmetic mean (= median = mode)
σ = (arithmetic) standard deviation (σ^2 = variance)

The inflection points in the probability density distributions (frequency curves) correspond to $F(x)$ = 15.9 % and $F(x)$ = 84.1 % in the cumulative curve. Using probability paper, the two corresponding x values can be read off and the standard deviation can be calculated directly using the relation

$$\sigma = \frac{x_{84.1} - x_{15.9}}{2}$$

2. Log-normal distribution:

$$f(x) = \frac{1}{\log \sigma_G \sqrt{2\pi}} \exp\left[-\frac{1}{2}\left(\frac{\log x - \log \bar{x}_G}{\log \sigma_G}\right)^2\right]$$

$\bar{x}_G$ = geometric mean
σ_G = (geometric) standard deviation

3. Gaudin-Schumann distribution (Závesky-Špaček, power-law) for $0 \le x \le x_{\max}$:

$$F(x) = \left(\frac{x}{x_{\max}}\right)^n,$$

Ningde Amperex Tech. Exhibit No. 2043
Zhuhai CosMX Battery Co. Ltd. v. Ningde Amperex Tech.
IPR2025-00432, U.S. Patent No. 11,575,148
Page 59 of 123

$$f(x) = \frac{n}{x_{\max}^{n}} \cdot x^{n-1}.$$

The cumulative curve of this distribution does not exhibit inflection points, and the frequency curve does exhibit a maximum (mode). The fit parameters $x_{\max}$ ("theoretical maximum grain size") and n ("grain size exponent") can be determined graphically by linear regression on log-log paper accoding to the relation

$$\log F(x) = n \log x - n \log x_{\max}.$$

(slope = n, intercept at $F(x) = 100\ \%$ gives $x_{\max}$).

4. Weibull distribution (or RRSB – Rosin-Rammler-Sperling-Bennett – distribution, a combination of exponential and power law) for $x > 0$:

$$F(x) = 1 - \exp\left[-\left(\frac{x}{x_W}\right)^{m}\right],$$

$$f(x) = \frac{m}{x_W}\left(\frac{x}{x_W}\right)^{m-1} \exp\left[-\left(\frac{x}{x_W}\right)^{m}\right].$$

The fit parameters (position parameter x_W and Weibull modulus m) can be determined using double-log graphs. This distribution can describe sigmoidal cumulative curves with inflection points.

CPPS-4-B. Comparison of moment notation and moment-ratio notation

Distribution type and mean value	Moment notation	Moment-ratio notation
Number-weighted, geometric		$\overline{D}_{0,0}$
Number-weighted, arithmetic (mean length)	$\overline{x}_{1,0}$	$\overline{D}_{1,0}$
Length-weighted, geometric		$\overline{D}_{1,1}$
Length-weighted, arithmetic	$\overline{x}_{1,1}$	$\overline{D}_{2,1}$
Mean surface	$\overline{x}_{2,0}$	$\overline{D}_{2,0}$
Surface-weighted, arithmetic (Sauter mean)	$\overline{x}_{1,2}$	$\overline{D}_{3,2}$
Mean volume	$\overline{x}_{3,0}$	$\overline{D}_{3,0}$
Volume-weighted, geometric		$\overline{D}_{3,3}$
Volume-weighted, arithmetic (De Brouckere mean)	$\overline{x}_{1,3}$	$\overline{D}_{4,3}$

Ningde Amperex Tech. Exhibit No. 2043
Zhuhai CosMX Battery Co. Ltd. v. Ningde Amperex Tech.
IPR2025-00432, U.S. Patent No. 11,575,148
Page 60 of 123

Appendix-CPPS-7

Meas.No. 300	Date 21.2.2007	Time 10:25	Operator	ID	Serial No. 778

Al2O3, D50 = 1 micron

Measuring Range	0.1 [µm] - 100.9 [µm]	Pump	50 [%]
Resolution	102 Channels (20 mm / 38 mm)		
Absorption	10.00 [%]	Ultrasonic	On
Measurement Duration	100 [Scans]		

Regularization / Modell 5793.601

Fraunhofer Calculation selected.

Mean	Values...						
D43 =	1.23 µm	D42 =	.99 µm	D41 =	.81 µm	D40 =	.67 µm
D32 =	.81 µm	D31 =	.66 µm	D30 =	.55 µm		
D21 =	.54 µm	D20 =	.46 µm				
D10 =	.42 µm						

Statistical Means...			
Arithmetic Mean Diameter	1.226 µm	Variance	.706 µm2
Geometric Mean Diameter	.995 µm	Mean Squre Deviation	.84 µm
Quadratic Square Mean Diameter	1.484 µm	Average Deviation	.631 µm
Harmonic Mean Diameter	.807 µm	Coefficiant of Variation	68.579 %
Statistical Modes...			
Skewness	1.591	Mode	.932 µm
Curtosis	3.307	Median	.992 µm
Span	1.952	Mean/Median Ratio	1.235
Uniformity	.61		
Specific Surface Area	74388.21 cm2/cm3		
Density	1. g/cc		
Form Factor	1. g/cc		

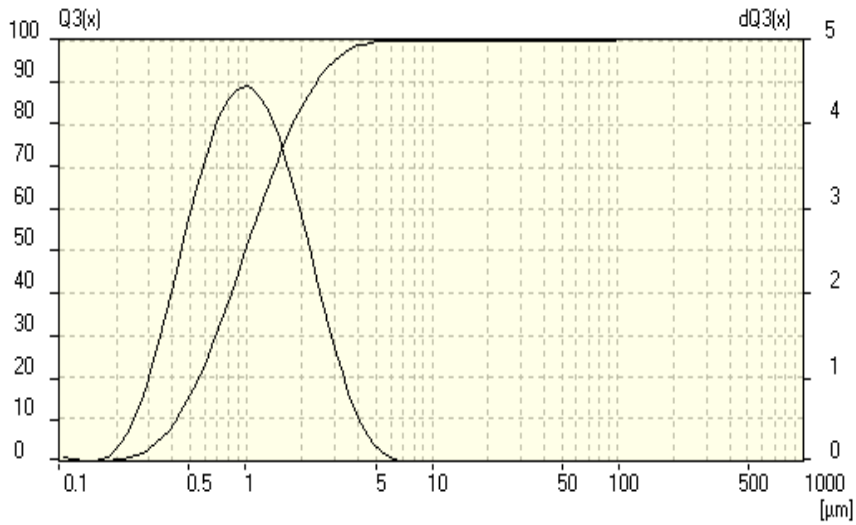

Ningde Amperex Tech. Exhibit No. 2043
Zhuhai CosMX Battery Co. Ltd. v. Ningde Amperex Tech.
IPR2025-00432, U.S. Patent No. 11,575,148
Page 61 of 123

Interpolation Values... C:\Program Files\a22___32\fritsch\equal-size-intervals.FPS

****** %	<=	0.100 µm	0.1 %	<=	0.150 µm	0.3 %	<=	0.200 µm
1.2 %	<=	0.250 µm	2.9 %	<=	0.300 µm	5.4 %	<=	0.350 µm
8.4 %	<=	0.400 µm	12.0 %	<=	0.450 µm	15.7 %	<=	0.500 µm
19.5 %	<=	0.550 µm	23.3 %	<=	0.600 µm	27.1 %	<=	0.650 µm
30.8 %	<=	0.700 µm	34.4 %	<=	0.750 µm	37.8 %	<=	0.800 µm
41.1 %	<=	0.850 µm	44.4 %	<=	0.900 µm	47.5 %	<=	0.950 µm
50.4 %	<=	1.000 µm	53.2 %	<=	1.050 µm	55.8 %	<=	1.100 µm
58.3 %	<=	1.150 µm	60.6 %	<=	1.200 µm	62.8 %	<=	1.250 µm
64.9 %	<=	1.300 µm	67.0 %	<=	1.350 µm	68.8 %	<=	1.400 µm
70.6 %	<=	1.450 µm	72.2 %	<=	1.500 µm	73.9 %	<=	1.550 µm
75.3 %	<=	1.600 µm	76.7 %	<=	1.650 µm	78.1 %	<=	1.700 µm
79.3 %	<=	1.750 µm	80.5 %	<=	1.800 µm	81.7 %	<=	1.850 µm
82.7 %	<=	1.900 µm	83.7 %	<=	1.950 µm	84.7 %	<=	2.000 µm
85.5 %	<=	2.050 µm	86.4 %	<=	2.100 µm	87.2 %	<=	2.150 µm
87.9 %	<=	2.200 µm	88.5 %	<=	2.250 µm	89.2 %	<=	2.300 µm
89.9 %	<=	2.350 µm	90.5 %	<=	2.400 µm	91.1 %	<=	2.450 µm
91.7 %	<=	2.500 µm	92.6 %	<=	2.600 µm	93.5 %	<=	2.700 µm
94.2 %	<=	2.800 µm	95.0 %	<=	2.900 µm	95.5 %	<=	3.000 µm
96.5 %	<=	3.200 µm	97.3 %	<=	3.400 µm	97.7 %	<=	3.500 µm
97.9 %	<=	3.600 µm	98.4 %	<=	3.800 µm	98.8 %	<=	4.000 µm
99.1 %	<=	4.200 µm	99.3 %	<=	4.400 µm	99.4 %	<=	4.500 µm
99.5 %	<=	4.600 µm	99.6 %	<=	4.800 µm	99.7 %	<=	5.000 µm
99.8 %	<=	5.200 µm	99.9 %	<=	5.400 µm	99.9 %	<=	5.500 µm
99.9 %	<=	5.600 µm	99.9 %	<=	5.800 µm	100.0 %	<=	6.000 µm
100.0 %	<=	6.200 µm	100.0 %	<=	6.400 µm	100.0 %	<=	6.500 µm
100.0 %	<=	6.600 µm	100.0 %	<=	6.800 µm	100.0 %	<=	7.000 µm
100.0 %	<=	7.200 µm	100.0 %	<=	7.400 µm	100.0 %	<=	7.500 µm
100.0 %	<=	7.600 µm	100.0 %	<=	7.800 µm	100.0 %	<=	8.000 µm
100.0 %	<=	7.200 µm	100.0 %	<=	7.400 µm	100.0 %	<=	7.500 µm
100.0 %	<=	7.600 µm	100.0 %	<=	7.800 µm	100.0 %	<=	8.000 µm
100.0 %	<=	8.500 µm	100.0 %	<=	9.000 µm	100.0 %	<=	9.500 µm
100.0 %	<=	10.000 µm	100.0 %	<=	12.000 µm	100.0 %	<=	14.000 µm
100.0 %	<=	16.000 µm	100.0 %	<=	18.000 µm	100.0 %	<=	20.000 µm

Interpolation Values... C:\Program Files\a22___32\fritsch\five-percent-steps.FPV

1.0 %	<=	0.244 µm	2.0 %	<=	0.278 µm	5.0 %	<=	0.343 µm
10.0 %	<=	0.423 µm	15.0 %	<=	0.491 µm	20.0 %	<=	0.557 µm
25.0 %	<=	0.623 µm	30.0 %	<=	0.690 µm	35.0 %	<=	0.759 µm
40.0 %	<=	0.832 µm	45.0 %	<=	0.910 µm	50.0 %	<=	0.993 µm
55.0 %	<=	1.085 µm	60.0 %	<=	1.187 µm	65.0 %	<=	1.302 µm
70.0 %	<=	1.433 µm	75.0 %	<=	1.589 µm	80.0 %	<=	1.779 µm
85.0 %	<=	2.019 µm	90.0 %	<=	2.361 µm	95.0 %	<=	2.907 µm
98.0 %	<=	3.619 µm	99.0 %	<=	4.120 µm	100.0 %	<=	10.490 µm

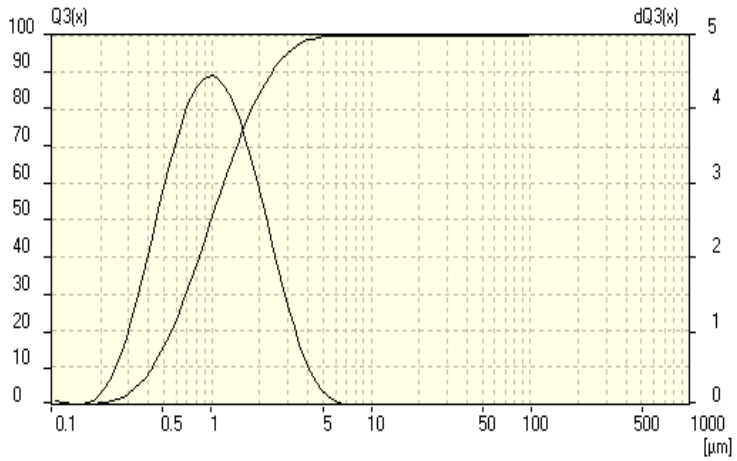

Meas.No. 300	Date 21.2.2007	Time 10:25	Operator	ID	Serial No. 778

Al2O3, D50 = 1 micron

Measuring Range	0.1 [µm] - 100.9 [µm]	Pump	50 [%]
Resolution	102 Channels (20 mm / 38 mm)		
Absorption	10.00 [%]	Ultrasonic	On
Measurement Duration	100 [Scans]		

Regularization / Modell 5793.601

Fraunhofer Calculation selected.

Mean	Values...						
D43 =	1.23 µm	D42 =	.99 µm	D41 =	.81 µm	D40 =	.67 µm
D32 =	.81 µm	D31 =	.66 µm	D30 =	.55 µm		
D21 =	.54 µm	D20 =	.46 µm				
D10 =	.3 µm						

Statistical Means...			
Arithmetic Mean Diameter	.807 µm	Variance	.342 µm2
Geometric Mean Diameter	.658 µm	Mean Squre Deviation	.584 µm
Quadratic Square Mean Diameter	.995 µm	Average Deviation	.415 µm
Harmonic Mean Diameter	.544 µm	Coefficiant of Variation	72.429 %
Statistical Modes...			
Skewness	2.169	Mode	.539 µm
Curtosis	7.093	Median	.634 µm
Span	1.938	Mean/Median Ratio	1.273
Uniformity	.61		
Specific Surface Area	110278.55 cm2/cm3		
Density	1. g/cc		
Form Factor	1. g/cc		

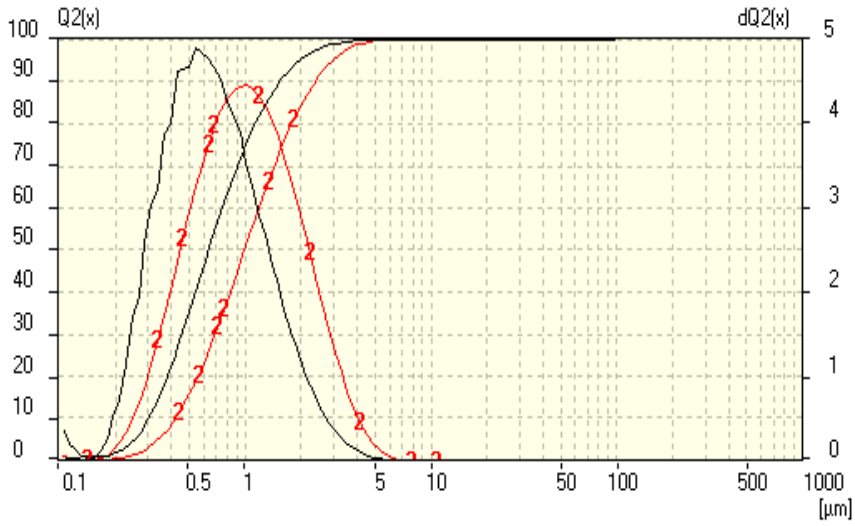

Interpolation Values... C:\Program Files\a22___32\fritsch\equal-size-intervals.FPS

****** %	<=	0.100 µm	0.8 %	<=	0.150 µm	1.6 %	<=	0.200 µm
4.6 %	<=	0.250 µm	9.7 %	<=	0.300 µm	15.8 %	<=	0.350 µm
22.4 %	<=	0.400 µm	29.1 %	<=	0.450 µm	35.4 %	<=	0.500 µm
41.2 %	<=	0.550 µm	46.6 %	<=	0.600 µm	51.5 %	<=	0.650 µm
55.9 %	<=	0.700 µm	59.9 %	<=	0.750 µm	63.5 %	<=	0.800 µm
66.8 %	<=	0.850 µm	69.8 %	<=	0.900 µm	72.4 %	<=	0.950 µm
74.9 %	<=	1.000 µm	77.1 %	<=	1.050 µm	79.0 %	<=	1.100 µm
80.8 %	<=	1.150 µm	82.4 %	<=	1.200 µm	83.9 %	<=	1.250 µm
85.2 %	<=	1.300 µm	86.5 %	<=	1.350 µm	87.5 %	<=	1.400 µm
88.6 %	<=	1.450 µm	89.4 %	<=	1.500 µm	90.3 %	<=	1.550 µm
91.1 %	<=	1.600 µm	91.8 %	<=	1.650 µm	92.4 %	<=	1.700 µm
93.0 %	<=	1.750 µm	93.5 %	<=	1.800 µm	94.0 %	<=	1.850 µm
94.5 %	<=	1.900 µm	94.9 %	<=	1.950 µm	95.3 %	<=	2.000 µm
95.6 %	<=	2.050 µm	96.0 %	<=	2.100 µm	96.3 %	<=	2.150 µm
96.5 %	<=	2.200 µm	96.8 %	<=	2.250 µm	97.0 %	<=	2.300 µm
97.3 %	<=	2.350 µm	97.5 %	<=	2.400 µm	97.7 %	<=	2.450 µm
97.9 %	<=	2.500 µm	98.1 %	<=	2.600 µm	98.4 %	<=	2.700 µm
98.6 %	<=	2.800 µm	98.8 %	<=	2.900 µm	99.0 %	<=	3.000 µm
99.3 %	<=	3.200 µm	99.5 %	<=	3.400 µm	99.5 %	<=	3.500 µm
99.6 %	<=	3.600 µm	99.7 %	<=	3.800 µm	99.8 %	<=	4.000 µm
99.8 %	<=	4.200 µm	99.9 %	<=	4.400 µm	99.9 %	<=	4.500 µm
99.9 %	<=	4.600 µm	99.9 %	<=	4.800 µm	100.0 %	<=	5.000 µm
100.0 %	<=	5.200 µm	100.0 %	<=	5.400 µm	100.0 %	<=	5.500 µm
100.0 %	<=	5.600 µm	100.0 %	<=	5.800 µm	100.0 %	<=	6.000 µm
100.0 %	<=	6.200 µm	100.0 %	<=	6.400 µm	100.0 %	<=	6.500 µm
100.0 %	<=	6.600 µm	100.0 %	<=	6.800 µm	100.0 %	<=	7.000 µm
100.0 %	<=	7.200 µm	100.0 %	<=	7.400 µm	100.0 %	<=	7.500 µm
100.0 %	<=	7.600 µm	100.0 %	<=	7.800 µm	100.0 %	<=	8.000 µm
100.0 %	<=	7.200 µm	100.0 %	<=	7.400 µm	100.0 %	<=	7.500 µm
100.0 %	<=	7.600 µm	100.0 %	<=	7.800 µm	100.0 %	<=	8.000 µm
100.0 %	<=	8.500 µm	100.0 %	<=	9.000 µm	100.0 %	<=	9.500 µm
100.0 %	<=	10.000 µm	100.0 %	<=	12.000 µm	100.0 %	<=	14.000 µm
100.0 %	<=	16.000 µm	100.0 %	<=	18.000 µm	100.0 %	<=	20.000 µm

Interpolation Values... C:\Program Files\a22___32\fritsch\five-percent-steps.FPV

1.0 %	<=	0.179 µm	2.0 %	<=	0.211 µm	5.0 %	<=	0.254 µm
10.0 %	<=	0.303 µm	15.0 %	<=	0.343 µm	20.0 %	<=	0.381 µm
25.0 %	<=	0.420 µm	30.0 %	<=	0.457 µm	35.0 %	<=	0.497 µm
40.0 %	<=	0.539 µm	45.0 %	<=	0.585 µm	50.0 %	<=	0.634 µm
55.0 %	<=	0.690 µm	60.0 %	<=	0.751 µm	65.0 %	<=	0.822 µm
70.0 %	<=	0.904 µm	75.0 %	<=	1.003 µm	80.0 %	<=	1.126 µm
85.0 %	<=	1.292 µm	90.0 %	<=	1.532 µm	95.0 %	<=	1.959 µm
98.0 %	<=	2.549 µm	99.0 %	<=	2.999 µm	100.0 %	<=	8.122 µm

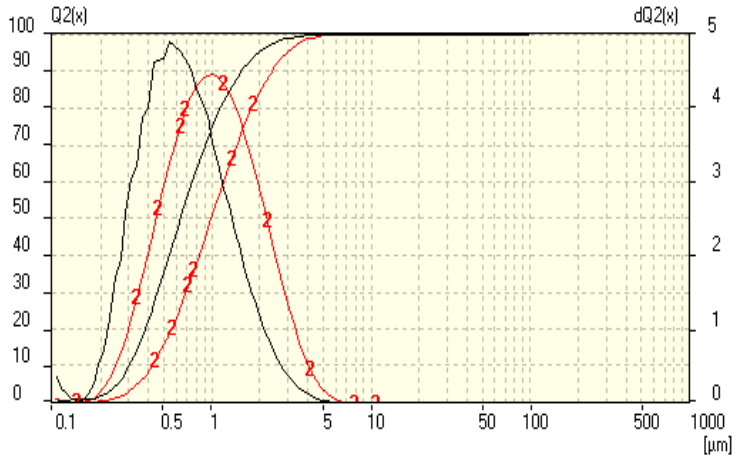

Meas.No. 300	Date 21.2.2007	Time 10:25	Operator	ID	Serial No. 778

Al2O3, D50 = 1 micron

Measuring Range	0.1 [µm] - 100.9 [µm]	Pump	50 [%]
Resolution	102 Channels (20 mm / 38 mm)		
Absorption	10.00 [%]	Ultrasonic	On
Measurement Duration	100 [Scans]		

Regularization / Modell 5793.601

Fraunhofer Calculation selected.

Mean	Values...						
D43 =	1.23 µm	D42 =	.99 µm	D41 =	.81 µm	D40 =	.67 µm
D32 =	.81 µm	D31 =	.66 µm	D30 =	.55 µm		
D21 =	.54 µm	D20 =	.46 µm				
D10 =	.23 µm						

Statistical Means...			
Arithmetic Mean Diameter	.544 µm	Variance	.145 µm2
Geometric Mean Diameter	.454 µm	Mean Squre Deviation	.38 µm
Quadratic Square Mean Diameter	.663 µm	Average Deviation	.259 µm
Harmonic Mean Diameter	.382 µm	Coefficiant of Variation	69.84 %
Statistical Modes...			
Skewness	2.615	Mode	.432 µm
Curtosis	11.899	Median	.439 µm
Span	1.707	Mean/Median Ratio	1.24
Uniformity	.55		
Specific Surface Area	157146.92 cm2/cm3		
Density	1. g/cc		
Form Factor	1. g/cc		

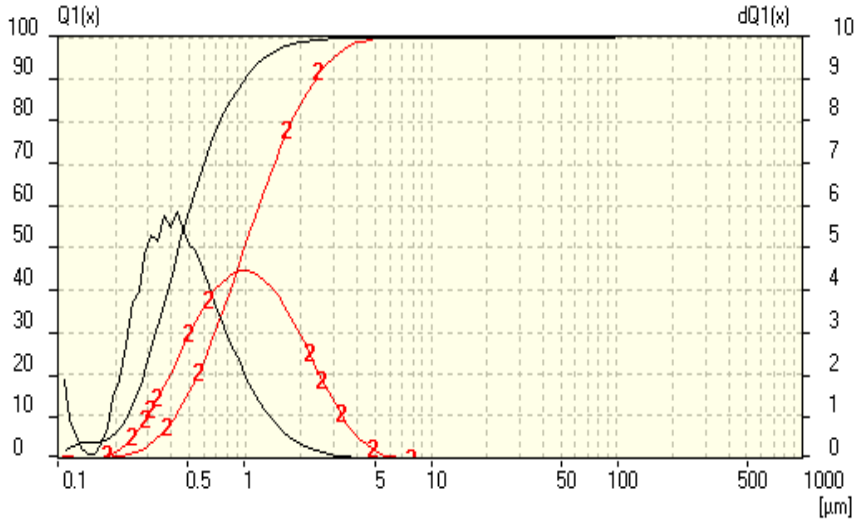

Interpolation Values... C:\Program Files\a22___32\fritsch\equal-size-intervals.FPS

****** %	<=	0.100 µm	3.7 %	<=	0.150 µm	6.0 %	<=	0.200 µm
13.3 %	<=	0.250 µm	23.3 %	<=	0.300 µm	33.6 %	<=	0.350 µm
43.2 %	<=	0.400 µm	51.8 %	<=	0.450 µm	58.9 %	<=	0.500 µm
65.0 %	<=	0.550 µm	70.1 %	<=	0.600 µm	74.4 %	<=	0.650 µm
77.9 %	<=	0.700 µm	81.0 %	<=	0.750 µm	83.5 %	<=	0.800 µm
85.6 %	<=	0.850 µm	87.5 %	<=	0.900 µm	89.1 %	<=	0.950 µm
90.5 %	<=	1.000 µm	91.6 %	<=	1.050 µm	92.6 %	<=	1.100 µm
93.5 %	<=	1.150 µm	94.2 %	<=	1.200 µm	94.9 %	<=	1.250 µm
95.4 %	<=	1.300 µm	96.0 %	<=	1.350 µm	96.4 %	<=	1.400 µm
96.8 %	<=	1.450 µm	97.1 %	<=	1.500 µm	97.4 %	<=	1.550 µm
97.7 %	<=	1.600 µm	97.9 %	<=	1.650 µm	98.1 %	<=	1.700 µm
98.3 %	<=	1.750 µm	98.5 %	<=	1.800 µm	98.6 %	<=	1.850 µm
98.8 %	<=	1.900 µm	98.9 %	<=	1.950 µm	99.0 %	<=	2.000 µm
99.1 %	<=	2.050 µm	99.2 %	<=	2.100 µm	99.2 %	<=	2.150 µm
99.3 %	<=	2.200 µm	99.4 %	<=	2.250 µm	99.4 %	<=	2.300 µm
99.5 %	<=	2.350 µm	99.5 %	<=	2.400 µm	99.6 %	<=	2.450 µm
99.6 %	<=	2.500 µm	99.7 %	<=	2.600 µm	99.7 %	<=	2.700 µm
99.8 %	<=	2.800 µm	99.8 %	<=	2.900 µm	99.8 %	<=	3.000 µm
99.9 %	<=	3.200 µm	99.9 %	<=	3.400 µm	99.9 %	<=	3.500 µm
99.9 %	<=	3.600 µm	100.0 %	<=	3.800 µm	100.0 %	<=	4.000 µm
100.0 %	<=	4.200 µm	100.0 %	<=	4.400 µm	100.0 %	<=	4.500 µm
100.0 %	<=	4.600 µm	100.0 %	<=	4.800 µm	100.0 %	<=	5.000 µm
100.0 %	<=	5.200 µm	100.0 %	<=	5.400 µm	100.0 %	<=	5.500 µm
100.0 %	<=	5.600 µm	100.0 %	<=	5.800 µm	100.0 %	<=	6.000 µm
100.0 %	<=	6.200 µm	100.0 %	<=	6.400 µm	100.0 %	<=	6.500 µm
100.0 %	<=	6.600 µm	100.0 %	<=	6.800 µm	100.0 %	<=	7.000 µm
100.0 %	<=	7.200 µm	100.0 %	<=	7.400 µm	100.0 %	<=	7.500 µm
100.0 %	<=	7.600 µm	100.0 %	<=	7.800 µm	100.0 %	<=	8.000 µm
100.0 %	<=	7.200 µm	100.0 %	<=	7.400 µm	100.0 %	<=	7.500 µm
100.0 %	<=	7.600 µm	100.0 %	<=	7.800 µm	100.0 %	<=	8.000 µm
100.0 %	<=	8.500 µm	100.0 %	<=	9.000 µm	100.0 %	<=	9.500 µm
100.0 %	<=	10.000 µm	100.0 %	<=	12.000 µm	100.0 %	<=	14.000 µm
100.0 %	<=	16.000 µm	100.0 %	<=	18.000 µm	100.0 %	<=	20.000 µm

Interpolation Values... C:\Program Files\a22___32\fritsch\five-percent-steps.FPV

1.0 %	<=	********* µm	2.0 %	<=	0.110 µm	5.0 %	<=	0.189 µm
10.0 %	<=	0.232 µm	15.0 %	<=	0.259 µm	20.0 %	<=	0.284 µm
25.0 %	<=	0.308 µm	30.0 %	<=	0.332 µm	35.0 %	<=	0.357 µm
40.0 %	<=	0.382 µm	45.0 %	<=	0.410 µm	50.0 %	<=	0.439 µm
55.0 %	<=	0.471 µm	60.0 %	<=	0.508 µm	65.0 %	<=	0.550 µm
70.0 %	<=	0.599 µm	75.0 %	<=	0.657 µm	80.0 %	<=	0.733 µm
85.0 %	<=	0.833 µm	90.0 %	<=	0.981 µm	95.0 %	<=	1.260 µm
98.0 %	<=	1.669 µm	99.0 %	<=	2.006 µm	100.0 %	<=	59.400 µm

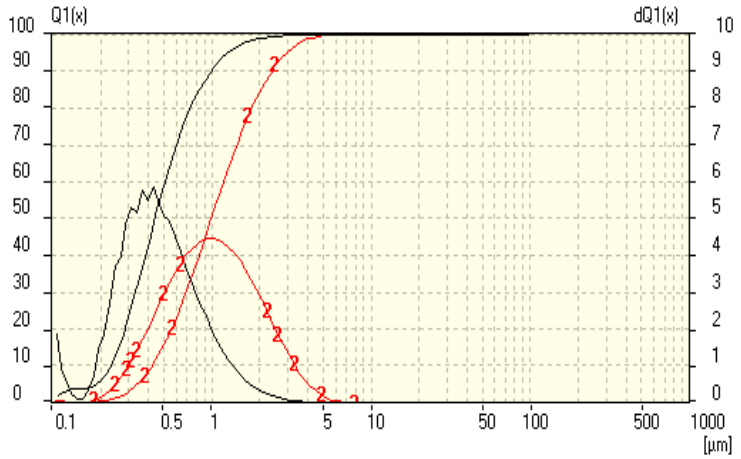

Meas.No. 300	Date 21.2.2007	Time 10:25	Operator	ID	Serial No. 778

Al2O3, D50 = 1 micron

Measuring Range	0.1 [µm] - 100.9 [µm]	Pump	50 [%]
Resolution	102 Channels (20 mm / 38 mm)		
Absorption	10.00 [%]	Ultrasonic	On
Measurement Duration	100 [Scans]		

Regularization / Modell 5793.601

Fraunhofer Calculation selected.

Mean	Values...						
D43 =	1.22 µm	D42 =	.99 µm	D41 =	.81 µm	D40 =	.67 µm
D32 =	.81 µm	D31 =	.66 µm	D30 =	.55 µm		
D21 =	.54 µm	D20 =	.46 µm				
D10 =	.12 µm						

Statistical Means...			
Arithmetic Mean Diameter	.382 µm	Variance	.063 µm2
Geometric Mean Diameter	.322 µm	Mean Squre Deviation	.25 µm
Quadratic Square Mean Diameter	.456 µm	Average Deviation	.171 µm
Harmonic Mean Diameter	.271 µm	Coefficiant of Variation	65.538 %
Statistical Modes...			
Skewness	2.601	Mode	.106 µm
Curtosis	13.851	Median	.325 µm
Span	1.68	Mean/Median Ratio	1.177
Uniformity	.5		
Specific Surface Area	221185.97 cm2/cm3		
Density	1. g/cc		
Form Factor	1. g/cc		

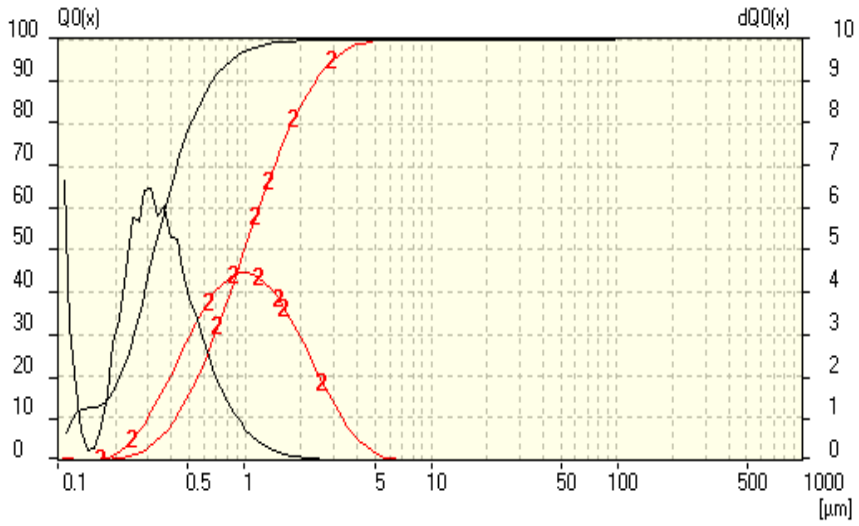

Interpolation Values... C:\Program Files\a22___32\fritsch\equal-size-intervals.FPS

****** %	<=	0.100 µm	12.5 %	<=	0.150 µm	17.4 %	<=	0.200 µm
29.5 %	<=	0.250 µm	43.5 %	<=	0.300 µm	55.6 %	<=	0.350 µm
65.4 %	<=	0.400 µm	73.2 %	<=	0.450 µm	78.9 %	<=	0.500 µm
83.3 %	<=	0.550 µm	86.8 %	<=	0.600 µm	89.4 %	<=	0.650 µm
91.4 %	<=	0.700 µm	93.0 %	<=	0.750 µm	94.2 %	<=	0.800 µm
95.2 %	<=	0.850 µm	96.1 %	<=	0.900 µm	96.7 %	<=	0.950 µm
97.3 %	<=	1.000 µm	97.7 %	<=	1.050 µm	98.0 %	<=	1.100 µm
98.3 %	<=	1.150 µm	98.6 %	<=	1.200 µm	98.8 %	<=	1.250 µm
99.0 %	<=	1.300 µm	99.1 %	<=	1.350 µm	99.2 %	<=	1.400 µm
99.3 %	<=	1.450 µm	99.4 %	<=	1.500 µm	99.5 %	<=	1.550 µm
99.6 %	<=	1.600 µm	99.6 %	<=	1.650 µm	99.7 %	<=	1.700 µm
99.7 %	<=	1.750 µm	99.7 %	<=	1.800 µm	99.8 %	<=	1.850 µm
99.8 %	<=	1.900 µm	99.8 %	<=	1.950 µm	99.8 %	<=	2.000 µm
99.9 %	<=	2.050 µm	99.9 %	<=	2.100 µm	99.9 %	<=	2.150 µm
99.9 %	<=	2.200 µm	99.9 %	<=	2.250 µm	99.9 %	<=	2.300 µm
99.9 %	<=	2.350 µm	99.9 %	<=	2.400 µm	99.9 %	<=	2.450 µm
100.0 %	<=	2.500 µm	100.0 %	<=	2.600 µm	100.0 %	<=	2.700 µm
100.0 %	<=	2.800 µm	100.0 %	<=	2.900 µm	100.0 %	<=	3.000 µm
100.0 %	<=	3.200 µm	100.0 %	<=	3.400 µm	100.0 %	<=	3.500 µm
100.0 %	<=	3.600 µm	100.0 %	<=	3.800 µm	100.0 %	<=	4.000 µm
100.0 %	<=	4.200 µm	100.0 %	<=	4.400 µm	100.0 %	<=	4.500 µm
100.0 %	<=	4.600 µm	100.0 %	<=	4.800 µm	100.0 %	<=	5.000 µm
100.0 %	<=	5.200 µm	100.0 %	<=	5.400 µm	100.0 %	<=	5.500 µm
100.0 %	<=	5.600 µm	100.0 %	<=	5.800 µm	100.0 %	<=	6.000 µm
100.0 %	<=	6.200 µm	100.0 %	<=	6.400 µm	100.0 %	<=	6.500 µm
100.0 %	<=	6.600 µm	100.0 %	<=	6.800 µm	100.0 %	<=	7.000 µm
100.0 %	<=	7.200 µm	100.0 %	<=	7.400 µm	100.0 %	<=	7.500 µm
100.0 %	<=	7.600 µm	100.0 %	<=	7.800 µm	100.0 %	<=	8.000 µm
100.0 %	<=	7.200 µm	100.0 %	<=	7.400 µm	100.0 %	<=	7.500 µm
100.0 %	<=	7.600 µm	100.0 %	<=	7.800 µm	100.0 %	<=	8.000 µm
100.0 %	<=	8.500 µm	100.0 %	<=	9.000 µm	100.0 %	<=	9.500 µm
100.0 %	<=	10.000 µm	100.0 %	<=	12.000 µm	100.0 %	<=	14.000 µm
100.0 %	<=	16.000 µm	100.0 %	<=	18.000 µm	100.0 %	<=	20.000 µm

Interpolation Values... C:\Program Files\a22___32\fritsch\five-percent-steps.FPV

1.0 %	<=	********* µm	2.0 %	<=	********* µm	5.0 %	<=	********* µm
10.0 %	<=	0.118 µm	15.0 %	<=	0.187 µm	20.0 %	<=	0.213 µm
25.0 %	<=	0.234 µm	30.0 %	<=	0.252 µm	35.0 %	<=	0.270 µm
40.0 %	<=	0.288 µm	45.0 %	<=	0.306 µm	50.0 %	<=	0.325 µm
55.0 %	<=	0.347 µm	60.0 %	<=	0.371 µm	65.0 %	<=	0.398 µm
70.0 %	<=	0.429 µm	75.0 %	<=	0.465 µm	80.0 %	<=	0.511 µm
85.0 %	<=	0.572 µm	90.0 %	<=	0.664 µm	95.0 %	<=	0.835 µm
98.0 %	<=	1.094 µm	99.0 %	<=	1.313 µm	100.0 %	<=	5.045 µm

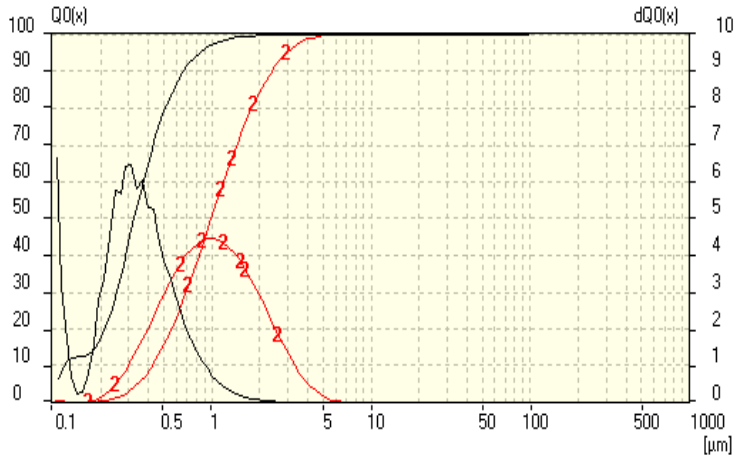

Meas.No. 300	Date 21.2.2007	Time 10:25	Operator	ID	Serial No. 778

Al2O3, D50 = 1 micron

Measuring Range	0.1 [µm] - 100.9 [µm]	Pump	50 [%]
Resolution	102 Channels (20 mm / 38 mm)		
Absorption	10.00 [%]	Ultrasonic	On
Measurement Duration	100 [Scans]		

Regularization / Modell 5793.601

Fraunhofer Calculation selected.

Mean	Values...						
D43 =	1.23 µm	D42 =	.99 µm	D41 =	.81 µm	D40 =	.67 µm
D32 =	.81 µm	D31 =	.66 µm	D30 =	.55 µm		
D21 =	.54 µm	D20 =	.46 µm				
D10 =	.42 µm						

Statistical Means...			
Arithmetic Mean Diameter	1.226 µm	Variance	.706 µm2
Geometric Mean Diameter	.995 µm	Mean Squre Deviation	.84 µm
Quadratic Square Mean Diameter	1.484 µm	Average Deviation	.631 µm
Harmonic Mean Diameter	.807 µm	Coefficiant of Variation	68.579 %
Statistical Modes...			
Skewness	1.591	Mode	.932 µm
Curtosis	3.307	Median	.992 µm
Span	1.952	Mean/Median Ratio	1.235
Uniformity	.61		
Specific Surface Area	74388.21 cm2/cm3		
Density	1. g/cc		
Form Factor	1. g/cc		

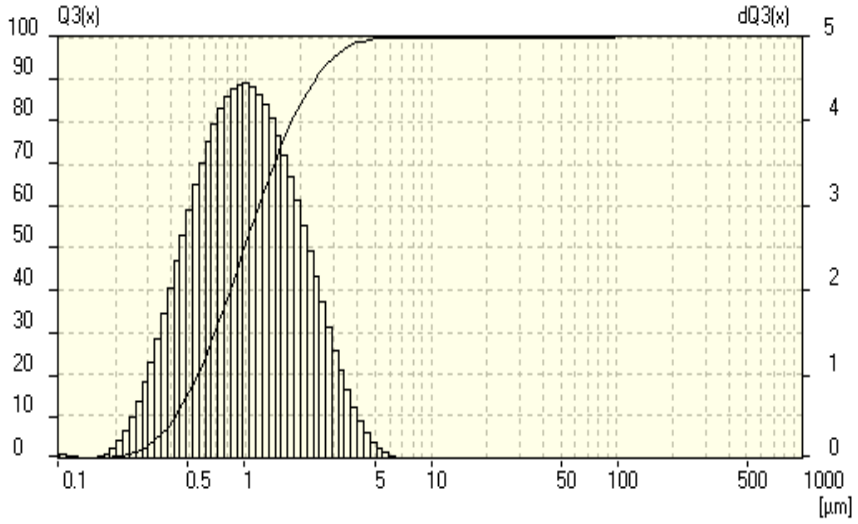

Ningde Amperex Tech. Exhibit No. 2043
Zhuhai CosMX Battery Co. Ltd. v. Ningde Amperex Tech.
IPR2025-00432, U.S. Patent No. 11,575,148
Page 69 of 123

Meas.No. 300	Date 21.2.2007	Time 10:25	Operator	ID	Serial No. 778

Al2O3, D50 = 1 micron

Measuring Range	0.1 [µm] - 100.9 [µm]	Pump	50 [%]
Resolution	102 Channels (20 mm / 38 mm)		
Absorption	10.00 [%]	Ultrasonic	On
Measurement Duration	100 [Scans]		

Regularization / Modell 5793.601

Fraunhofer Calculation selected.

Mean	Values...						
D43 =	1.23 µm	D42 =	.99 µm	D41 =	.81 µm	D40 =	.67 µm
D32 =	.81 µm	D31 =	.66 µm	D30 =	.55 µm		
D21 =	.54 µm	D20 =	.46 µm				
D10 =	.42 µm						

Statistical Means...			
Arithmetic Mean Diameter	1.226 µm	Variance	.706 µm2
Geometric Mean Diameter	.995 µm	Mean Squre Deviation	.84 µm
Quadratic Square Mean Diameter	1.484 µm	Average Deviation	.631 µm
Harmonic Mean Diameter	.807 µm	Coefficiant of Variation	68.579 %
Statistical Modes...			
Skewness	1.591	Mode	.932 µm
Curtosis	3.307	Median	.992 µm
Span	1.952	Mean/Median Ratio	1.235
Uniformity	.61		
Specific Surface Area	74388.21 cm2/cm3		
Density	1. g/cc		
Form Factor	1. g/cc		

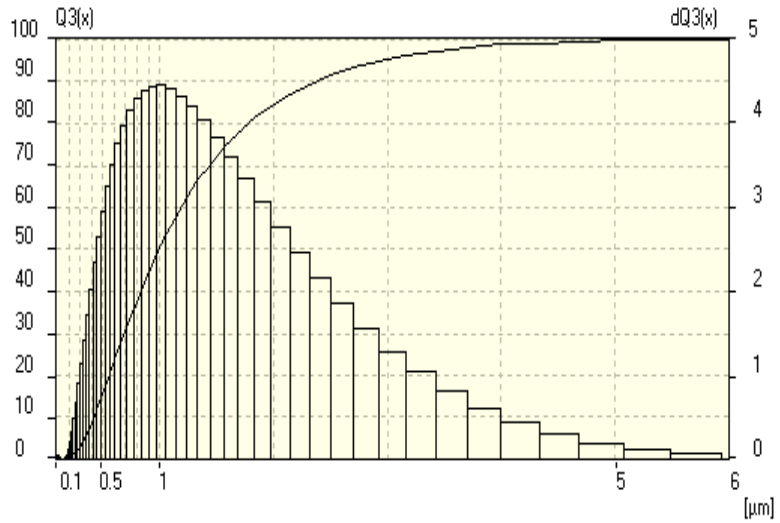

Ningde Amperex Tech. Exhibit No. 2043
Zhuhai CosMX Battery Co. Ltd. v. Ningde Amperex Tech.
IPR2025-00432, U.S. Patent No. 11,575,148
Page 70 of 123

Meas.No. 300	Date 21.2.2007	Time 10:25	Operator	ID	Serial No. 778

Al2O3, D50 = 1 micron

Measuring Range	0.1 [µm] - 100.9 [µm]	Pump	50 [%]
Resolution	102 Channels (20 mm / 38 mm)		
Absorption	10.00 [%]	Ultrasonic	On
Measurement Duration	100 [Scans]		

Regularization / Modell 5793.601

Fraunhofer Calculation selected.

Mean	Values...						
D43 =	1.23 µm	D42 =	.99 µm	D41 =	.81 µm	D40 =	.67 µm
D32 =	.81 µm	D31 =	.66 µm	D30 =	.55 µm		
D21 =	.54 µm	D20 =	.46 µm				
D10 =	.42 µm						

Statistical Means...			
Arithmetic Mean Diameter	1.226 µm	Variance	.706 µm2
Geometric Mean Diameter	.995 µm	Mean Squre Deviation	.84 µm
Quadratic Square Mean Diameter	1.484 µm	Average Deviation	.631 µm
Harmonic Mean Diameter	.807 µm	Coefficiant of Variation	68.579 %
Statistical Modes...			
Skewness	1.591	Mode	.932 µm
Curtosis	3.307	Median	.992 µm
Span	1.952	Mean/Median Ratio	1.235
Uniformity	.61		
Specific Surface Area	74388.21 cm2/cm3		
Density	1. g/cc		
Form Factor	1. g/cc		

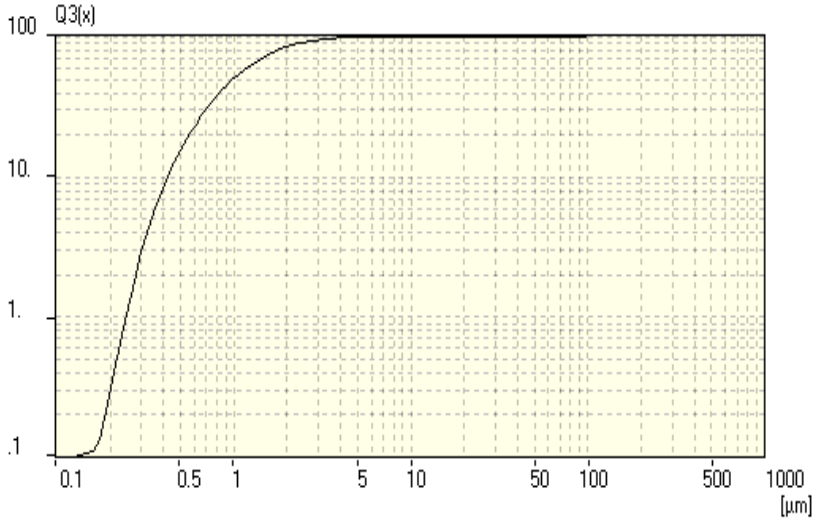

Ningde Amperex Tech. Exhibit No. 2043
Zhuhai CosMX Battery Co. Ltd. v. Ningde Amperex Tech.
IPR2025-00432, U.S. Patent No. 11,575,148
Page 71 of 123

Meas.No. 300	Date 21.2.2007	Time 10:25	Operator	ID	Serial No. 778

Al2O3, D50 = 1 micron

Measuring Range	0.1 [µm] - 100.9 [µm]	Pump	50 [%]
Resolution	102 Channels (20 mm / 38 mm)		
Absorption	10.00 [%]	Ultrasonic	On
Measurement Duration	100 [Scans]		

Regularization / Modell 5793.601

Fraunhofer Calculation selected.

Mean	Values...						
D43 =	1.23 µm	D42 =	.99 µm	D41 =	.81 µm	D40 =	.67 µm
D32 =	.81 µm	D31 =	.66 µm	D30 =	.55 µm		
D21 =	.54 µm	D20 =	.46 µm				
D10 =	.42 µm						

Statistical Means...			
Arithmetic Mean Diameter	1.226 µm	Variance	.706 µm2
Geometric Mean Diameter	.995 µm	Mean Squre Deviation	.84 µm
Quadratic Square Mean Diameter	1.484 µm	Average Deviation	.631 µm
Harmonic Mean Diameter	.807 µm	Coefficiant of Variation	68.579 %
Statistical Modes...			
Skewness	1.591	Mode	.932 µm
Curtosis	3.307	Median	.992 µm
Span	1.952	Mean/Median Ratio	1.235
Uniformity	.61		
Specific Surface Area	74388.21 cm2/cm3		
Density	1. g/cc		
Form Factor	1. g/cc		

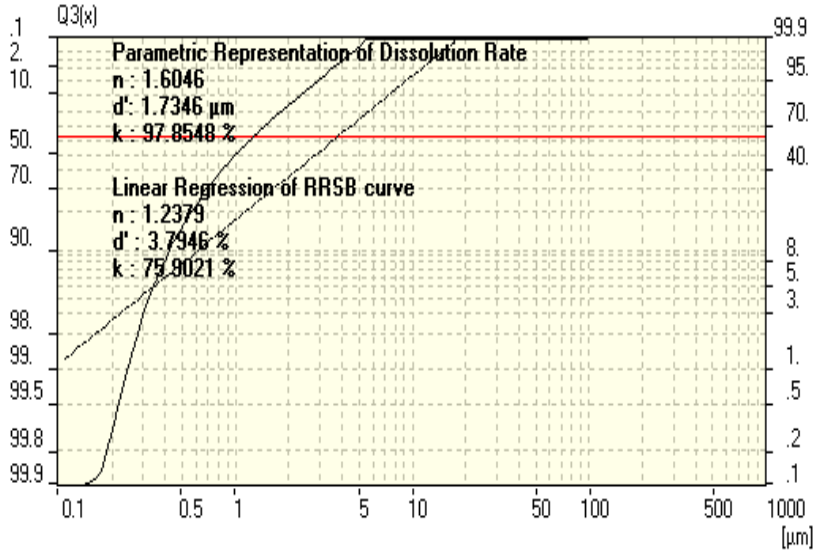

Meas.No. 300	Date 21.2.2007	Time 10:25	Operator	ID	Serial No. 778

Al2O3, D50 = 1 micron

Measuring Range	0.1 [µm] - 100.9 [µm]	Pump	50 [%]
Resolution	102 Channels (20 mm / 38 mm)		
Absorption	10.00 [%]	Ultrasonic	On
Measurement Duration	100 [Scans]		

Regularization / Modell 5793.601

Fraunhofer Calculation selected.

Mean	Values...						
D43 =	1.23 µm	D42 =	.99 µm	D41 =	.81 µm	D40 =	.67 µm
D32 =	.81 µm	D31 =	.66 µm	D30 =	.55 µm		
D21 =	.54 µm	D20 =	.46 µm				
D10 =	.42 µm						

Statistical Means...			
Arithmetic Mean Diameter	1.226 µm	Variance	.706 µm2
Geometric Mean Diameter	.995 µm	Mean Squre Deviation	.84 µm
Quadratic Square Mean Diameter	1.484 µm	Average Deviation	.631 µm
Harmonic Mean Diameter	.807 µm	Coefficiant of Variation	68.579 %
Statistical Modes...			
Skewness	1.591	Mode	.932 µm
Curtosis	3.307	Median	.992 µm
Span	1.952	Mean/Median Ratio	1.235
Uniformity	.61		
Specific Surface Area	74388.21 cm2/cm3		
Density	1. g/cc		
Form Factor	1. g/cc		

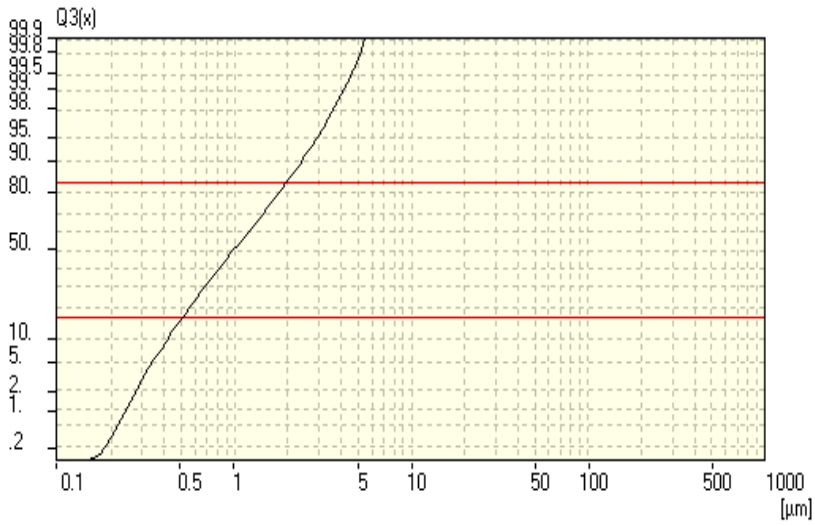

Ningde Amperex Tech. Exhibit No. 2043
Zhuhai CosMX Battery Co. Ltd. v. Ningde Amperex Tech.
IPR2025-00432, U.S. Patent No. 11,575,148
Page 73 of 123

Meas.No. 300	Date 21.2.2007	Time 10:25	Operator	ID	Serial No. 778

Al2O3, D50 = 1 micron

Measuring Range	0.1 [µm] - 100.9 [µm]	Pump	50 [%]
Resolution	102 Channels (20 mm / 38 mm)		
Absorption	10.00 [%]	Ultrasonic	On
Measurement Duration	100 [Scans]		

Regularization / Modell 5793.601

Fraunhofer Calculation selected.

Mean	Values...						
D43 =	1.23 µm	D42 =	.99 µm	D41 =	.81 µm	D40 =	.67 µm
D32 =	.81 µm	D31 =	.66 µm	D30 =	.55 µm		
D21 =	.54 µm	D20 =	.46 µm				
D10 =	.3 µm						

Statistical Means...			
Arithmetic Mean Diameter	.807 µm	Variance	.342 µm2
Geometric Mean Diameter	.658 µm	Mean Squre Deviation	.584 µm
Quadratic Square Mean Diameter	.995 µm	Average Deviation	.415 µm
Harmonic Mean Diameter	.544 µm	Coefficiant of Variation	72.429 %
Statistical Modes...			
Skewness	2.169	Mode	.539 µm
Curtosis	7.093	Median	.634 µm
Span	1.938	Mean/Median Ratio	1.273
Uniformity	.61		
Specific Surface Area	110278.55 cm2/cm3		
Density	1. g/cc		
Form Factor	1. g/cc		

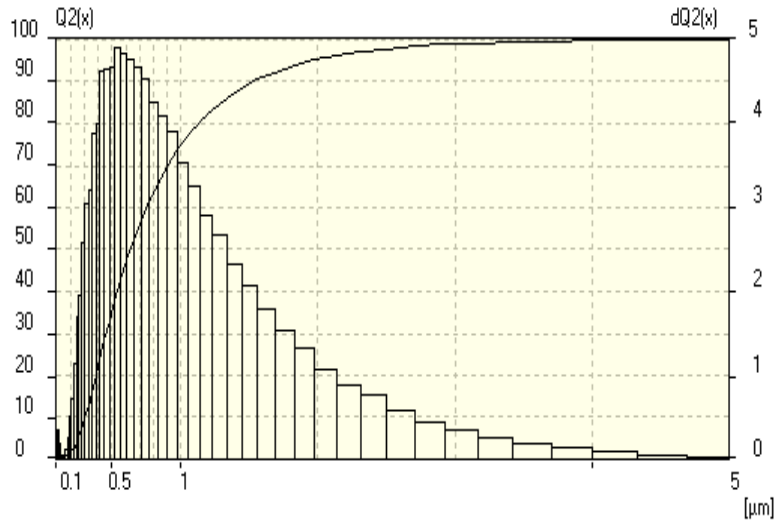

Ningde Amperex Tech. Exhibit No. 2043
Zhuhai CosMX Battery Co. Ltd. v. Ningde Amperex Tech.
IPR2025-00432, U.S. Patent No. 11,575,148
Page 74 of 123

Meas.No. 300	Date 21.2.2007	Time 10:25	Operator	ID	Serial No. 778

Al2O3, D50 = 1 micron

Measuring Range	0.1 [µm] - 100.9 [µm]	Pump	50 [%]
Resolution	102 Channels (20 mm / 38 mm)		
Absorption	10.00 [%]	Ultrasonic	On
Measurement Duration	100 [Scans]		

Regularization / Modell 5793.601

Fraunhofer Calculation selected.

Mean	Values...						
D43 =	1.23 µm	D42 =	.99 µm	D41 =	.81 µm	D40 =	.67 µm
D32 =	.81 µm	D31 =	.66 µm	D30 =	.55 µm		
D21 =	.54 µm	D20 =	.46 µm				
D10 =	.3 µm						

Statistical Means...			
Arithmetic Mean Diameter	.807 µm	Variance	.342 µm2
Geometric Mean Diameter	.658 µm	Mean Squre Deviation	.584 µm
Quadratic Square Mean Diameter	.995 µm	Average Deviation	.415 µm
Harmonic Mean Diameter	.544 µm	Coefficiant of Variation	72.429 %
Statistical Modes...			
Skewness	2.169	Mode	.539 µm
Curtosis	7.093	Median	.634 µm
Span	1.938	Mean/Median Ratio	1.273
Uniformity	.61		
Specific Surface Area	110278.55 cm2/cm3		
Density	1. g/cc		
Form Factor	1. g/cc		

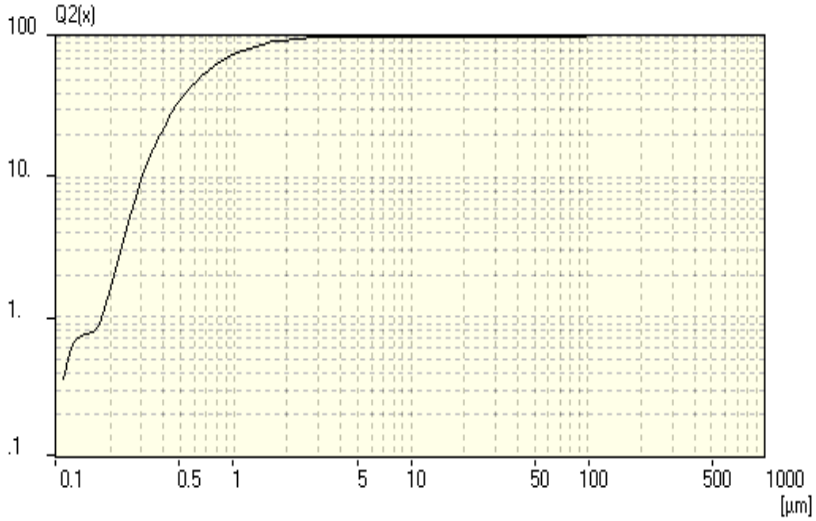

Ningde Amperex Tech. Exhibit No. 2043
Zhuhai CosMX Battery Co. Ltd. v. Ningde Amperex Tech.
IPR2025-00432, U.S. Patent No. 11,575,148
Page 75 of 123

Meas.No. 300	Date 21.2.2007	Time 10:25	Operator	ID	Serial No. 778

Al2O3, D50 = 1 micron

Measuring Range	0.1 [µm] - 100.9 [µm]	Pump	50 [%]
Resolution	102 Channels (20 mm / 38 mm)		
Absorption	10.00 [%]	Ultrasonic	On
Measurement Duration	100 [Scans]		

Regularization / Modell 5793.601

Fraunhofer Calculation selected.

Mean	Values...						
D43 =	1.23 µm	D42 =	.99 µm	D41 =	.81 µm	D40 =	.67 µm
D32 =	.81 µm	D31 =	.66 µm	D30 =	.55 µm		
D21 =	.54 µm	D20 =	.46 µm				
D10 =	.3 µm						

Statistical Means...			
Arithmetic Mean Diameter	.807 µm	Variance	.342 µm2
Geometric Mean Diameter	.658 µm	Mean Squre Deviation	.584 µm
Quadratic Square Mean Diameter	.995 µm	Average Deviation	.415 µm
Harmonic Mean Diameter	.544 µm	Coefficiant of Variation	72.429 %
Statistical Modes...			
Skewness	2.169	Mode	.539 µm
Curtosis	7.093	Median	.634 µm
Span	1.938	Mean/Median Ratio	1.273
Uniformity	.61		
Specific Surface Area	110278.55 cm2/cm3		
Density	1. g/cc		
Form Factor	1. g/cc		

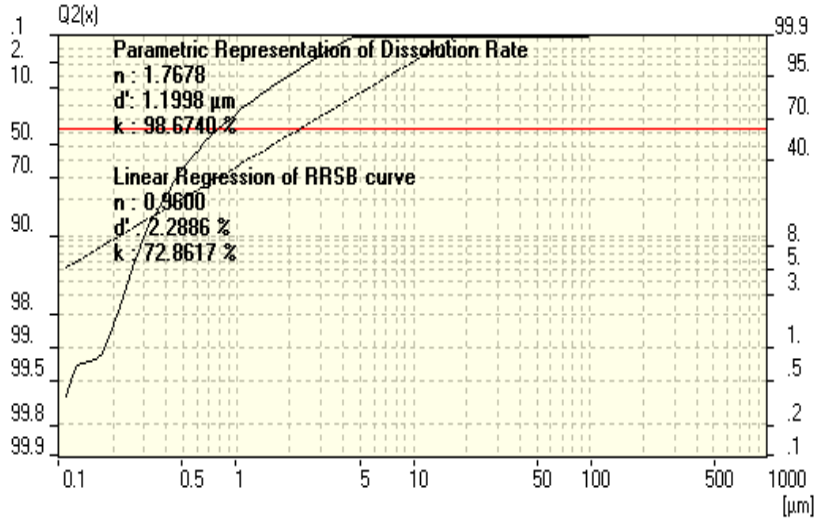

Meas.No. 300	Date 21.2.2007	Time 10:25	Operator	ID	Serial No. 778

Al2O3, D50 = 1 micron

Measuring Range	0.1 [µm] - 100.9 [µm]	Pump	50 [%]
Resolution	102 Channels (20 mm / 38 mm)		
Absorption	10.00 [%]	Ultrasonic	On
Measurement Duration	100 [Scans]		

Regularization / Modell 5793.601

Fraunhofer Calculation selected.

Mean	Values...						
D43 =	1.23 µm	D42 =	.99 µm	D41 =	.81 µm	D40 =	.67 µm
D32 =	.81 µm	D31 =	.66 µm	D30 =	.55 µm		
D21 =	.54 µm	D20 =	.46 µm				
D10 =	.3 µm						

Statistical Means...			
Arithmetic Mean Diameter	.807 µm	Variance	.342 µm2
Geometric Mean Diameter	.658 µm	Mean Squre Deviation	.584 µm
Quadratic Square Mean Diameter	.995 µm	Average Deviation	.415 µm
Harmonic Mean Diameter	.544 µm	Coefficiant of Variation	72.429 %
Statistical Modes...			
Skewness	2.169	Mode	.539 µm
Curtosis	7.093	Median	.634 µm
Span	1.938	Mean/Median Ratio	1.273
Uniformity	.61		
Specific Surface Area	110278.55 cm2/cm3		
Density	1. g/cc		
Form Factor	1. g/cc		

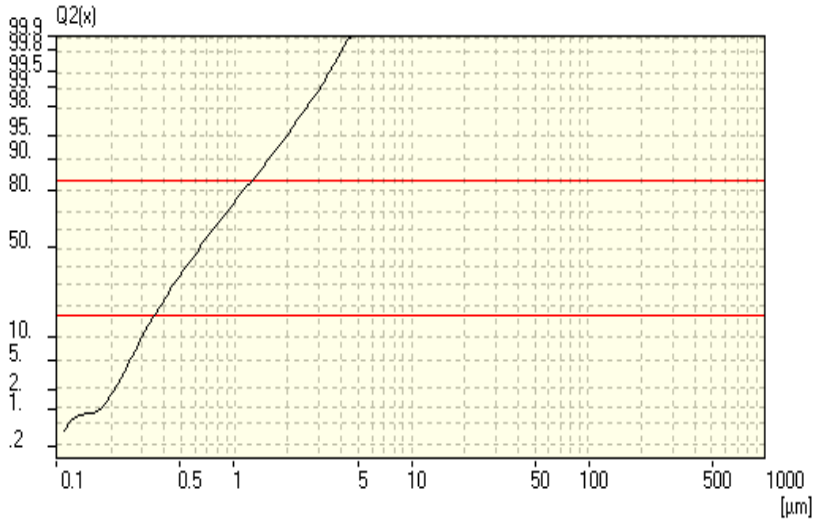

Ningde Amperex Tech. Exhibit No. 2043
Zhuhai CosMX Battery Co. Ltd. v. Ningde Amperex Tech.
IPR2025-00432, U.S. Patent No. 11,575,148
Page 77 of 123

Meas.No. 300	Date 21.2.2007	Time 10:25	Operator	ID	Serial No. 778

Al2O3, D50 = 1 micron

Measuring Range	0.1 [µm] - 100.9 [µm]	Pump	50 [%]
Resolution	102 Channels (20 mm / 38 mm)		
Absorption	10.00 [%]	Ultrasonic	On
Measurement Duration	100 [Scans]		

Regularization / Modell 5793.601

Fraunhofer Calculation selected.

Mean	Values...						
D43 =	1.23 µm	D42 =	.99 µm	D41 =	.81 µm	D40 =	.67 µm
D32 =	.81 µm	D31 =	.66 µm	D30 =	.55 µm		
D21 =	.54 µm	D20 =	.46 µm				
D10 =	.23 µm						

Statistical Means...			
Arithmetic Mean Diameter	.544 µm	Variance	.145 µm2
Geometric Mean Diameter	.454 µm	Mean Squre Deviation	.38 µm
Quadratic Square Mean Diameter	.663 µm	Average Deviation	.259 µm
Harmonic Mean Diameter	.382 µm	Coefficiant of Variation	69.84 %
Statistical Modes...			
Skewness	2.615	Mode	.432 µm
Curtosis	11.899	Median	.439 µm
Span	1.707	Mean/Median Ratio	1.24
Uniformity	.55		
Specific Surface Area	157146.92 cm2/cm3		
Density	1. g/cc		
Form Factor	1. g/cc		

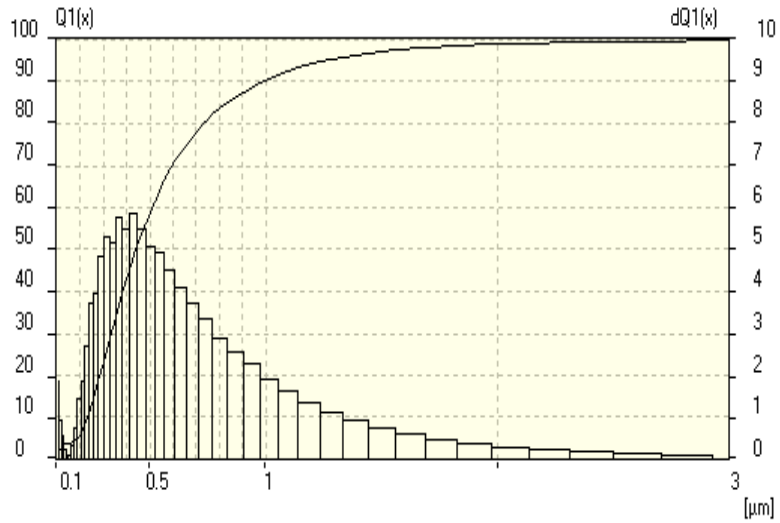

Meas.No. 300	Date 21.2.2007	Time 10:25	Operator	ID	Serial No. 778

Al2O3, D50 = 1 micron

Measuring Range	0.1 [µm] - 100.9 [µm]	Pump	50 [%]
Resolution	102 Channels (20 mm / 38 mm)		
Absorption	10.00 [%]	Ultrasonic	On
Measurement Duration	100 [Scans]		

Regularization / Modell 5793.601

Fraunhofer Calculation selected.

Mean	Values...						
D43 =	1.23 µm	D42 =	.99 µm	D41 =	.81 µm	D40 =	.67 µm
D32 =	.81 µm	D31 =	.66 µm	D30 =	.55 µm		
D21 =	.54 µm	D20 =	.46 µm				
D10 =	.23 µm						

Statistical Means...			
Arithmetic Mean Diameter	.544 µm	Variance	.145 µm2
Geometric Mean Diameter	.454 µm	Mean Squre Deviation	.38 µm
Quadratic Square Mean Diameter	.663 µm	Average Deviation	.259 µm
Harmonic Mean Diameter	.382 µm	Coefficiant of Variation	69.84 %
Statistical Modes...			
Skewness	2.615	Mode	.432 µm
Curtosis	11.899	Median	.439 µm
Span	1.707	Mean/Median Ratio	1.24
Uniformity	.55		
Specific Surface Area	157146.92 cm2/cm3		
Density	1. g/cc		
Form Factor	1. g/cc		

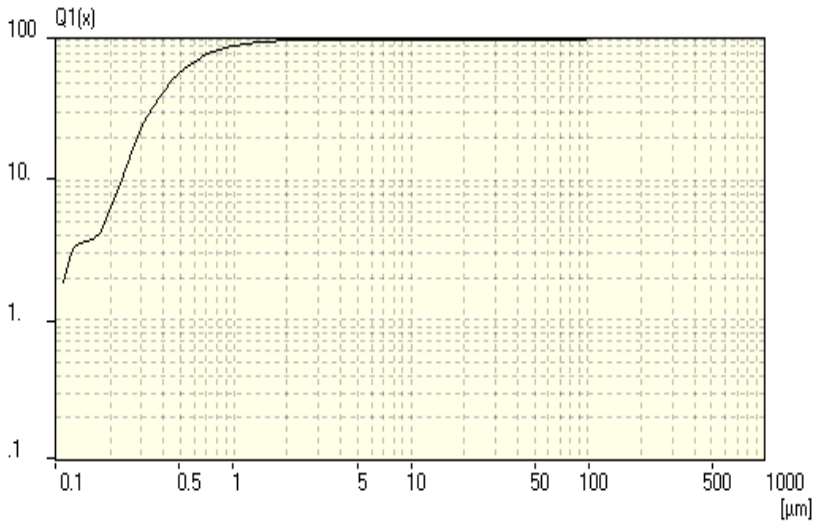

Ningde Amperex Tech. Exhibit No. 2043
Zhuhai CosMX Battery Co. Ltd. v. Ningde Amperex Tech.
IPR2025-00432, U.S. Patent No. 11,575,148
Page 79 of 123

Meas.No. 300	Date 21.2.2007	Time 10:25	Operator	ID	Serial No. 778

Al2O3, D50 = 1 micron

Measuring Range	0.1 [µm] - 100.9 [µm]	Pump	50 [%]
Resolution	102 Channels (20 mm / 38 mm)		
Absorption	10.00 [%]	Ultrasonic	On
Measurement Duration	100 [Scans]		

Regularization / Modell 5793.601

Fraunhofer Calculation selected.

Mean	Values...						
D43 =	1.23 µm	D42 =	.99 µm	D41 =	.81 µm	D40 =	.67 µm
D32 =	.81 µm	D31 =	.66 µm	D30 =	.55 µm		
D21 =	.54 µm	D20 =	.46 µm				
D10 =	.23 µm						

Statistical Means...			
Arithmetic Mean Diameter	.544 µm	Variance	.145 µm2
Geometric Mean Diameter	.454 µm	Mean Squre Deviation	.38 µm
Quadratic Square Mean Diameter	.663 µm	Average Deviation	.259 µm
Harmonic Mean Diameter	.382 µm	Coefficiant of Variation	69.84 %
Statistical Modes...			
Skewness	2.615	Mode	.432 µm
Curtosis	11.899	Median	.439 µm
Span	1.707	Mean/Median Ratio	1.24
Uniformity	.55		
Specific Surface Area	157146.92 cm2/cm3		
Density	1. g/cc		
Form Factor	1. g/cc		

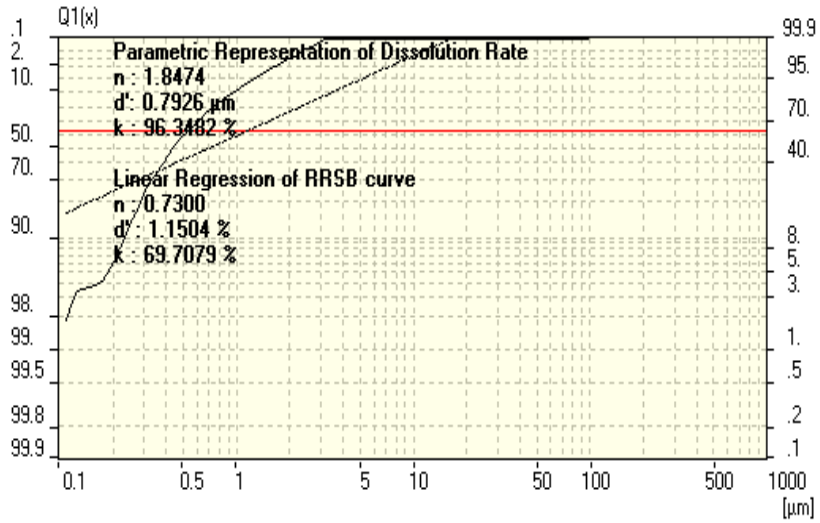

Ningde Amperex Tech. Exhibit No. 2043
Zhuhai CosMX Battery Co. Ltd. v. Ningde Amperex Tech.
IPR2025-00432, U.S. Patent No. 11,575,148
Page 80 of 123

Meas.No. 300	Date 21.2.2007	Time 10:25	Operator	ID	Serial No. 778

Al2O3, D50 = 1 micron

Measuring Range	0.1 [µm] - 100.9 [µm]	Pump	50 [%]
Resolution	102 Channels (20 mm / 38 mm)		
Absorption	10.00 [%]	Ultrasonic	On
Measurement Duration	100 [Scans]		

Regularization / Modell 5793.601

Fraunhofer Calculation selected.

Mean	Values...						
D43 =	1.23 µm	D42 =	.99 µm	D41 =	.81 µm	D40 =	.67 µm
D32 =	.81 µm	D31 =	.66 µm	D30 =	.55 µm		
D21 =	.54 µm	D20 =	.46 µm				
D10 =	.23 µm						

Statistical Means...			
Arithmetic Mean Diameter	.544 µm	Variance	.145 µm2
Geometric Mean Diameter	.454 µm	Mean Squre Deviation	.38 µm
Quadratic Square Mean Diameter	.663 µm	Average Deviation	.259 µm
Harmonic Mean Diameter	.382 µm	Coefficiant of Variation	69.84 %
Statistical Modes...			
Skewness	2.615	Mode	.432 µm
Curtosis	11.899	Median	.439 µm
Span	1.707	Mean/Median Ratio	1.24
Uniformity	.55		
Specific Surface Area	157146.92 cm2/cm3		
Density	1. g/cc		
Form Factor	1. g/cc		

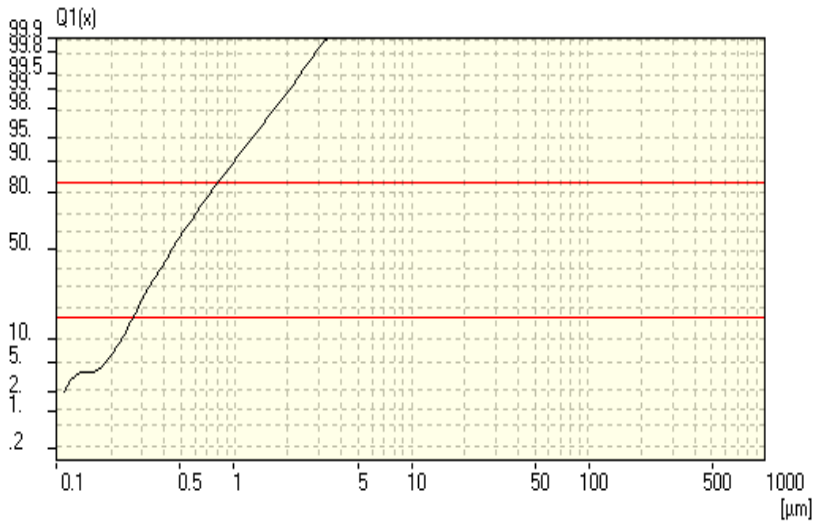

Ningde Amperex Tech. Exhibit No. 2043
Zhuhai CosMX Battery Co. Ltd. v. Ningde Amperex Tech.
IPR2025-00432, U.S. Patent No. 11,575,148
Page 81 of 123

Meas.No. 300	Date 21.2.2007	Time 10:25	Operator	ID	Serial No. 778

Al2O3, D50 = 1 micron

Measuring Range	0.1 [µm] - 100.9 [µm]	Pump	50 [%]
Resolution	102 Channels (20 mm / 38 mm)		
Absorption	10.00 [%]	Ultrasonic	On
Measurement Duration	100 [Scans]		

Regularization / Modell 5793.601

Fraunhofer Calculation selected.

Mean	Values...						
D43 =	1.22 µm	D42 =	.99 µm	D41 =	.81 µm	D40 =	.67 µm
D32 =	.81 µm	D31 =	.66 µm	D30 =	.55 µm		
D21 =	.54 µm	D20 =	.46 µm				
D10 =	.12 µm						

Statistical Means...			
Arithmetic Mean Diameter	.382 µm	Variance	.063 µm2
Geometric Mean Diameter	.322 µm	Mean Squre Deviation	.25 µm
Quadratic Square Mean Diameter	.456 µm	Average Deviation	.171 µm
Harmonic Mean Diameter	.271 µm	Coefficiant of Variation	65.538 %
Statistical Modes...			
Skewness	2.601	Mode	.106 µm
Curtosis	13.851	Median	.325 µm
Span	1.68	Mean/Median Ratio	1.177
Uniformity	.5		
Specific Surface Area	221185.97 cm2/cm3		
Density	1. g/cc		
Form Factor	1. g/cc		

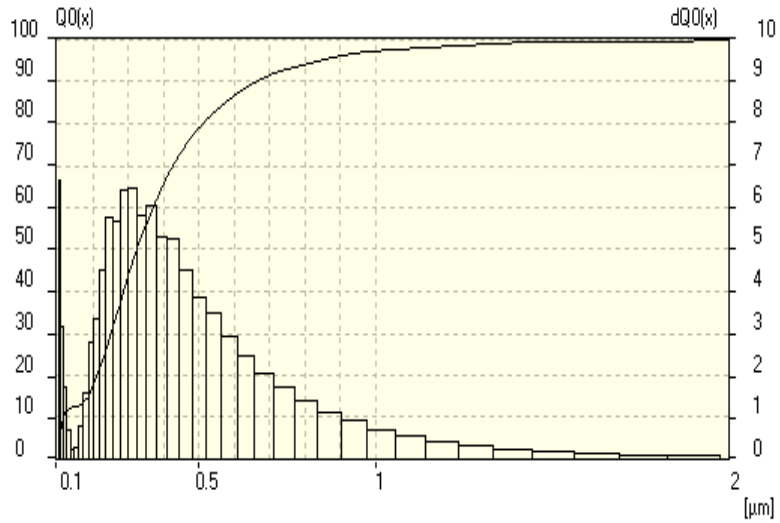

Meas.No. 300	Date 21.2.2007	Time 10:25	Operator	ID	Serial No. 778

Al2O3, D50 = 1 micron

Measuring Range	0.1 [µm] - 100.9 [µm]	Pump	50 [%]
Resolution	102 Channels (20 mm / 38 mm)		
Absorption	10.00 [%]	Ultrasonic	On
Measurement Duration	100 [Scans]		

Regularization / Modell 5793.601

Fraunhofer Calculation selected.

Mean	Values...						
D43 =	1.22 µm	D42 =	.99 µm	D41 =	.81 µm	D40 =	.67 µm
D32 =	.81 µm	D31 =	.66 µm	D30 =	.55 µm		
D21 =	.54 µm	D20 =	.46 µm				
D10 =	.12 µm						

Statistical Means...			
Arithmetic Mean Diameter	.382 µm	Variance	.063 µm2
Geometric Mean Diameter	.322 µm	Mean Squre Deviation	.25 µm
Quadratic Square Mean Diameter	.456 µm	Average Deviation	.171 µm
Harmonic Mean Diameter	.271 µm	Coefficiant of Variation	65.538 %
Statistical Modes...			
Skewness	2.601	Mode	.106 µm
Curtosis	13.851	Median	.325 µm
Span	1.68	Mean/Median Ratio	1.177
Uniformity	.5		
Specific Surface Area	221185.97 cm2/cm3		
Density	1. g/cc		
Form Factor	1. g/cc		

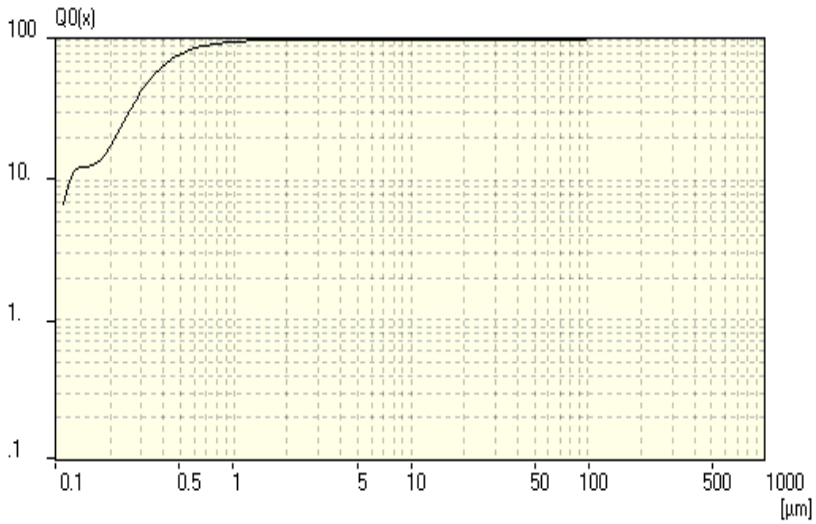

Ningde Amperex Tech. Exhibit No. 2043
Zhuhai CosMX Battery Co. Ltd. v. Ningde Amperex Tech.
IPR2025-00432, U.S. Patent No. 11,575,148
Page 83 of 123

Meas.No. 300	Date 21.2.2007	Time 10:25	Operator	ID	Serial No. 778

Al2O3, D50 = 1 micron

Measuring Range	0.1 [µm] - 100.9 [µm]	Pump	50 [%]
Resolution	102 Channels (20 mm / 38 mm)		
Absorption	10.00 [%]	Ultrasonic	On
Measurement Duration	100 [Scans]		

Regularization / Modell 5793.601

Fraunhofer Calculation selected.

Mean	Values...						
D43 =	1.22 µm	D42 =	.99 µm	D41 =	.81 µm	D40 =	.67 µm
D32 =	.81 µm	D31 =	.66 µm	D30 =	.55 µm		
D21 =	.54 µm	D20 =	.46 µm				
D10 =	.12 µm						

Statistical Means...			
Arithmetic Mean Diameter	.382 µm	Variance	.063 µm2
Geometric Mean Diameter	.322 µm	Mean Squre Deviation	.25 µm
Quadratic Square Mean Diameter	.456 µm	Average Deviation	.171 µm
Harmonic Mean Diameter	.271 µm	Coefficiant of Variation	65.538 %
Statistical Modes...			
Skewness	2.601	Mode	.106 µm
Curtosis	13.851	Median	.325 µm
Span	1.68	Mean/Median Ratio	1.177
Uniformity	.5		
Specific Surface Area	221185.97 cm2/cm3		
Density	1. g/cc		
Form Factor	1. g/cc		

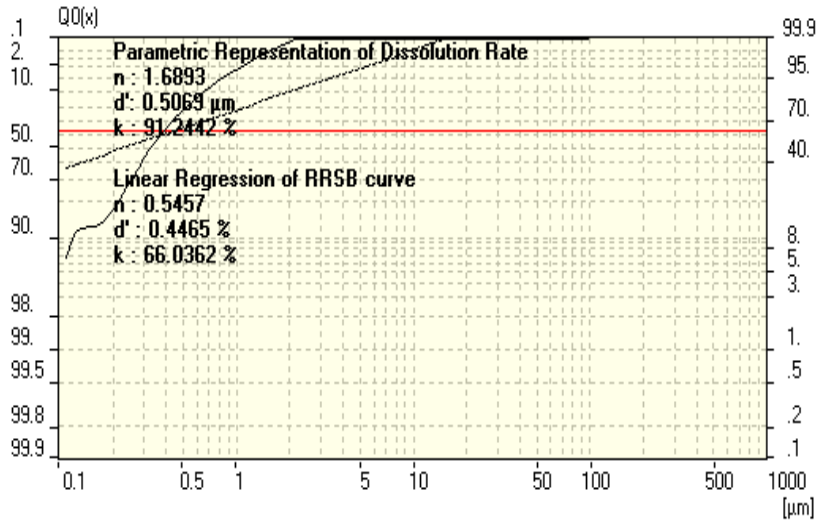

Ningde Amperex Tech. Exhibit No. 2043
Zhuhai CosMX Battery Co. Ltd. v. Ningde Amperex Tech.
IPR2025-00432, U.S. Patent No. 11,575,148
Page 84 of 123

Meas.No. 300	Date 21.2.2007	Time 10:25	Operator	ID	Serial No. 778

Al2O3, D50 = 1 micron

Measuring Range	0.1 [µm] - 100.9 [µm]	Pump	50 [%]
Resolution	102 Channels (20 mm / 38 mm)		
Absorption	10.00 [%]	Ultrasonic	On
Measurement Duration	100 [Scans]		

Regularization / Modell 5793.601

Fraunhofer Calculation selected.

Mean	Values...						
D43 =	1.22 µm	D42 =	.99 µm	D41 =	.81 µm	D40 =	.67 µm
D32 =	.81 µm	D31 =	.66 µm	D30 =	.55 µm		
D21 =	.54 µm	D20 =	.46 µm				
D10 =	.12 µm						

Statistical Means...			
Arithmetic Mean Diameter	.382 µm	Variance	.063 µm2
Geometric Mean Diameter	.322 µm	Mean Squre Deviation	.25 µm
Quadratic Square Mean Diameter	.456 µm	Average Deviation	.171 µm
Harmonic Mean Diameter	.271 µm	Coefficiant of Variation	65.538 %
Statistical Modes...			
Skewness	2.601	Mode	.106 µm
Curtosis	13.851	Median	.325 µm
Span	1.68	Mean/Median Ratio	1.177
Uniformity	.5		
Specific Surface Area	221185.97 cm2/cm3		
Density	1. g/cc		
Form Factor	1. g/cc		

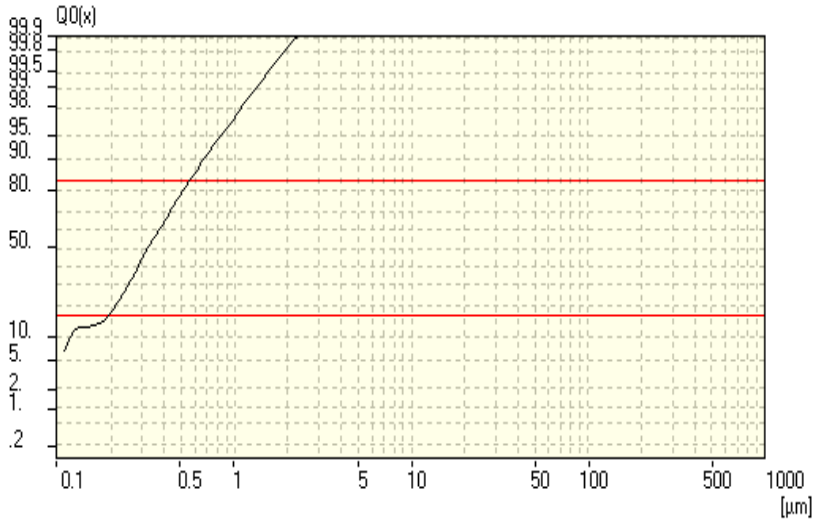

Ningde Amperex Tech. Exhibit No. 2043
Zhuhai CosMX Battery Co. Ltd. v. Ningde Amperex Tech.
IPR2025-00432, U.S. Patent No. 11,575,148
Page 85 of 123

Meas.No. 300	Date 21.2.2007	Time 10:25	Operator	ID	Serial No. 778

Al2O3, D50 = 1 micron

Measuring Range	0.1 [µm] - 100.9 [µm]	Pump	50 [%]
Resolution	102 Channels (20 mm / 38 mm)		
Absorption	10.00 [%]	Ultrasonic	On
Measurement Duration	100 [Scans]		

Regularization / Modell 5793.601

Fraunhofer Calculation selected.

Mean	Values...						
D43 =	1.22 µm	D42 =	.99 µm	D41 =	.81 µm	D40 =	.67 µm
D32 =	.81 µm	D31 =	.66 µm	D30 =	.55 µm		
D21 =	.54 µm	D20 =	.46 µm				
D10 =	.12 µm						

Statistical Means...			
Arithmetic Mean Diameter	.382 µm	Variance	.063 µm2
Geometric Mean Diameter	.322 µm	Mean Squre Deviation	.25 µm
Quadratic Square Mean Diameter	.456 µm	Average Deviation	.171 µm
Harmonic Mean Diameter	.271 µm	Coefficiant of Variation	65.538 %
Statistical Modes...			
Skewness	2.601	Mode	.106 µm
Curtosis	13.851	Median	.325 µm
Span	1.68	Mean/Median Ratio	1.177
Uniformity	.5		
Specific Surface Area	221185.97 cm2/cm3		
Density	1. g/cc		
Form Factor	1. g/cc		

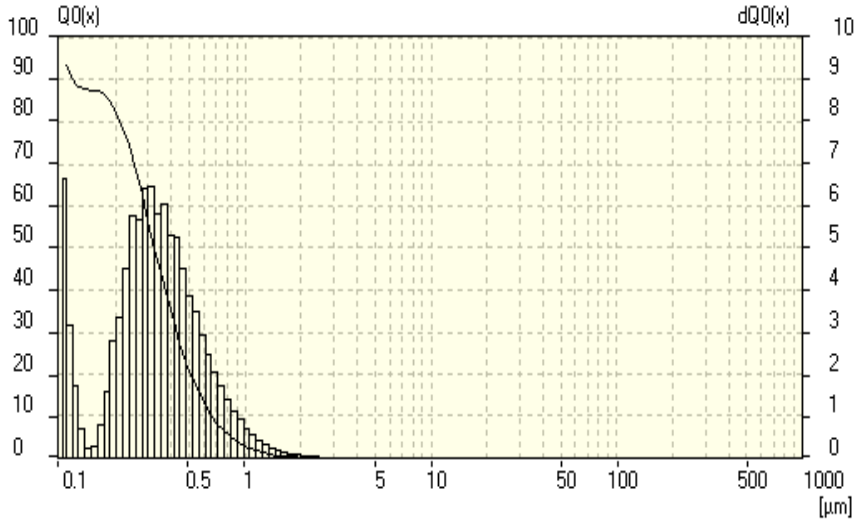

Ningde Amperex Tech. Exhibit No. 2043
Zhuhai CosMX Battery Co. Ltd. v. Ningde Amperex Tech.
IPR2025-00432, U.S. Patent No. 11,575,148
Page 86 of 123

Meas.No. 300	Date 21.2.2007	Time 10:25	Operator	ID	Serial No. 778

Al2O3, D50 = 1 micron

Measuring Range	0.1 [µm] - 100.9 [µm]	Pump	50 [%]
Resolution	102 Channels (20 mm / 38 mm)		
Absorption	10.00 [%]	Ultrasonic	On
Measurement Duration	100 [Scans]		

Regularization / Modell 5793.601

Fraunhofer Calculation selected.

Mean	Values...						
D43 =	1.22 µm	D42 =	.99 µm	D41 =	.81 µm	D40 =	.67 µm
D32 =	.81 µm	D31 =	.66 µm	D30 =	.55 µm		
D21 =	.54 µm	D20 =	.46 µm				
D10 =	.12 µm						

Statistical Means...			
Arithmetic Mean Diameter	.382 µm	Variance	.063 µm2
Geometric Mean Diameter	.322 µm	Mean Squre Deviation	.25 µm
Quadratic Square Mean Diameter	.456 µm	Average Deviation	.171 µm
Harmonic Mean Diameter	.271 µm	Coefficiant of Variation	65.538 %
Statistical Modes...			
Skewness	2.601	Mode	.106 µm
Curtosis	13.851	Median	.325 µm
Span	1.68	Mean/Median Ratio	1.177
Uniformity	.5		
Specific Surface Area	221185.97 cm2/cm3		
Density	1. g/cc		
Form Factor	1. g/cc		

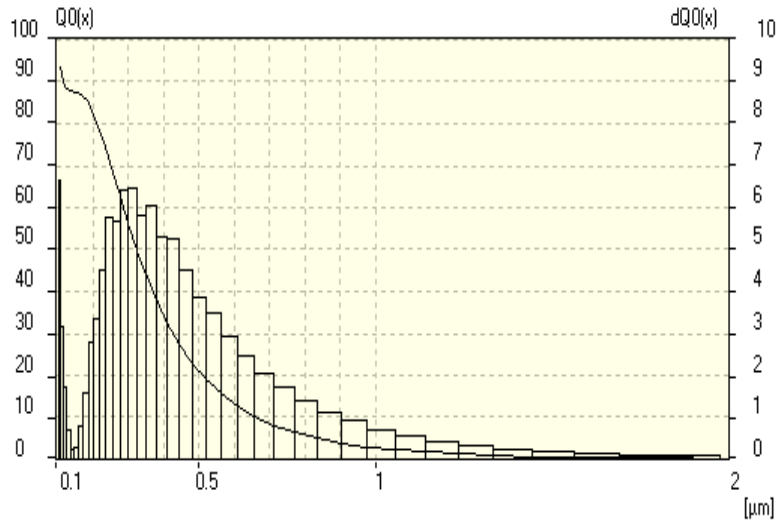

Ningde Amperex Tech. Exhibit No. 2043
Zhuhai CosMX Battery Co. Ltd. v. Ningde Amperex Tech.
IPR2025-00432, U.S. Patent No. 11,575,148
Page 87 of 123

Meas.No. 300	Date 21.2.2007	Time 10:25	Operator	ID	Serial No. 778

Al2O3, D50 = 1 micron

Measuring Range	0.1 [µm] - 100.9 [µm]	Pump	50 [%]
Resolution	102 Channels (20 mm / 38 mm)		
Absorption	10.00 [%]	Ultrasonic	On
Measurement Duration	100 [Scans]		

Regularization / Modell 5793.601

Fraunhofer Calculation selected.

Mean	Values...						
D43 =	1.22 µm	D42 =	.99 µm	D41 =	.81 µm	D40 =	.67 µm
D32 =	.81 µm	D31 =	.66 µm	D30 =	.55 µm		
D21 =	.54 µm	D20 =	.46 µm				
D10 =	.12 µm						

Statistical Means...			
Arithmetic Mean Diameter	.382 µm	Variance	.063 µm2
Geometric Mean Diameter	.322 µm	Mean Squre Deviation	.25 µm
Quadratic Square Mean Diameter	.456 µm	Average Deviation	.171 µm
Harmonic Mean Diameter	.271 µm	Coefficiant of Variation	65.538 %
Statistical Modes...			
Skewness	2.601	Mode	.106 µm
Curtosis	13.851	Median	.325 µm
Span	1.68	Mean/Median Ratio	1.177
Uniformity	.5		
Specific Surface Area	221185.97 cm2/cm3		
Density	1. g/cc		
Form Factor	1. g/cc		

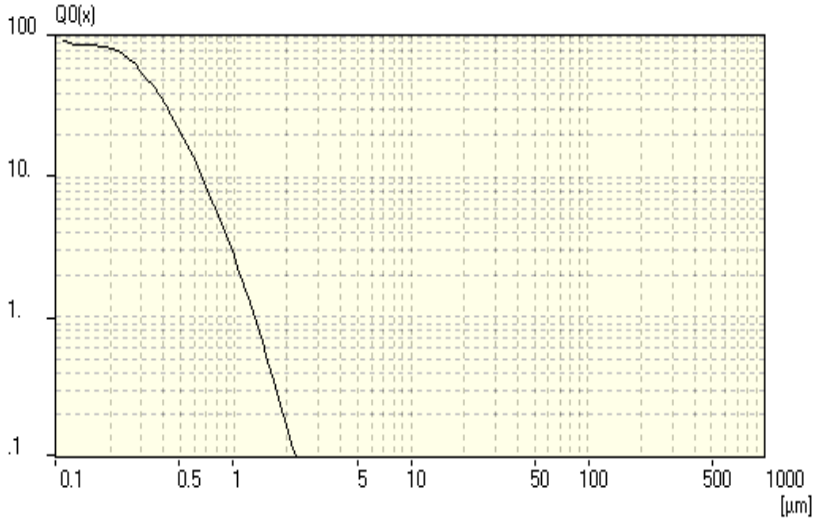

Ningde Amperex Tech. Exhibit No. 2043
Zhuhai CosMX Battery Co. Ltd. v. Ningde Amperex Tech.
IPR2025-00432, U.S. Patent No. 11,575,148
Page 88 of 123

Meas.No. 300	Date 21.2.2007	Time 10:25	Operator	ID	Serial No. 778

Al2O3, D50 = 1 micron

Measuring Range	0.1 [µm] - 100.9 [µm]	Pump	50 [%]
Resolution	102 Channels (20 mm / 38 mm)		
Absorption	10.00 [%]	Ultrasonic	On
Measurement Duration	100 [Scans]		

Regularization / Modell 5793.601

Fraunhofer Calculation selected.

Mean	Values...						
D43 =	1.22 µm	D42 =	.99 µm	D41 =	.81 µm	D40 =	.67 µm
D32 =	.81 µm	D31 =	.66 µm	D30 =	.55 µm		
D21 =	.54 µm	D20 =	.46 µm				
D10 =	.12 µm						

Statistical Means...			
Arithmetic Mean Diameter	.382 µm	Variance	.063 µm2
Geometric Mean Diameter	.322 µm	Mean Squre Deviation	.25 µm
Quadratic Square Mean Diameter	.456 µm	Average Deviation	.171 µm
Harmonic Mean Diameter	.271 µm	Coefficiant of Variation	65.538 %
Statistical Modes...			
Skewness	2.601	Mode	.106 µm
Curtosis	13.851	Median	.325 µm
Span	1.68	Mean/Median Ratio	1.177
Uniformity	.5		
Specific Surface Area	221185.97 cm2/cm3		
Density	1. g/cc		
Form Factor	1. g/cc		

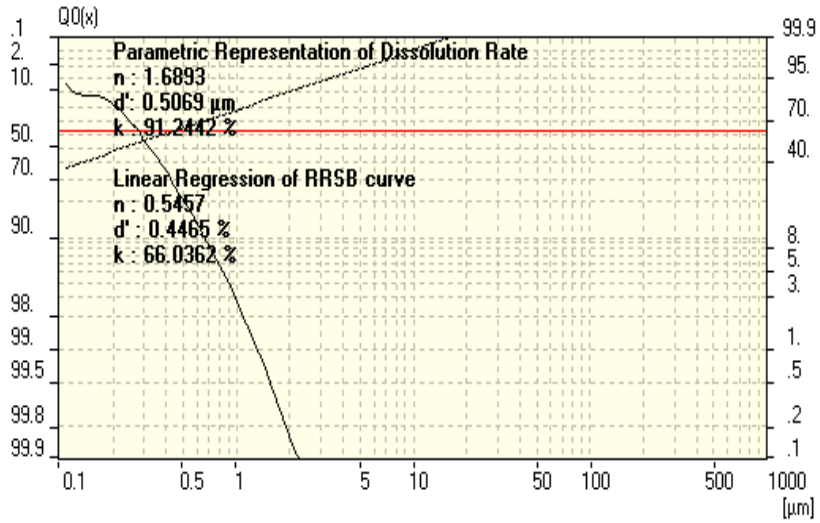

Meas.No. 300	Date 21.2.2007	Time 10:25	Operator	ID	Serial No. 778

Al2O3, D50 = 1 micron

Measuring Range	0.1 [µm] - 100.9 [µm]	Pump	50 [%]
Resolution	102 Channels (20 mm / 38 mm)		
Absorption	10.00 [%]	Ultrasonic	On
Measurement Duration	100 [Scans]		

Regularization / Modell 5793.601

Fraunhofer Calculation selected.

Mean	Values...						
D43 =	1.22 µm	D42 =	.99 µm	D41 =	.81 µm	D40 =	.67 µm
D32 =	.81 µm	D31 =	.66 µm	D30 =	.55 µm		
D21 =	.54 µm	D20 =	.46 µm				
D10 =	.12 µm						

Statistical Means...			
Arithmetic Mean Diameter	.382 µm	Variance	.063 µm2
Geometric Mean Diameter	.322 µm	Mean Squre Deviation	.25 µm
Quadratic Square Mean Diameter	.456 µm	Average Deviation	.171 µm
Harmonic Mean Diameter	.271 µm	Coefficiant of Variation	65.538 %
Statistical Modes...			
Skewness	2.601	Mode	.106 µm
Curtosis	13.851	Median	.325 µm
Span	1.68	Mean/Median Ratio	1.177
Uniformity	.5		
Specific Surface Area	221185.97 cm2/cm3		
Density	1. g/cc		
Form Factor	1. g/cc		

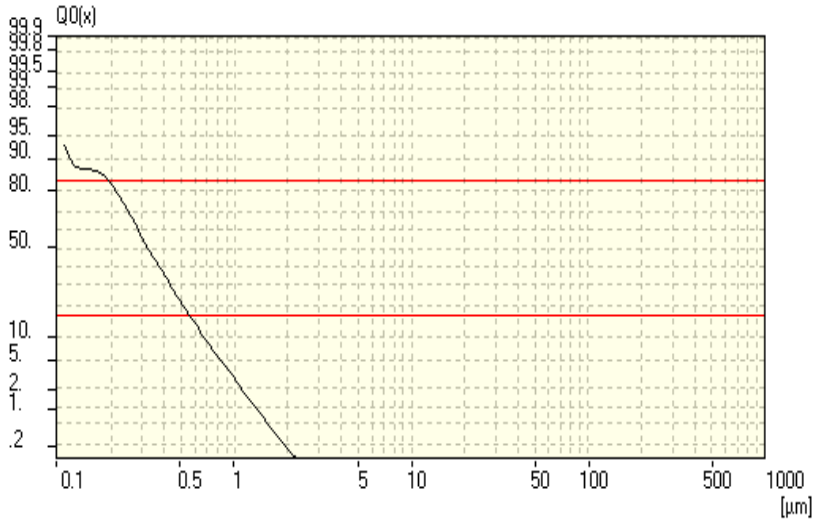

Ningde Amperex Tech. Exhibit No. 2043
Zhuhai CosMX Battery Co. Ltd. v. Ningde Amperex Tech.
IPR2025-00432, U.S. Patent No. 11,575,148
Page 90 of 123

Meas.No. 300	Date 21.2.2007	Time 10:25	Operator	ID	Serial No. 778

Al2O3, D50 = 1 micron

Measuring Range	0.1 [µm] - 100.9 [µm]	Pump	50 [%]
Resolution	102 Channels (20 mm / 38 mm)		
Absorption	10.00 [%]	Ultrasonic	On
Measurement Duration	100 [Scans]		

Regularization / Modell 5793.601

Fraunhofer Calculation selected.

Mean	Values...						
D43 =	1.23 µm	D42 =	.99 µm	D41 =	.81 µm	D40 =	.67 µm
D32 =	.81 µm	D31 =	.66 µm	D30 =	.55 µm		
D21 =	.54 µm	D20 =	.46 µm				
D10 =	.42 µm						

Statistical Means...			
Arithmetic Mean Diameter	1.226 µm	Variance	.706 µm2
Geometric Mean Diameter	.995 µm	Mean Squre Deviation	.84 µm
Quadratic Square Mean Diameter	1.484 µm	Average Deviation	.631 µm
Harmonic Mean Diameter	.807 µm	Coefficiant of Variation	68.579 %
Statistical Modes...			
Skewness	1.591	Mode	.932 µm
Curtosis	3.307	Median	.992 µm
Span	1.952	Mean/Median Ratio	1.235
Uniformity	.61		
Specific Surface Area	74388.21 cm2/cm3		
Density	1. g/cc		
Form Factor	1. g/cc		

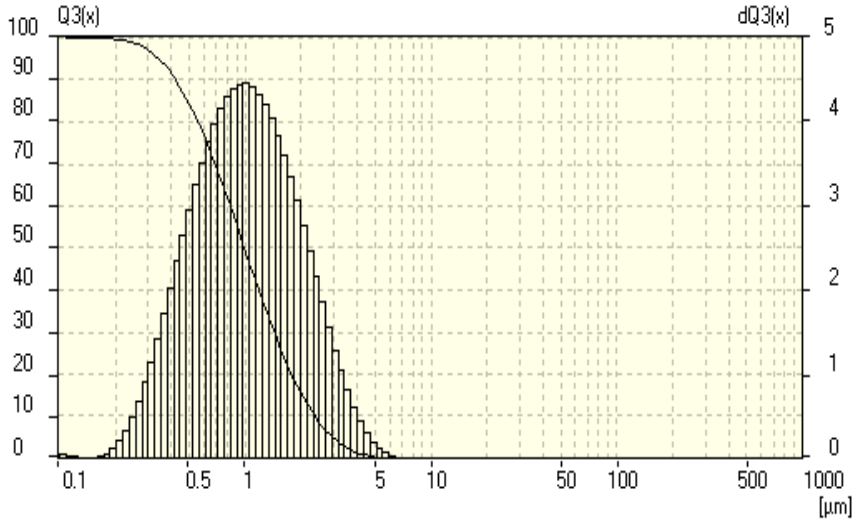

Meas.No. 300	Date 21.2.2007	Time 10:25	Operator	ID	Serial No. 778

Al2O3, D50 = 1 micron

Measuring Range	0.1 [µm] - 100.9 [µm]	Pump	50 [%]
Resolution	102 Channels (20 mm / 38 mm)		
Absorption	10.00 [%]	Ultrasonic	On
Measurement Duration	100 [Scans]		

Regularization / Modell 5793.601

Fraunhofer Calculation selected.

Mean	Values...						
D43 =	1.23 µm	D42 =	.99 µm	D41 =	.81 µm	D40 =	.67 µm
D32 =	.81 µm	D31 =	.66 µm	D30 =	.55 µm		
D21 =	.54 µm	D20 =	.46 µm				
D10 =	.42 µm						

Statistical Means...			
Arithmetic Mean Diameter	1.226 µm	Variance	.706 µm2
Geometric Mean Diameter	.995 µm	Mean Squre Deviation	.84 µm
Quadratic Square Mean Diameter	1.484 µm	Average Deviation	.631 µm
Harmonic Mean Diameter	.807 µm	Coefficiant of Variation	68.579 %
Statistical Modes...			
Skewness	1.591	Mode	.932 µm
Curtosis	3.307	Median	.992 µm
Span	1.952	Mean/Median Ratio	1.235
Uniformity	.61		
Specific Surface Area	74388.21 cm2/cm3		
Density	1. g/cc		
Form Factor	1. g/cc		

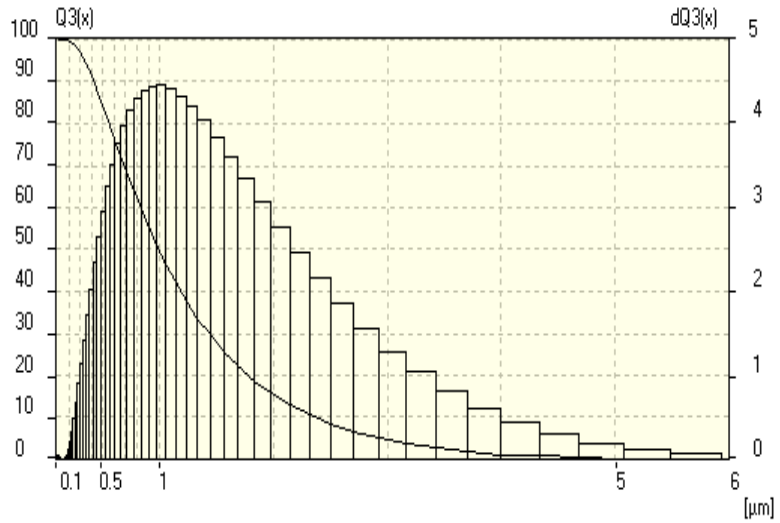

Ningde Amperex Tech. Exhibit No. 2043
Zhuhai CosMX Battery Co. Ltd. v. Ningde Amperex Tech.
IPR2025-00432, U.S. Patent No. 11,575,148
Page 92 of 123

Meas.No. 300	Date 21.2.2007	Time 10:25	Operator	ID	Serial No. 778

Al2O3, D50 = 1 micron

Measuring Range	0.1 [µm] - 100.9 [µm]	Pump	50 [%]
Resolution	102 Channels (20 mm / 38 mm)		
Absorption	10.00 [%]	Ultrasonic	On
Measurement Duration	100 [Scans]		

Regularization / Modell 5793.601

Fraunhofer Calculation selected.

Mean	Values...						
D43 =	1.23 µm	D42 =	.99 µm	D41 =	.81 µm	D40 =	.67 µm
D32 =	.81 µm	D31 =	.66 µm	D30 =	.55 µm		
D21 =	.54 µm	D20 =	.46 µm				
D10 =	.42 µm						

Statistical Means...			
Arithmetic Mean Diameter	1.226 µm	Variance	.706 µm2
Geometric Mean Diameter	.995 µm	Mean Squre Deviation	.84 µm
Quadratic Square Mean Diameter	1.484 µm	Average Deviation	.631 µm
Harmonic Mean Diameter	.807 µm	Coefficiant of Variation	68.579 %
Statistical Modes...			
Skewness	1.591	Mode	.932 µm
Curtosis	3.307	Median	.992 µm
Span	1.952	Mean/Median Ratio	1.235
Uniformity	.61		
Specific Surface Area	74388.21 cm2/cm3		
Density	1. g/cc		
Form Factor	1. g/cc		

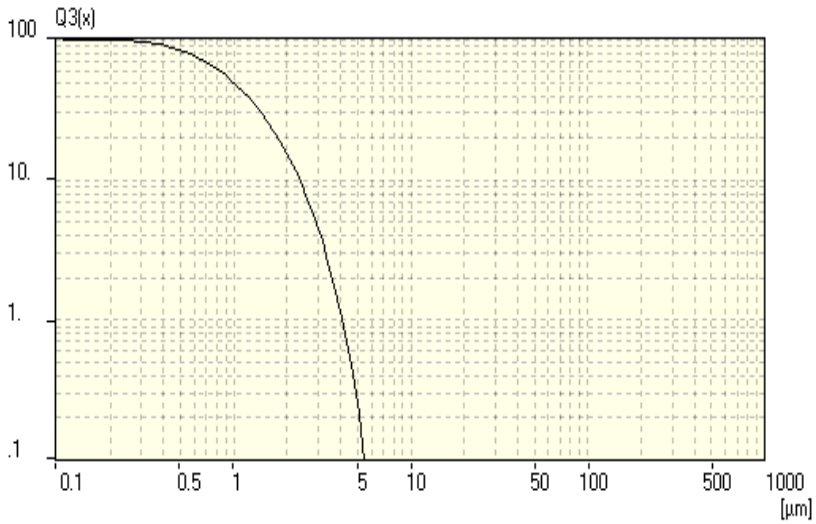

Ningde Amperex Tech. Exhibit No. 2043
Zhuhai CosMX Battery Co. Ltd. v. Ningde Amperex Tech.
IPR2025-00432, U.S. Patent No. 11,575,148
Page 93 of 123

Meas.No. 300	Date 21.2.2007	Time 10:25	Operator	ID	Serial No. 778

Al2O3, D50 = 1 micron

Measuring Range	0.1 [µm] - 100.9 [µm]	Pump	50 [%]
Resolution	102 Channels (20 mm / 38 mm)		
Absorption	10.00 [%]	Ultrasonic	On
Measurement Duration	100 [Scans]		

Regularization / Modell 5793.601

Fraunhofer Calculation selected.

Mean	Values...						
D43 =	1.23 µm	D42 =	.99 µm	D41 =	.81 µm	D40 =	.67 µm
D32 =	.81 µm	D31 =	.66 µm	D30 =	.55 µm		
D21 =	.54 µm	D20 =	.46 µm				
D10 =	.42 µm						

Statistical Means...			
Arithmetic Mean Diameter	1.226 µm	Variance	.706 µm2
Geometric Mean Diameter	.995 µm	Mean Squre Deviation	.84 µm
Quadratic Square Mean Diameter	1.484 µm	Average Deviation	.631 µm
Harmonic Mean Diameter	.807 µm	Coefficiant of Variation	68.579 %
Statistical Modes...			
Skewness	1.591	Mode	.932 µm
Curtosis	3.307	Median	.992 µm
Span	1.952	Mean/Median Ratio	1.235
Uniformity	.61		
Specific Surface Area	74388.21 cm2/cm3		
Density	1. g/cc		
Form Factor	1. g/cc		

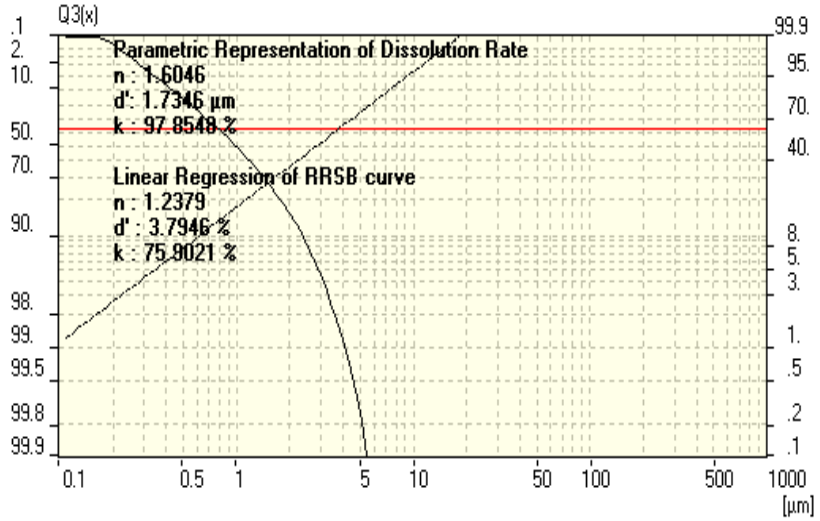

Ningde Amperex Tech. Exhibit No. 2043
Zhuhai CosMX Battery Co. Ltd. v. Ningde Amperex Tech.
IPR2025-00432, U.S. Patent No. 11,575,148
Page 94 of 123

Meas.No. 300	Date 21.2.2007	Time 10:25	Operator	ID	Serial No. 778

Al2O3, D50 = 1 micron

Measuring Range	0.1 [µm] - 100.9 [µm]	Pump	50 [%]
Resolution	102 Channels (20 mm / 38 mm)		
Absorption	10.00 [%]	Ultrasonic	On
Measurement Duration	100 [Scans]		

Regularization / Modell 5793.601

Fraunhofer Calculation selected.

Mean	Values...						
D43 =	1.23 µm	D42 =	.99 µm	D41 =	.81 µm	D40 =	.67 µm
D32 =	.81 µm	D31 =	.66 µm	D30 =	.55 µm		
D21 =	.54 µm	D20 =	.46 µm				
D10 =	.42 µm						

Statistical Means...			
Arithmetic Mean Diameter	1.226 µm	Variance	.706 µm2
Geometric Mean Diameter	.995 µm	Mean Squre Deviation	.84 µm
Quadratic Square Mean Diameter	1.484 µm	Average Deviation	.631 µm
Harmonic Mean Diameter	.807 µm	Coefficiant of Variation	68.579 %
Statistical Modes...			
Skewness	1.591	Mode	.932 µm
Curtosis	3.307	Median	.992 µm
Span	1.952	Mean/Median Ratio	1.235
Uniformity	.61		
Specific Surface Area	74388.21 cm2/cm3		
Density	1. g/cc		
Form Factor	1. g/cc		

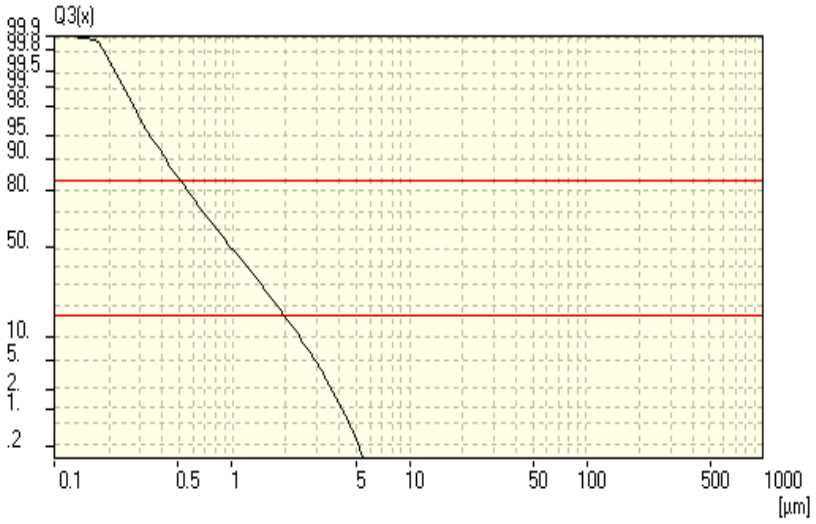

Ningde Amperex Tech. Exhibit No. 2043
Zhuhai CosMX Battery Co. Ltd. v. Ningde Amperex Tech.
IPR2025-00432, U.S. Patent No. 11,575,148
Page 95 of 123

Appendix-CPPS-9

Table 9-A. *Mean caliper diameter, surface and volume of standard shapes.*

Shape (and corresponding linear size measure)	Mean caliper diameter	Surface	Volume
Sphere with radius r	$2r$	$4\pi r^2 \approx 12.6 r^2$	$\left(\frac{4}{3}\right)\pi r^3 \approx 4.2 r^3$
Hemisphere with radius r	$\left(1+\frac{\pi}{4}\right)r$	$3\pi r^2$	$\left(\frac{2}{3}\right)\pi r^3$
Oblate spheroid with semiaxes $a=b$ and c ($c<a$) where $\varepsilon=\left[1-\left(\frac{c}{a}\right)^2\right]^{1/2}$	$c+\left(\frac{a}{\varepsilon}\right)\arcsin\varepsilon$	$2\pi a^2 + \pi\left(\frac{c^2}{\varepsilon}\right)\ln\left[\frac{1+\varepsilon}{1-\varepsilon}\right]$	$\left(\frac{4}{3}\right)\pi a^2 c$
Prolate spheroid with semiaxes $a=b$ and c ($c>a$), where $\varepsilon=\left[\left(\frac{c}{a}\right)^2-1\right]^{1/2}$	$c+\left(\frac{a}{\varepsilon}\right)\operatorname{arcsinh}\varepsilon$	$2\pi a^2 + 2\pi\left(\frac{c^2}{\varepsilon}\right)\arcsin\left(\frac{a\varepsilon}{c}\right)$	$\left(\frac{4}{3}\right)\pi a^2 c$
Cylinder of length l and radius r	$\frac{1}{2}(l+\pi r)$	$2\pi r(l+r)$	$\pi l r^2$
Thin rod (needle), i.e. $r\to 0$	$\frac{l}{2}$	$\to 0$	$\to 0$
Thin disc (platelet), i.e. $l\to 0$	$\frac{\pi r}{2}$	$2\pi r^2$	$\to 0$
Tetrahedron of edge length a	$a\left(\frac{3}{\pi}\right)\arccos\left(\frac{1}{3}\right)^{1/2} \approx 0.91a$	$\sqrt{3}a^2 \approx 1.73a^2$	$\left(\frac{\sqrt{2}}{12}\right)a^3 \approx 0.12a^3$
Cube of edge length a	$\left(\frac{3}{2}\right)a$	$6a^2$	a^3
Octahedron of edge length a	$a\left(\frac{6}{\pi}\right)\arccos\left(\frac{2}{3}\right)^{1/2} \approx 1.18a$	$2\sqrt{3}a^2 \approx 3.46a^2$	$\left(\frac{2}{9}\right)^{1/2}a^3 \approx 0.47a^3$

Ningde Amperex Tech. Exhibit No. 2043
Zhuhai CosMX Battery Co. Ltd. v. Ningde Amperex Tech.
IPR2025-00432, U.S. Patent No. 11,575,148
Page 96 of 123

Dodecahedron of edge length a	$a\left(\frac{15}{\pi}\right)\arccos\left[\left(\frac{1}{2}\right)+\left(\frac{\sqrt{5}}{10}\right)\right]^{1/2}$ $\approx 2.64\,a$	$3\left[5\left(5+2\sqrt{5}\right)\right]^{1/2}a^2$ $\approx 20.6\,a^2$	$\left(\frac{15+7\sqrt{5}}{4}\right)a^3$ $\approx 7.66\,a^3$
Tetrakaidecahedron of edge length a	$3\,a$	$6\left(1+2\sqrt{3}\right)a^2$ $\approx 26.8\,a^2$	$8\sqrt{2}\,a^3 \approx 11.3\,a^3$
Icosahedron of edge length a	$a\left(\frac{15}{\pi}\right)\arccos\left[\frac{1+\left(2\sqrt{5}/5\right)}{\left(\frac{3}{2}\right)+\left(\frac{3\sqrt{5}}{10}\right)}\right]^{1/2}$ $\approx 1.74\,a$	$5\sqrt{3}\,a^2 \approx 8.66\,a^2$	$\left(\frac{5\left(3+\sqrt{5}\right)}{12}\right)a^3$ $\approx 2.18\,a^3$
Parallelepiped of edge lengths a, b and c	$\frac{a+b+c}{2}$	$2\left(ab+bc+ca\right)$	$a\,b\,c$

Ningde Amperex Tech. Exhibit No. 2043
Zhuhai CosMX Battery Co. Ltd. v. Ningde Amperex Tech.
IPR2025-00432, U.S. Patent No. 11,575,148
Page 97 of 123

Appendix-CPPS-14

14-A. Introduction to suspension rheology

14-A-1. States of matter (basic rheological classification)

- gas (compressible fluid)
- liquid (incompressible fluid)
- solid

Deborah number: $De = \frac{t_{material}}{t_{process}} = \frac{characteristic\ material\ time\ (relaxation\ time)}{characteristic\ \ process\ time\ (deformation\ time)}$

- fluids ($De << 1$, for purely viscous fluids $De \to 0$)
- visco-elastic and elastico-viscous materials ($De \approx 1$, Maxwell fluid, Kelvin solid)
- solids ($De >> 1$, for purely elastic solids $De \to \infty$)

Order of magnitude of viscosities for different classes of materials (only orientational values for typical materials of the respective class !)

Material	Viscosity	Remark
Gases	10 μPas	at room temperature
Water, ethanol, mercury	1 mPas	at room temperature
Metal melts	1 mPas	at high temperature
Ceramic suspensions	10 mPas – 1000 mPas	apparent viscosity
Oil	1 Pas	apparent viscosity
Ceramic pastes	10 Pas – 1000 Pas	apparent viscosity
Glass melts	10 Pas	at high temperature
Solid glass	10^{18} Pas	Extrapolated value

14-A-2. Basic 1-D rheological models

Model	Constitutive equation (1-D)	Mechanical analogue	Rheological characteristic	Response
Hooke	$\tau = G\,\gamma$	spring	ideally viscous	– on de-loading: deformation and stresses restore instantaneously
Newton	$\tau = \mu\,\dot{\gamma}$	dashpot	perfectly elastic	– on de-loading: deformation remains, stresses restore instantaneously
Maxwell	$\dot{\gamma} = \frac{\dot{\tau}}{G} + \frac{\tau}{\mu}$	spring and dashpot in series	stress relaxation	– on de-loading: stresses relax slowly

Ningde Amperex Tech. Exhibit No. 2043
Zhuhai CosMX Battery Co. Ltd. v. Ningde Amperex Tech.
IPR2025-00432, U.S. Patent No. 11,575,148
Page 98 of 123

			with $t_{relax} = \frac{\mu}{G}$	$\tau = \tau_0 \cdot e^{-\frac{t}{t_{relax}}}$
Kelvin	$\tau = G\,\gamma + \mu\,\dot{\gamma}$	spring and dashpot parallel	Delayed response with $t_{delay} = \frac{\mu}{G}$	– on de-loading: deformation relaxes slowly $\gamma = \gamma_0 \cdot e^{-\frac{t}{t_{delay}}}$ – on loading: $\gamma = \gamma_{final} \cdot \left(1 - e^{-\frac{t}{t_{delay}}}\right)$

(only here γ is the shear deformation, $\dot{\gamma}$ the shear rate !)

!!! In the following γ is the shear rate !!!

Definition of the 1-D shear stress τ and shear rate γ for important geometries and flow types:

- In (rectangular) Cartesian coordinates with flow in direction x (plane Couette flow):
  - Shear stress $\tau \equiv \tau_{xy}$ (= x-y-component of the stress tensor),
  - shear rate $\gamma \equiv \frac{dv_x}{dy}$ (= y-direction gradient of the x-component of the velocity vector = x-y-component of the rate of deformation tensor)
- In cylindrical (semi-polar) coordinates with flow in axial direction (cylindrical Poiseuille flow):
  - Shear stress $\tau \equiv \tau_{rz}$ (= r-z-component of the stress tensor),
  - shear rate $\gamma \equiv \frac{dv_z}{dr}$ (= radial gradient of the axial velocity component = r-z-component of the rate of deformation tensor)
- In cylindrical (semi-polar) coordinates with flow in tangential direction (cylindrical Couette flow):
  - Shear stress $\tau \equiv \tau_{r\theta}$ (= r-θ-component of the stress tensor),
  - shear rate $\gamma \equiv \frac{dv_\theta}{dr} = \omega$ (= radial gradient of the angular velocity = r-θ-component of the rate of deformation tensor)

Ningde Amperex Tech. Exhibit No. 2043
Zhuhai CosMX Battery Co. Ltd. v. Ningde Amperex Tech.
IPR2025-00432, U.S. Patent No. 11,575,148
Page 99 of 123

14-A-3. Principle of rheology – fluid flow along solid surfaces

Critical assumption (boundary condition):

Fluid sticks on the solid surface (absence of wall slip)

Note: All "normal" monophase liquids (not gases ! not suspensions !) are assumed to stick on solid surfaces during flow, irrespective of their physico-chemical adherence or wetting behavior with respect to these surfaces ! Even mercury sticks on the glass surface during flow through capillaries ! (Coleman, Markovitz & Noll, 1966)

14-A-4. Simple viscometers (basic formulae)

- Falling ball viscometer: $\eta = \dfrac{D^2\,(\rho_s - \rho_l)\,g}{18\,v}$ (Stokes equation)

- Capillary viscometer: $\tau = \dfrac{D\Delta p}{4L}$ (Δp = pressure difference)

  $\gamma = \dfrac{8\,\bar{v}_z}{D}$ ($\bar{v}_z$ = mean velocity)

- Rotational viscometer: $\tau = \dfrac{M}{2\pi\,R_1^2 h}$ (M = torque)

  $\gamma = \dfrac{\omega}{1 - \left(R_1 / R_2 \right)^2}$ (ω = angular velocity)

14-A-5. Rational theory of viscometry

$$\mathbf{T} = \mathbf{T}\,(\mathbf{D})$$

- Linear case – Newtonian fluids (Navier-Stokes fluids = 3-D "Newtonian fluids", compressible or incompressible):

$$\mathbf{T} = \xi\,(tr\ \mathbf{D})\,\mathbf{1} + 2\,\mu\,\mathbf{D}$$

- Non-linear case – non-Newtonian fluids (purely viscous, Reiner-Rivlin fluids, compressible or incompressible)

$$\mathbf{T} = \phi_0(...)\,\mathbf{1} + \phi_1(...)\,\mathbf{D} + \phi_2(...)\,\mathbf{D}^2$$

where the ϕ_i are scalar functions of ρ, T and the three principal invariants I_D, II_D and III_D.

Ningde Amperex Tech. Exhibit No. 2043
Zhuhai CosMX Battery Co. Ltd. v. Ningde Amperex Tech.
IPR2025-00432, U.S. Patent No. 11,575,148
Page 100 of 123

- For incompressible fluids (= liquids) $div\ \mathbf{v} = tr\ \mathbf{D} = I_D = 0$ and for viscometric flows (equivalent to simple shear flows) $\det \mathbf{D} = III_D = 0$. Furthermore for incompressible fluids the pressure is hydrostatic and therefore an arbitrary scalar, into which the first above r.h.s. term can be absorbed. For viscometric flows the third r.h.s. term determines normal stresses only. When these are without concern we have for the stress tensor

$$\mathbf{T} = -p\mathbf{1} + \phi_1(II_D)\,\mathbf{D}$$

Since $II_D = \frac{1}{2}\left[(tr\ \mathbf{D})^2 - tr\left(\mathbf{D}^2\right)\right]$ and $tr\ \mathbf{D} = 0$ we have for the shear stress tensor

$$\boldsymbol{\tau} = \phi_1\left(-tr\ (\mathbf{D}^2)\right)\mathbf{D}$$

("generalized Newtonian fluids", only incompressible !)

Specialization to 1-D shear stresses

- Linear case – Newtonian fluids $\tau = \mu\,\gamma$
  where μ = viscosity (coefficient of dynamic shear viscosity).

- Nonlinear case – Generalized Newtonian fluids $\tau = \eta(\gamma)\,\gamma$
  where $\eta(\gamma)$ = apparent viscosity.

  Special models for non-Newtonian liquids in 1-D:

  – Power law (Ostwald - De Waele model): $\tau = K\gamma^n$
  – Bingham model: $\tau = \tau_0 + K\gamma$
  – Herschel-Bulkley model (generalized Bingham model): $\tau = \tau_0 + K\gamma^n$
  – Bird-Carreau model, (modified) Cross model, Prandtl-Powell-Eyring model

14-A-6. Temperature dependence of viscosity

- AFE - type equations: $\eta = \eta_0\ e^{B/T}$ (Arrhenius, Andrade, Frenkel, Eyring)

  (theory of reaction rates)

- WLF - type equations: $\eta = \eta_0\ e^{\frac{A(T-T_0)}{B+(T-T_0)}}$ (William, Landel, Ferry)

  (free volume theory)

- VFT - type equations: $\eta = \eta_0\ e^{\frac{A}{T-T_0}}$ (Vogel, Fulcher, Tamann)

  (modified free volume theory)

- Purely empirical fit equations e.g. $\eta = \eta_0\ e^{-A(T-T_0)}$

Ningde Amperex Tech. Exhibit No. 2043
Zhuhai CosMX Battery Co. Ltd. v. Ningde Amperex Tech.
IPR2025-00432, U.S. Patent No. 11,575,148
Page 101 of 123

14-A-7. Concentration dependence of viscosity

For dilute systems:

Definition: Relative viscosity $\eta_r = \frac{\eta}{\eta_0} = \frac{viscosity\ of\ \ suspension}{viscosity\ of\ \ pure\ liquid}$

- Einstein formula: $\eta_r = 1 + 2.5\,\phi$ (ϕ = volume fraction of solids)

  (for perfectly rigid non-interacting spheres)

- Second-order formulae for rigid spheres with first-order interaction effects:

$$\eta_r = 1 + 2.5\,\phi + B\,\phi^2 + \ldots \qquad (B = 4.4 - 14.1)$$

For concentrated systems:

Definition: Reduced volume fraction $\phi_r = \frac{\phi}{\phi_{\max}} = \frac{volume\ \ fraction}{maximum\ volume\ \ fraction}$

Note: The highest possible $\phi_{\max}$ for a system of monosized spheres corresponds to closest packing, i.e. 74 %. For real systems the value $\phi_{\max}$ is often close to the value of random close packing of monosized spheres, i.e. 64 %.

- Shell model formulae for monodisperse systems $\eta_r = C\left(\frac{\sqrt[3]{\phi_r}}{1-\sqrt[3]{\phi_r}}\right)$

  (where C is a model-dependent parameter ranging from 0.589 to 1.125)

- Eilers formula: $\eta_r = \left(1 + 1.25\,\phi \cdot \frac{1}{1-\phi_r}\right)^2$

- Mooney formula: $\eta_r = \exp\left(C\phi \cdot \frac{1}{1-\phi_r}\right)$

  (reduces to Einstein if C is chosen to be 2.5)

- Krieger formula: $\eta_r = \left(\frac{1}{1-\phi_r}\right)^N$

  (reduces to Einstein if N is chosen to be $2.5\,\phi_{\max}$)

Ningde Amperex Tech. Exhibit No. 2043
Zhuhai CosMX Battery Co. Ltd. v. Ningde Amperex Tech.
IPR2025-00432, U.S. Patent No. 11,575,148
Page 102 of 123

14-B. Rheology of suspensions with anisometric particles

14-B-1. Effective, relative and intrinsic viscosity

Effective properties are the macroscopic (i.e. overall or large-scale), properties of multiphase materials. In general they are dependent on the constituent (i.e. phase) properties and the microstructure of the material. For two-phase solid-liquid mixtures with matrix-inclusion type microstructure (suspensions) the effective shear viscosity η (simply called "effective viscosity" in the sequel) can be assumed to be a function of the solids volume fraction ϕ. Note, however, that the assumption of a dependence exclusively on ϕ is only justifiable on pragmatic grounds, i.e. when higher-order microstructural information is lacking. Note further, that in assuming the existence of a unique (i.e. not shear-rate dependent) shear viscosity, one implicitly assumes purely viscous behavior (i.e. no viscoelastic effects) and Newtonian (linear) behavior of the whole suspension (and not only for the suspending medium). In the dilute limit, i.e. for volume fractions $\phi \to 0$, the effective viscosity η of suspensions with rigid, spherical particles is given by the Einstein relation

$$\eta = \eta_0 \, (1 + 2.5\,\phi) \, .$$

In this equation, ϕ is the solids volume fraction, η denotes the effective suspension viscosity and η_0 the viscosity of the suspending medium (pure liquid). In order to simplify notation in the following text, we introduce the relative viscosity η_r,

$$\eta_r \equiv \frac{\eta}{\eta_0} \, ,$$

and the so-called intrinsic viscosity $[\eta]$,

$$[\eta] \equiv \lim_{\phi \to 0} \frac{\eta_r - 1}{\phi} \, .$$

Using intrinsic viscosity, the Einstein relation can be formally generalized to suspensions of anisometric particles, i.e.

$$\eta_r = 1 + [\eta]\,\phi \, .$$

Jeffery, in a rigorous treatment of the motion of a rigid ellipsoids and spheroids of a certain aspect ratio, was the first to calculate definite values for $[\eta]$ as a function of the particle aspect ratio. Therefore this can be called Jeffery-Einstein relation.

14-B-2. Intrinsic viscosity as a function of the particle aspect ratio

Jeffery (1922) calculated the motion of a single ellipsoidal particle immersed in a viscous liquid. He solved the equations of motion for the case of slow laminar (creeping) shear flow and showed that for a rotationally symmetric ellipsoid (spheroids) this motion is in general periodic, with its axis of revolution describing a cone about the perpendicular to the plane of

Ningde Amperex Tech. Exhibit No. 2043
Zhuhai CosMX Battery Co. Ltd. v. Ningde Amperex Tech.
IPR2025-00432, U.S. Patent No. 11,575,148
Page 103 of 123

the undisturbed motion of the liquid (Jeffery's orbit). Jeffery's investigation reveals no tendency of the spheroid to set its axis in any particular direction with regard to the undisturbed motion of the liquid. This finding is in agreement with modern research on fiber suspensions. Note, however, that the result has been derived for dilute suspensions (i.e. suspensions with non-interacting fibers or platelets) in shear flow, and cannot be assumed to be valid for either non-dilute suspensions (i.e. suspensions with interacting fibers or platelets) or other flow types, i.e. elongational flow.

According to Jeffery, only lower and upper bounds can be given for the intrinsic viscosity of spheroid suspensions. The lower bound (i.e. the minimum value of $[\eta]$) corresponds to the smallest dissipation of energy, the upper bound (i.e. the maximum value of $[\eta]$) to the largest. In modern notation, these bounds are given by the following formulae:

1. Minimum intrinsic viscosity

$$[\eta]_{\min} = \frac{1}{Ahd^4},$$

2. Maximum intrinsic viscosity

$$[\eta]_{\max} = \frac{1}{hd^3(h+d)^2}\left[\frac{h}{2A} + \frac{2d}{B} + \frac{hd^2}{C}\right].$$

In these equations, h is the length of the long axis ("height") and d the length of the short axis ("diameter"), and the coefficients A, B, C are

$$A = \frac{1}{4\,h^5\,\sin^4\theta}\left[\left(2 - 5\cos^2\theta\right)\frac{1}{\cos^4\theta} + 3\,\frac{1}{\sin\theta}\,\ln\tan\left(\frac{\theta}{2} + \frac{\pi}{4}\right)\right]$$

$$B = \frac{1}{h^5\,\sin^4\theta}\left[2 + \frac{1}{\cos^2\theta} - 3\,\frac{1}{\sin\theta}\,\ln\tan\left(\frac{\theta}{2} + \frac{\pi}{4}\right)\right]$$

$$C = \frac{1}{h^3\,\sin^4\theta}\left[\left(2 + \cos^2\theta\right)\frac{1}{\sin\theta}\,\ln\tan\left(\frac{\theta}{2} + \frac{\pi}{4}\right) - 3\right]$$

for prolate spheroids, for which $\theta \equiv \arccos\left(\frac{h}{d}\right)$, and

$$A = \frac{1}{4\,d^5\,\sin^4\theta}\left[-\left(5 - 2\cos^2\theta\right)\cos\theta + 3\,\frac{\theta}{\sin\theta}\right]$$

$$B = \frac{1}{d^5\,\sin^4\theta}\left[-\left(2 + \cos^2\theta\right)\frac{1}{\cos\theta} - 3\,\frac{\theta}{\sin\theta}\right]$$

$$C = \frac{1}{d^3\,\sin^4\theta}\left[\left(1 + 2\cos^2\theta\right)\frac{\theta}{\sin\theta} - 3\cos\theta\right]$$

Ningde Amperex Tech. Exhibit No. 2043
Zhuhai CosMX Battery Co. Ltd. v. Ningde Amperex Tech.
IPR2025-00432, U.S. Patent No. 11,575,148
Page 104 of 123

and for oblate spheroids, for which $\theta \equiv \arccos\left(\frac{d}{h}\right)$. Numerical values of the minimum and maximum intrinsic viscosity of spheroid suspensions are listed in Table 14-B-1 as a function of the aspect ratio $R \equiv h/d$.

Table 14-B-1. *Minimum and maximum intrinsic viscosity values of a suspension with oblate and prolate spheroids as a function of the particle aspect ratio (calculated according to Jeffery).*

Aspect ratio R	**Minimum of** $[\eta]$	**Maximum of** $[\eta]$
0	2.061	∞
1/100	2.067	86.3
1/50	2.072	43.9
1/40	2.075	35.4
1/30	2.080	26.9
1/20	2.089	18.4
1/10	2.116	9.96
1/9	2.122	9.11
1/8	2.130	8.27
1/7	2.139	7.43
1/6	2.151	6.58
1/5	2.168	5.74
1/4	2.193	4.91
1/3	2.232	4.08
1/2	2.306	3.27
1	2.5	2.5
2	2.174	2.819
3	2.088	3.088
4	2.053	3.327
5	2.035	3.548
6	2.025	3.753
7	2.019	3.948
8	2.015	4.134
9	2.012	4.312
10	2.010	4.485
20	2.002	5.999
30	2.001	7.316
40	2.001	8.529
50	2.000	9.677
100	2.000	14.9
∞	2.000	∞

Ningde Amperex Tech. Exhibit No. 2043
Zhuhai CosMX Battery Co. Ltd. v. Ningde Amperex Tech.
IPR2025-00432, U.S. Patent No. 11,575,148
Page 105 of 123

According to Brenner (1974), in simple shear flow the intrinsic viscosity of a suspension with axisymmetric particles (possessing fore-aft symmetry) is given by the expression

$$[\eta] = 5Q_1 - \frac{15}{4}Q_2\left\langle \sin^2\theta \right\rangle - \frac{5}{4B}\left(3Q_2 + 4Q_4\right)\left\langle \sin^2\theta\cos 2\phi \right\rangle + \frac{15}{2BP}\left(3Q_2 + 4Q_3\right)\left\langle \sin^2\theta\sin 2\phi \right\rangle$$

In this expression

$$B = \frac{5N}{3K_r}$$

is a dimensionless parameter and

$$P = \frac{\gamma}{D_r}$$

the rotary Péclet number, with γ being the shear rate and the rotary Brownian diffusion coefficient D_r given by the Stokes-Einstein equation

$$D_r = \frac{kT}{6V\eta_0 K_r},$$

where k is the Boltzmann constant, T the absolute temperature, V the particle volume and η_0 the viscosity of the suspending medium. The material constants N and K_r (connected to the rotation of the axisymmetric particle about a transverse axis) are dependent on the model shape chosen and the aspect ratio (true axis ratio, particle axis ratio) $R = a/b$, where a is the polar radius (for prolate shapes half of the length, for oblate shapes half of the thickness) and b the equatorial radius (for prolate shapes half of the thickness, for oblate shapes half of the diameter). For spheroids in general

$$K_r = \frac{2\left(R^2+1\right)}{3\left(R^2\alpha_1+\alpha_2\right)}$$

and

$$N = \frac{2\left(R^2-1\right)}{5\left(R^2\alpha_1+\alpha_2\right)}.$$

Moreover,

$$Q_1 = \frac{1}{5\alpha_3}$$

$$Q_2 = \frac{2}{15\alpha_3}\left(1-\frac{\alpha_5}{\alpha_6}\right)$$

Ningde Amperex Tech. Exhibit No. 2043
Zhuhai CosMX Battery Co. Ltd. v. Ningde Amperex Tech.
IPR2025-00432, U.S. Patent No. 11,575,148
Page 106 of 123

$$Q_3 = \frac{1}{5\alpha_3}\left[\frac{R(\alpha_1+\alpha_2)}{R^2\alpha_1+\alpha_2}\left(\frac{\alpha_3}{\alpha_4}\right)-1\right]$$

and

$$Q_4 = \frac{1}{5\alpha_3}\left[\frac{2R\alpha_3}{(R^2+1)\alpha_4}-1\right]$$

In these expressions the α 's are defined as

$$\alpha_1 = \frac{2}{R^2-1}\left(\beta R^2-1\right)$$

$$\alpha_2 = \frac{R^2}{R^2-1}(1-\beta)$$

$$\alpha_3 = \frac{R^2}{4\left(R^2-1\right)^2}\left(3\beta+2R^2-5\right)$$

$$\alpha_4 = \frac{R}{\left(R^2-1\right)^2}\left(R^2+2-3\beta R^2\right)$$

$$\alpha_5 = \frac{R^2}{4\left(R^2-1\right)^2}\left(2R^2+1-\left(4R^2-1\right)\beta\right)$$

$$\alpha_6 = \frac{R^2}{\left(R^2-1\right)^2}\left[\left(2R^2+1\right)\beta-3\right]$$

where

$$\beta = \frac{\cosh^{-1}R}{R\sqrt{R^2-1}}$$

for prolate spheroids ($R>1$) and

$$\beta = \frac{\cos^{-1}R}{R\sqrt{1-R^2}}$$

for prolate spheroids ($R<1$). As a consequence

$$B = \frac{R^2-1}{R^2+1}$$

Ningde Amperex Tech. Exhibit No. 2043
Zhuhai CosMX Battery Co. Ltd. v. Ningde Amperex Tech.
IPR2025-00432, U.S. Patent No. 11,575,148
Page 107 of 123

for all spheroids. The volume of a spheroid is

$$V = \frac{4\pi}{3} ab^2 .$$

In the limiting case $R >> 1$ (long thin prolate spheroid)

$$K_r = \frac{R^2}{3\left(\ln 2R - 0.5\right)}$$

and

$$B = 1 - \frac{2}{R^2}$$

Moreover, for long thin prolate spheroids,

$$Q_1 = \frac{2}{5} - \frac{6\ln 2R}{5R^2}$$

$$Q_2 = -\frac{R^2}{15\left(\ln 2R - 1.5\right)} + \frac{2}{5}$$

$$Q_3 = \frac{R^2}{10\left(\ln 2R - 0.5\right)}$$

$$Q_4 = \frac{6\ln 2R}{5R^2} .$$

For long slender ($R >> 1$, but finite and blunt-ended) cylindrical rods (with $L \approx 5.45$)

$$K_r = \frac{2}{9}\left[\frac{R^2}{\ln R}\left(1 + \frac{\ln 2 - 1}{\ln R}\right) + \frac{3L}{8\pi}\right]$$

and

$$B = 1 - \frac{3L\ln R}{4\pi R^2} .$$

Moreover, for long slender cylindrical rods,

$$Q_1 = \frac{2}{5}$$

Ningde Amperex Tech. Exhibit No. 2043
Zhuhai CosMX Battery Co. Ltd. v. Ningde Amperex Tech.
IPR2025-00432, U.S. Patent No. 11,575,148
Page 108 of 123

$$Q_2 = -\frac{2R^2}{45\left(\ln 2R + \ln 2 - 17/6\right)}$$

$$Q_3 = \frac{1}{15}\cdot\left(1 - \frac{3L\ln R}{4\pi R^2}\right)\cdot\left[\frac{R^2}{\ln R}\left(1 + \frac{\ln 2 - 1}{\ln R}\right) - \frac{3L}{8\pi}\right]$$

$$Q_4 = 0$$

The volume of a circular cylinder is

$$V = 2\pi a b^2 .$$

The material constants in the limiting case $R << 1$ (infinitesimally thin circular disk of radius b) can be obtained from the general results for an oblate spheroid, by letting the polar radius a tend to zero. Since, however, the volume V of such a disk and accordingly also its volume fraction ϕ is zero, the results must be presented in a different form, using the number density n (number of disks per unit volume) as a concentration measure. According to Brenner (1974)

$$6VK_r \to \frac{32}{3} b^3$$

and

$$B = -1$$

(corresponding to $R = 0$). Moreover, the following replacements have to be made:

$$\phi\, Q_1 \to n\frac{32}{45} b^3$$

$$\phi\, Q_2 \to n\frac{16}{45} b^3$$

$$\phi\, Q_3 \to -n\frac{8}{45} b^3$$

$$\phi\, Q_4 \to -n\frac{32}{45} b^3 .$$

In the special case of spheres ($R = 1$) the α integrals reduce to $\alpha_1 = \alpha_2 = \frac{2}{3}$, $\alpha_3 = \alpha_4 = \frac{2}{5}$ and $\alpha_5 = \alpha_6 = \frac{4}{15}$ and thus the material constants are

$$K_r = 1 ,$$

Ningde Amperex Tech. Exhibit No. 2043
Zhuhai CosMX Battery Co. Ltd. v. Ningde Amperex Tech.
IPR2025-00432, U.S. Patent No. 11,575,148
Page 109 of 123

$$B = 0,$$

$$Q_1 = \frac{1}{2},$$

$$Q_2 = Q_3 = Q_4$$

The volume of a sphere (with radius b) is

$$V = \frac{\pi b^3}{6}.$$

For all axisymmetric particles with fore-aft symmetry the material parameters Q_1 through Q_4, as well as K_r, N, and B completely determine the behavior of the suspension in arbitrary flow processes. Only five of these parameters are independent. Note that for all model shapes described above $|B| \leq 1$. The inverse case $|B| \geq 1$ occurs only for relatively uncommon model shapes (e.g. certain peanut-shaped bodies). The parameter Q_4 is derived from

$$Q_4 = Q_3 - \frac{1}{2} BN.$$

All material parameters are uniquely defined by the aspect ratio R. Based on the knowledge of K_r and particle size (volume V) [1] the rotary Péclet number can be estimated in order to assess the influence of Brownian motion. It is common practice to distinguish three regimes:

- Dominant Brownian motion:

  $$P << 1$$

  In this case ("zero shear rate limit") the intrinsic viscosity is maximal. The upper bound of the intrinsic viscosity is

  $$[\eta]_0 = 5Q_1 - Q_2 + 2Q_3.$$

  According to Brenner (1974) this result holds not only for simple shear flows (as stated in earlier derivations), but for any (homogeneous) shear flow, including e.g. uniaxial extension. For long thin prolate spheroids ($R >> 1$) this equation reduces to the well-known approximate result of Kuhn and Kuhn (1945)

[1] Apart from diluteness of the suspension, the particle system is assumed to be monodisperse, with a constant aspect ratio. This has to be kept in mind when a comparison with real suspensions is intended. The extrapolation of viscosity measurement results in the non-dilute region to the dilute region may or may not be justified. Due to interactions effective in the non-dilute region, such an extrapolation may lead to higher intrinsic viscosity values. Similarly, the effect of polydispersity of real systems on the results is difficult to assess, especially when additionally the aspect ratio is not size-invariant or has a distribution with finite width.

Ningde Amperex Tech. Exhibit No. 2043
Zhuhai CosMX Battery Co. Ltd. v. Ningde Amperex Tech.
IPR2025-00432, U.S. Patent No. 11,575,148
Page 110 of 123

$$[\eta]_0 = \frac{R^2}{15}\left[\frac{3}{\ln 2R - 0.5} + \frac{1}{\ln 2R - 1.5}\right] + \frac{8}{5}.$$

Table 14-B-2 lists the upper bound of the intrinsic viscosity $[\eta]_0$ (i.e. in the case $P = 0$) for dilute suspensions of prolate and oblate spheroids in dependence of the aspect ratio, according to the exact numerical calculation of Scheraga, cf. Brenner (1974).

Table 14-B-2. *Upper bound of the intrinsic viscosity $[\eta]_0$ (i.e. in the case $P = 0$) for dilute suspensions of prolate and oblate spheroids in dependence of the aspect ratio.*

R or $1/R$	Prolate	Oblate
1	2.5	2.5
2	2.908	2.854
4	4.663	4.059
5	5.806	4.708
10	13.63	8.043
16	27.18	12.10
25	55.19	18.19
50	176.8	35.16

- Intermediate Brownian motion:

$$R_e^{\,3} + R_e^{\,-3} >> P >> 1$$

In this case (which necessarily requires $R >> 1$ for prolate and $R << 1$ for oblate particles) the intrinsic viscosity is

$$[\eta] = 5\left(Q_1 + Q_4\right) + \frac{5}{4}$$

- Weak Brownian motion:

$$P >> 1 \qquad \text{and} \qquad P >> R_e^{\,3} + R_e^{\,-3}$$

where R_e is an "equivalent aspect ratio" (emerging in a natural way in hydrodynamic theory), which is equal to the true aspect ratio (i.e. $R_e = R$) in the case of spheroids and

$$R_e = \sqrt{\frac{8\pi}{3L}}\,\frac{R}{\sqrt{\ln R}}$$

in the case of long slender cylindrical rods. Table 14-B-3 lists equivalent aspect ratios of slender rods in dependence of the true aspect ratio.

Ningde Amperex Tech. Exhibit No. 2043
Zhuhai CosMX Battery Co. Ltd. v. Ningde Amperex Tech.
IPR2025-00432, U.S. Patent No. 11,575,148
Page 111 of 123

Table 14-B-3. *Equivalent aspect ratios of slender rods in dependence of the true aspect ratio.*

R	R_e
1	-
2	2.98
4	4.21
5	4.89
10	8.17
16	11.9
25	17.3
50	31.3
100	57.8
1000	472

In the case of weak Brownian motion the goniometric factors are given in Table 14-B-4 in dependence of the equivalent aspect ratio, according to the asymptotic results of Hinch & Leal, cf. Brenner (1974).

Table 14-B-4. *Goniometric factors in dependence of the equivalent aspect ratio.*

R_e	$\langle \sin^2\theta \rangle$	$P\langle \sin^2\theta \sin 2\phi \rangle$	$\langle \sin^2\theta \cos 2\phi \rangle$
1	0.667	0	0
2	0.690	2.1653	-0.2716
4	0.758	8.6551	-0.5136
5	0.784	13.302	-0.5810
10	0.862	51.090	-0.7530
16	0.905	128.92	-0.8366
25	0.936	312.55	-0.8918
50	0.968	1244.68	-0.9388
100	0.986	4998.81	-0.9578
∞	1	$\propto R^2/2$	-1

The values in this table refer to the case $1 \le R_e \le \infty$ (prolate particles). In order to obtain the values of the goniometric factors in the range $0 \le R_e \le 1$ (oblate particles) the following replacements have to be made:

$$R_e \to 1/R_e$$

$$\langle \sin^2\theta \rangle \to \langle \sin^2\theta \rangle$$

$$\langle \sin^2\theta \sin 2\phi \rangle \to -\langle \sin^2\theta \sin 2\phi \rangle$$

$$\langle \sin^2\theta \cos 2\phi \rangle \to -\langle \sin^2\theta \cos 2\phi \rangle .$$

Ningde Amperex Tech. Exhibit No. 2043
Zhuhai CosMX Battery Co. Ltd. v. Ningde Amperex Tech.
IPR2025-00432, U.S. Patent No. 11,575,148
Page 112 of 123

For long slender bodies ($R_e >> 1$, i.e. $B \to 1$), i.e. when $P^{1/3} >> R_e >> 1$, the following asymptotic approximations can be used, cf. Brenner (1974):

$$\left\langle \sin^2\theta \right\rangle = 1 - \frac{1.792}{R_e}$$

$$\left\langle \sin^2\theta \sin 2\phi \right\rangle = \frac{{R_e}^2}{2P}$$

$$\left\langle \sin^2\theta \cos 2\phi \right\rangle = -1 + \frac{3.0524}{R_e}.$$

The corresponding intrinsic viscosity is

$$[\eta] = 0.315 \frac{R}{\ln R}.$$

In the total absence of Brownian motion (i.e. absence of rotary diffusion, corresponding to the limit $P \to \infty$) bodies with $|B| \le 1$ (common case) undergo in simple shear flow a time-periodic rotation of the type first described by Jeffery (1922). The equations governing rotation of an axisymmetric body suspended in a liquid medium exposed to simple shear flow are

$$\dot{\theta} = \frac{1}{4}\gamma\, B \sin 2\theta \sin 2\phi \qquad \text{and} \qquad \dot{\phi} = \frac{1}{2}\gamma\left(1 + B\cos 2\phi\right).$$

Inspection of these equations shows, however, that bodies with $|B| \ge 1$ undergo an aperiodic motion in simple shear flow, ultimately adopting a stable terminal orientation. In this case the terminal orientations are $\theta^\infty = \pi/2, \tan\phi^\infty = R$ and $\theta^\infty = \pi/2$, $\tan\phi^\infty = -R$ for $B \ge 1$ and $B \le -1$, respectively. As a consequence, in the absence of rotary Brownian motion the orientational distribution function is the Dirac delta function (distribution) and the following goniometric factors may be employed to calculate the intrinsic viscosity in simple shear flow

$$\left\langle \sin^2\theta \right\rangle = 1$$

$$\left\langle \sin^2\theta \sin 2\phi \right\rangle = \frac{\sqrt{B^2 - 1}}{B}$$

$$\left\langle \sin^2\theta \cos 2\phi \right\rangle = -\frac{1}{B}.$$

In concluding we note that the intrinsic viscosity is in general bounded from below by the inequality $[\eta] > 1$.

Ningde Amperex Tech. Exhibit No. 2043
Zhuhai CosMX Battery Co. Ltd. v. Ningde Amperex Tech.
IPR2025-00432, U.S. Patent No. 11,575,148
Page 113 of 123

14-C. Rheology and thermal conductivity of nanofluids

14-C-1. Concentration measures and mixture rules

Transformation of mass fractions (weight fractions) w into volume fractions ϕ and vice versa:

$$\phi = \frac{\rho_f w}{\rho_s (1-w) + \rho_f w}$$

$$w = \frac{\rho_s \phi}{\rho_f (1-\phi) + \rho_s \phi}$$

In these relations ρ_s is the density of the solid particles and ρ_f the density of the base fluid, i.e. the liquid medium; ϕ and w (for convenience without subscript) refer to the dispersed phase, i.e. the solid particles. Accordingly, the effective density of the suspension is

$$\rho = \phi\, \rho_s + (1-\phi)\, \rho_f \,.$$

The primary aim of suspension rheology is the description of the effective viscosity of a suspension η at constant temperature in dependence of the volume fraction of solids ϕ. In the classical approach to nanofluids, volume fractions, mass fractions and densities are related by the same relations as for ordinary suspensions (see above). Moreover, if the nanofluid is in thermal equilibrium, the effective volumetric heat capacity $C_p = \rho\, c_p$ (effective specific heat at constant pressure, referred to unit volume) is usually assumed to be

$$C_P = \phi\, C_{Ps} + (1-\phi)\, C_{Pf} \,.$$

Although from a theoretical point of view this simple additivity of the volumetric heat capacities with respect to volume fractions is questionable (an exact treatment has to take compressibility and thermal expansion into account), this relation can be expected to be a reasonable approximation to reality. The exact relation is based on the additivity of the specific heats (i.e. heat capacities referred to unit mass) with respect to mass fractions, i.e.

$$c_P = w\, c_{Ps} + (1-w)\, c_{Pf} \,.$$

Note that for the calculation of the effective (volumetric) thermal expansion coefficient β of suspensions, including nanofluids, the thermal expansion of the solid phase particles can usually be neglected, i.e.

$$\beta = (1-\phi)\, \beta_f \,,$$

where β_f is the volumetric thermal expansion coefficient of the base fluid.

Ningde Amperex Tech. Exhibit No. 2043
Zhuhai CosMX Battery Co. Ltd. v. Ningde Amperex Tech.
IPR2025-00432, U.S. Patent No. 11,575,148
Page 114 of 123

14-C-2. Effective viscosity and thermal conductivity

Predictive relations for the effective viscosity of nanofluids are in principle analogous to those for ordinary suspensions (see above), i.e. the Einstein and Brinkman relation. Additionally, several other extensions or modifications of the Einstein relation as well as several relations of empirical origin (obtained from fitting experimental data), have been proposed, e.g.

$$\eta_r \approx 1 + 10\,\phi$$

$$\eta_r = 1 + 10.6\,\phi + (10.6\,\phi)^2$$

$$\eta_r = 1 + 2.5\,\phi + (2.5\,\phi)^2 + (2.5\,\phi)^3 + (2.5\,\phi)^4 + \ldots$$

$$\eta_r = 1 + 39.1\,\phi + 534\,\phi^2$$

The fact (empirical finding) that the linear Einstein relation always underestimates the actual viscosity increase with solid volume fraction, can be accounted for either by using a nonlinear relation or, sometimes, by reinterpreting the volume fraction in terms of an "effective", "equivalent", or "apparent" volume fraction. In nanofluids, and to a certain extent in ordinary suspensions as well, the physical interpretation of this apparently enhanced volume fraction may be agglomeration (since "porous" agglomerates formed by clustering of primary particles can act as secondary particles during flow processes). For nanofluids, additionally, the fluid surface layer on the dispersed nanoparticles, which is known to exhibit structure and properties different from the bulk fluid, may be volumetrically significant. One the most interesting models for practical use is the Chen model [Chen et al. 2007]. Under reasonable assumptions, this model contains one adjustable parameter which can be determined from experimentally measured data and interpreted in physical terms, viz. as an effectively enhanced volume fraction due to agglomeration. The Chen model is based on a Krieger-type relation, modified for agglomerated suspensions, i.e.

$$\eta_r = \left(1 - \frac{\phi_a}{\phi_{\max}}\right)^{-[\eta]\phi_{\max}},$$

where $\phi_{\max}$ is the maximum concenration (solids volume fraction) at which flow can occur (approx. 0.605 for high shear rate flows), $[\eta]$ is the intrinsic viscosity (approx. 2.5 for isometric particles) and ϕ_a is the apparent volume fraction of the agglomerated solid particles, which is related to the true volume fraction ϕ via the fractal dimension D,

$$\phi_a = \phi \cdot \left(\frac{r_a}{r}\right)^{3-D},$$

where r and r_a are the radii of the primary particles and the secondary particles (agglomerates), respectively. Assuming that agglomeration is a diffusion limited aggregation process (DLA process) the fractal dimension D is approx. 1.8 for nanofluids. The resulting relation

Ningde Amperex Tech. Exhibit No. 2043
Zhuhai CosMX Battery Co. Ltd. v. Ningde Amperex Tech.
IPR2025-00432, U.S. Patent No. 11,575,148
Page 115 of 123

$$\eta_r = \left(1 - \frac{\phi}{0.605}\left(\frac{r_a}{r}\right)^{1.2}\right)^{-1.5125}$$

can thus be used to extract an effective agglomerate size (radius r_a) from the measured concentration dependence of the viscosity (η_r versus ϕ curve) when the primary particle size is known. Note that the above Krieger-type expression can be expanded in polynomial form,

$$\eta_r = 1 + [\eta]\phi_a + ([\eta]\phi_a)^2 + ([\eta]\phi_a)^3 + \ldots$$

In other words, when the apparent volume fraction of agglomerated particles is taken instead of the true volume fraction, Einstein-type equations and its extensions are obtained (see above). Indeed, experimentally it is often found, that the ratio r_a/r is between 3 and 4, so that the intrinsic viscosity remains at a value close to 2.5, as expected for approximately isometric agglomerates. Note further, that the temperature dependence of the effective viscosity of nanofluids, and suspensions in general, is almost entirely determined by that of the base fluid (liquid medium) and can be described e.g. by the Vogel-Fulcher-Tamann relation. In concluding this subsection we would like to emphasize that the rheology of nanofluids is a hot topic of current research and many open questions remain. For strongly anisometric nanoparticles (e.g. carbon nanotubes) the viscosity increase with solids volume fraction can be expected to be much stronger than predicted by any of the above models.

Nanofluids usually exhibit enhanced thermal conductivity in comparison to the base fluid. There is some controversy on whether this enhancement is even larger than predicted by classical models (recent critical work [Zhang et al. 2007] denies this and claims that systematic measurement errors are responsible for erroneously high thermal conductivity values beyond the classical predictions), but it is commonly agreed that there is measurable enhancement of thermal conductivity even for very low volume fractions of solids (< 1 %). Principally this enhancement is simply a plausible consequence of the fact that most solids have higher – sometimes considerably higher – thermal conductivity than the base fluid, cf. Table 14-C-1.

Table 14-C-1. *Thermal conductivity values of materials of interest for nanofluids.*

Material	Thermal conductivity [W/mK] at R.T.
Base fluids	
Water	0.613
Ethylene glycol	0.25
Oil	0.11
Nanoparticles	
MW-CNT (carbon nanotubes)	3000
CuO	76.5
Al_2O_3	33 (up to 42-46 ?)
SiO_2	1.4
Fullerene	0.4

Ningde Amperex Tech. Exhibit No. 2043
Zhuhai CosMX Battery Co. Ltd. v. Ningde Amperex Tech.
IPR2025-00432, U.S. Patent No. 11,575,148
Page 116 of 123

The most popular models for thermal conductivity prediction are the Maxwell (or Maxwell-Eucken) model for spherical particles [Maxwell 1892, Eucken 1932], sometimes erroneously attributed to Wasp [Wasp 1977],

$$k_r = \frac{k}{k_f} = \frac{k_s + 2\,k_f + 2\left(k_s - k_f\right)\phi}{k_s + 2\,k_f - \left(k_s - k_f\right)\phi},$$

the Bruggeman-Landauer mean field model [Bruggeman 1935, Landauer 1952],

$$k_r = \frac{1}{4}\left\{\lambda + \sqrt{\lambda^2 + 8\frac{k_s}{k_f}}\right\} \qquad \text{with} \qquad \lambda = \left(3\phi - 1\right)\frac{k_s}{k_f} - \left(3\phi - 2\right),$$

and the Hamilton-Crosser model for non-spherical particles [Hamilton & Crosser 1962],

$$k_r = \frac{k}{k_f} = \frac{k_s + \left(n-1\right)\cdot k_f + \left(n-1\right)\cdot\left(k_s - k_f\right)\phi}{k_s + \left(n-1\right)\cdot k_f - \left(k_s - k_f\right)\phi},$$

where n is a shape factor, which is $n = 3/\Psi$, where Ψ is the sphericity, defined as the ratio of the surface area of a volume-equivalent sphere to that of the particle in question. Note that for spheres $n = 3$, i.e. the Hamilton-Crosser model contains the Maxwell model as a special case. High aspect ratio particles have high values of n and therefore generally more potential for thermal conductivity enhancement than isometric nanoparticles of the same material (however, also the viscosity is extremely enhanced, which sets certain limitations to the exploitation of this potential in practical applications – the volume fraction has to be kept low enough to ensure sufficient fluidity). In the case of carbon nanotubes, which are intrinsically high-aspect ratio materials, the extremely high thermal conductivity clearly outweighs the requirement of extremely low concentrations to ensure fluidity.

Specific models for anisometric particles, in particular high aspect ratio fibers and carbon nanotubes, are the Yamada-Ota unit-cell model [Yamada & Ota 1980],

$$k_r = \frac{k_s + C\,k_f + C\left(k_s - k_f\right)\phi}{k_s + C\,k_f - \left(k_s - k_f\right)\phi},$$

which can also be considered as a modification of the Maxwell model (where C is a shape factor given for cylindrical particles by $C = 2\,\phi^{0.2}\left(l_P/d_P\right)$, where l_P/d_P is the aspect ratio, i.e. the ratio of fiber length and diameter) and the Jang-Choi model [Jang & Choi 2004],

$$k_r = 1 - \phi + \left\langle\cos^2\theta\right\rangle\zeta\,\frac{k_s}{k_f}\,\phi + C_1\,\frac{r_{fm}}{r_{sp}}\,\mathrm{Re}_p{}^2\,\mathrm{Pr}\,\phi = 1 + \left(\left\langle\cos^2\theta\right\rangle\zeta\,\frac{k_s}{k_f} + C_1\,\frac{r_{fm}}{r_{sp}}\,\mathrm{Re}_p{}^2\,\mathrm{Pr} - 1\right)\phi,$$

where ζ is the Kapitza resistance (often treated as an adjustable parameter), r_{fm} is the radius of the molecules of the base fluid, r_{sp} the radius of the solid particles, Re_p the (nano-)particle Reynolds number, Pr the Prandtl number and the cos-term determines the fiber orientation (via θ): $\left\langle\cos^2\theta\right\rangle = 1$ for well aligned fibers and $\left\langle\cos^2\theta\right\rangle = 1/3$ for completely random

Ningde Amperex Tech. Exhibit No. 2043
Zhuhai CosMX Battery Co. Ltd. v. Ningde Amperex Tech.
IPR2025-00432, U.S. Patent No. 11,575,148
Page 117 of 123

orientation. This model predicts an additional thermal conductivity contribution via the particle interfaces and a inverse dependence on particle size (last term). Similarly, the model by Kumar et al. [Kumar 2004]

$$k_r = 1 + \frac{C_2 v_P}{k_f} \cdot \frac{r_{fm}}{r_{sp}} \cdot \frac{\phi}{1-\phi},$$

where C_2 is a constant and v_P is given by the Stokes-Einstein relation

$$v_P = \frac{8 k_B T}{\pi \eta r_P^2},$$

predicts that the thermal conductivity enhancement increases with particles size as $1/r_P^3$ (however, it also predicts a temperature dependence in addition to that of the base fluid; which has not been experimentally confirmed so far). Note that in the absence of microconvection (caused by particle motion), the Jang-Choi model simplifies to

$$k_r = 1 - \phi + \left\langle \cos^2 \theta \right\rangle \cdot \zeta \cdot \frac{k_s}{k_f} \cdot \phi .$$

In order to account for thermal conductivity increases beyond the predictions, the bulk thermal conductivity of the solid particles can be replaced by an "effective" (apparent, equivalent) thermal conductivity, e.g. that of agglomerates (aggregates), cf. [Chen et al. 2007] for a combined Maxwell-and-Bruggeman model, or the nanoparticles with its adsorbed partially ordered liquid layer (which exhibits structure and properties significantly different from the bulk fluid and approaching the corresponding solid phase structure and properties) can be modeled as composite shells, i.e. the nanoparticles are modeled as non-overlapping equivalent particles of greater size and the ordered liquid layer is assumed to have higher thermal conductivity than the bulk thermal conductivity of the base fluid. The Maxwell relation as modified by the Yu-Choi model is

$$k_r = \frac{k_{pe} + 2\,k_f + 2\left(k_{pe} - k_f\right)\left(1+\varepsilon\right)^3 \phi}{k_{pe} + 2\,k_f - \left(k_{pe} - k_f\right)\left(1+\varepsilon\right)^3 \phi},$$

where ε is the ratio of the ordered layer thickness to the nanoparticle radius and k_{pe} is the effective thermal conductivity of the composite-shell particles given by

$$k_{pe} = \frac{\left[2\left(1-\gamma\right) + \left(1+\varepsilon\right)^3 \left(1+2\gamma\right)\right] \cdot \gamma}{-\left(1-\gamma\right) + \left(1+\varepsilon\right)^3 \left(1+2\gamma\right)} \cdot k_s ,$$

where γ is the ratio of the thermal conductivity of the ordered layer to that of the solid particle core.

Denoting the ratio between the thermal conductivity of the solid particles and the fluid ("phase contrast") as $\kappa = k_s / k_f$, a short-hand notation of the above relations can be given. In this short-hand notation further models occuring in the literature can be given as follows:

Ningde Amperex Tech. Exhibit No. 2043
Zhuhai CosMX Battery Co. Ltd. v. Ningde Amperex Tech.
IPR2025-00432, U.S. Patent No. 11,575,148
Page 118 of 123

1. Jeffrey model [Jeffrey 1973]:

$$k_r = 1 + 3\vartheta\,\phi + \left(3\vartheta^2 + \frac{3\vartheta^2}{4} + \frac{9\vartheta^3}{16}\frac{\kappa+2}{2\kappa+3} + \ldots\right)\phi^2$$

2. Davis model [Davis 1986]:

$$k_r = 1 + \frac{3\,(\kappa-1)}{(\kappa+2)-(\kappa-1)\,\phi}\cdot\left[\phi + f(\kappa)\,\phi^2 + O(\phi^3)\right]$$

3. Lu-Lin relation [Lu & Lin 1996]:

$$k_r = 1 + \kappa\,\phi + b\,\phi^2$$

Ningde Amperex Tech. Exhibit No. 2043
Zhuhai CosMX Battery Co. Ltd. v. Ningde Amperex Tech.
IPR2025-00432, U.S. Patent No. 11,575,148
Page 119 of 123

CPPS-References. References to the Lecture Course "Characterization of Particles and Particle Systems"

1. Adamczyk Z.: *Particles at Interfaces – Interactions, Deposition, Structure*. Elsevier, Amsterdam 2006.
2. Allen T.: *Particle Size Measurement, Volume 1 – Powder Sampling and Particle Size Measurement, Volume 2 – Surface Area Measurement* (fifth edition). Chapman and Hall, London 1997.
3. Aste T., Weaire D.: *The Pursuit of Perfect Packing*. Institute of Physics Publishing. Bristol and Philadelphia 2000.

4. Bergaya F., Theng B. K. G., Lagaly G. (eds.): *Handbook of Clay Science*. Elsevier, Amsterdam 2006.
5. Bernhardt C.: *Granulometrie – Klassier- und Sedimentationsmethoden.* Deutscher Verlag für Grundstoffindustrie, Leipzig 1990.
6. Bernhardt C.: *Particle Size Analysis – Classification and Sedimentation Methods.* Chapman & Hall, London 1994.
7. Boccara N., Daoud M. (eds.): *Physics of Finely Divided Matter*. Springer, Berlin 1985.
8. Bohren C. F., Huffman D. R.: *Absorption and Scattering of Light by Small Particles.* Wiley-VCH, Weinheim 2004.
9. Born M., Wolf E.: *Principles of Optics*. Third edition. Pergamon Press, Oxford 1965.

10. Champeney D. C.: *Fourier Transforms and Their Physical Applications.* Academic Press, New York 1973.
11. Choi. S. U. S., Zhang Z. G., Keblinski P.: Nanofluids, pp. 757-773 in Nalwa H. S. (ed.): *Encyclopedia of Nanoscience and Nanotechnology – Vol. 6.* American Scientific Publishers, Valencia / CA 2004.

12. Dettmann J.: Fullerene. Birkhauser, Basel 1994.
13. Dinger D. R.: *Particle Calculations for Ceramists*. Dinger Ceramic Consulting Services, Clemson 2001.

14. Fejes Tóth L.: Reguläre Figuren. Teubner, Leipzig 1965.
15. Friedrich J.: Formanalyse von Partikelkollektiven (Fortschrittsberichte VDI, Reihe 3 – Verfahrenstechnik, Nr. 268). VDI Verlag, Düsseldorf 1992.

16. German R. M.: Particle Packing Characteristics. Metal Powder Industries Federation, Princeton 1989.

17. Happel J., Brenner H.: Low Reynolds Number Hydrodynamics. Martinus Nijhoff / Kluwer, The Hague 1983.
18. Heffels C.: On-line Particle Size and Shape Characterization by Narrow Angle Light Scattering. Ph.D. Thesis, Technical University Delft, Delft 1996.
19. Herdan G.: *Small Particle Statistics*. Butterworths, London 1960.
20. Hilbert D., Cohn-Vossen S.: Anschauliche Geometrie. Springer, Berlin 1932.
21. Hilliard J. E., Lawson L. R.: Stereology and Stochastic Geometry. Kluwer Academic Publishers, Dordrecht 2003.
22. Hulst, H. C. van de: Light Scattering by Small Particles. Wiley, New York 1957.

Ningde Amperex Tech. Exhibit No. 2043
Zhuhai CosMX Battery Co. Ltd. v. Ningde Amperex Tech.
IPR2025-00432, U.S. Patent No. 11,575,148
Page 120 of 123

23. Jackson J. D.: Classical Electrodynamics. Second edition. Wiley, New York 1975.
24. Jasmund K., Lagaly G. (eds.): Tonminerale und Tone – Struktur, Eigenschaften, Anwendungen und Einsatz in Industrie und Umwelt. Steinkopff Verlag, Darmstadt 1993.
25. Jelínek Z. K.: *Particle Size Analysis*. John Wiley and Sons, New York 1974.
26. Jillavenkatesa A., Dapkunas S.J., Lum L.-S. H.: *Particle Size Characterization* (National Institute of Standards and Technology Special Publication NIST 960-1, downloadable from http://www.nist.gov/practiceguide). US Government Printing Office, Washington 2001.
27. Johnson C. S., Gabriel D. A.: Laser Light Scattering. Dover, New York 1994.
28. Jonasz M., Fournier G. R.: Light Scattering by Particles in Water – Theoretical and Experimental Foundations. Elsevier, Amsterdam 2007.
29. Jones D. S.: The Theory of Electromagnetism. Pergamon, Oxford 1964.

30. Kaye B. H.: *A Random Walk Through Fractal Dimensions* (second edition). VCH, Weinheim 1994.
31. Kendall D. G., Barden D., Carne T. K., Le H.: Shape and Shape Theory. John Wiley & Sons, Chichester 1999.
32. Kerker M.: The Scattering of Light and Other Electromagnetic Radiation. Academic Press, New York 1969.
33. Klug H. P., Alexander L. E.: *X-ray Diffraction Procedures for Polycrystalline and Amorphous Materials*. Second edition. John Wiley & Sons, New York 1974.
34. Kopp H.: Bildverarbeitung interaktiv. Teubner, Stuttgart 1997.
35. Köster E.: Granulometrische und morphometrische Messmethoden an Mineralkörnern, Steinen und sonstigen Stoffen. Enke, Stuttgart 1964.
36. Kumar C. (ed.): *Nanomaterials – Toxicity, Health and Environmental Issues.* Wiley-VCH, Weinheim 2006.

37. Landau L. D., Lifshitz E. M.: Electrodynamics of Continuous Media. Pergamon Press, Oxford 1960.
38. Lee K. W., Kwon S.-B.: Aerosol Nanoparticles – Theory of Coagulation, pp. 35–44 in Schwartz J. A., Contescu C. I., Putyera K. (eds.): *Dekker Encyclopedia of Nanoscience and Nanotechnology*. Marcel Dekker, New York 2004.
39. Leschonski K.: Partikelmeßtechnik …
40. Lowell S., Shields J. E., Thomas M. A., Thommes M.: *Characterization of Porous Solids and Powders – Surface Area, Pore Size and Density*. Kluwer Academic Publishers, Dordrecht 2004.

41. Mandelbrot B. B.: *Fractals – Form, Chance and Dimension.* Freeman, San Francisco 1977 (Czech translation …).
42. Mandelbrot B. B.: *The Fractal Geometry of Nature.* Freeman, San Francisco 1982 (German translation …).
43. Maxwell J. C.: *A Treatise on Electricity and Magnetism – Vol. 1*. Third edition. Dover, New York 1954.
44. McCrone W., Draftz R. G., Delly J. G.: The Particle Atlas. Ann Arbor Science Publishers, Ann Arbor, 1967.
45. Mecke K., Stoyan D. (eds.): *Morphology of Condensed Matter – Physics and Geometry of Spatially Complex Systems*. Springer, Berlin 2002.

Ningde Amperex Tech. Exhibit No. 2043
Zhuhai CosMX Battery Co. Ltd. v. Ningde Amperex Tech.
IPR2025-00432, U.S. Patent No. 11,575,148
Page 121 of 123

46. Mecke K., Stoyan D. (eds.): *Statistical Physics and Spatial Statistics*. Springer, Berlin 2000.
47. Michaelides E. E.: *Particles, Bubbles and Drops – Their Motion, Heat and Mass Transfer*. World Scientific, New Jersey 2006.
48. Mie G.: Beitrage zur Optik trüber Medien, speziell kolloidaler Metallösungen, *Ann. Phys.* **25**, 377-445 (1908).
49. Milling A. J. (ed.): Surface Characterization Methods – Principles, Techniques, and Applications. Marcel Dekker, New York 1999.
50. Mittemeijer E. J., Scardi P. (eds.): Diffraction Analysis of the Microstructure of Materials. Springer, Berlin 2004.
51. Morrison I. D., Ross S.: *Colloidal Dispersions – Suspensions, Emulsions and Foams*. Wiley Interscience, New York 2002.
52. Mühlenweg H.: Investigation of the Influence of Particle Shape on Diffraction Spectroscopy. DFG Scholarship Report 1997.
53. Müller G.: Methoden der Sediment-Untersuchung (= Volume I of von Engelhardt W., Füchtbauer H., Müller G. (eds.): Sediment-Petrologie). Schweizerbart, Stuttgart 1964.
54. Munshi P. (ed.): Computerized Tomography for Scientists and Engineers. CRC Press (Taylor & Francis), Boca Raton 2007.
55. Nalwa H. S. (ed.): Encyclopedia of Nanoscience and Nanotechnology (10 volumes). American Scientific Publishers, Valencia 2004.
56. Ohser J., Mücklich F.: Statistical Analysis of Microstructures in Materials Science. John Wiley, Chichester 2000.
57. Pierre A. C.: Introduction to Sol-Gel Processing. Kluwer Academic Publishers, Boston 1998.
58. Rayleigh, Lord: On the light from the sky, its polarization and colour, *Philos. Mag.* **41**, 107-120, 274-279 (1871).
59. Reist P. C.: *Aerosol Science and Technology* (second edition). McGraw-Hill, New York 1993.
60. Ruck B.: Laser-Doppler-Anemometrie. AT Fachverlag, Stuttgart 1987.
61. Russ J. C., Dehoff R. T.: Practical Stereology. Second edition. Kluwer Academic / Plenum Publishers, New York 2000.
62. Russ J. C.: The Image Processing Handbook. Fifth edition. CRC Press (Taylor & Francis), Boca Raton 2007.
63. Russel W. B., Saville D. A., Schowalter W. R.: Colloidal Dispersions. Cambridge University Press, Cambridge 1989.
64. Sahimi M.: Applications of Percolation Theory. Taylor & Francis, London 1994.
65. Saltykov S. A.: Stereometrische Metallographie. VEB Deutscher Verlag für Grundstoffindustrie, Leipzig 1974.
66. Saxl I.: Stereology of Objects with Internal Structure. Academia, Prague 1989.
67. Scarlett B.: Characterization of particles and powders, pp. 99–125 in Brook (volume ed.): *Processing of Ceramics Part 1* (= Vol 17 A of Cahn R. W., Haasen P. and Kramer E. J. (series eds.): *Materials Science and Technology – A Comprehensive Treatment*, softcover edition). Wiley – VCH, Weinheim 2005.
68. Sinton C. W.: Raw Materials for Glass and Ceramics – Sources, Processes and Quality Control. John Wiley & Sons, Hoboken / NJ 2006.

Ningde Amperex Tech. Exhibit No. 2043
Zhuhai CosMX Battery Co. Ltd. v. Ningde Amperex Tech.
IPR2025-00432, U.S. Patent No. 11,575,148
Page 122 of 123

69. Stauffer D., Aharony A.: Perkolationstheorie – Eine Einführung. VCH, Weinheim 1995.
70. Stauffer D., Aharony A.: Introduction to Percolation Theory. Revised second edition. Taylor & Francis, London 1994.
71. Stoyan D., Mecke J.: *Stochastische Geometrie*. Akademie-Verlag, Berlin 1983.
72. Stoyan D., Kendall W. S., Mecke J.: *Stochastic Geometry and its Applications*. Second edition. John Wiley & Sons, Chichester 1995.
73. Stratton J. A.: Electromagnetic Theory. McGra-Hill, New York 1941.
74. Sugimoto T.: Monodispersed Particles. Elsevier, Amsterdam 2001.
75. Sunagawa I. (ed.): Morphology of Crystals – Part A. Terra Scientific and Reidel Publishing Company, Tokyo and Dordrecht 1987.
76. Syvitski J. P. M. (ed.): Principles, Methods, and Application of Particle Size Analysis. Cambridge University Press, Cambridge 1991.

77. Valvoda V., Polcarová M., Lukáč P.: Základy strukturní analýzy. Univerzita Karlova, Prague 1992.

78. Warren B. E.: *X-ray Diffraction*. Addison-Wesley Publishing Company, Reading 1969.
79. Wasp F. J.: *Solid-Liquid Slurry Pipeline Transportation*. Trans Tech Publications, Berlin 1977.
80. Williams C. S., Becklund O. A.: Optics – a Short Course for Engineers and Scientists. Wiley-Interscience, New York 1972.
81. Wojnar L.: *Image Analysis – Applications in Materials Engineering*. CRC Press, Baco Raton 1999.

82. Xu R.: *Particle Characterization – Light Scattering Methods*. Kluwer Academic Publishers, Dordrecht 2000.

83. Zong C.: Sphere Packings. Springer, New York 1999.

Ningde Amperex Tech. Exhibit No. 2043
Zhuhai CosMX Battery Co. Ltd. v. Ningde Amperex Tech.
IPR2025-00432, U.S. Patent No. 11,575,148
Page 123 of 123